
Deep Composition of Tensor Trains using Squared Inverse Rosenblatt Transports

Tiangang Cui · Sergey Dolgov

the date of receipt and acceptance should be inserted later

Abstract Characterising intractable high-dimensional random variables is one of the fundamental challenges in stochastic computation. The recent surge of transport maps offers a mathematical foundation and new insights for tackling this challenge by coupling intractable random variables with tractable reference random variables. This paper generalises a recently developed functional tensor-train (FTT) approximation of the inverse Rosenblatt transport [14] to a wide class of high-dimensional nonnegative functions, such as unnormalised probability density functions. First, we extend the inverse Rosenblatt transform to enable the transport to general reference measures other than the uniform measure. We develop an efficient procedure to compute this transport from a squared FTT decomposition which preserves the monotonicity. More crucially, we integrate the proposed monotonicity-preserving FTT transport into a nested variable transformation framework inspired by deep neural networks. The resulting deep inverse Rosenblatt transport significantly expands the capability of tensor approximations and transport maps to random variables with complicated nonlinear interactions and concentrated density functions. We demonstrate the efficacy of the proposed approach on a range of applications in statistical learning and uncertainty quantification, including parameter estimation for dynamical systems and inverse problems constrained by partial differential equations.

Keywords tensor-train · inverse problems · uncertainty quantification · Rosenblatt transport · deep transport maps

Mathematics Subject Classification (2010) 65D15 · 65D32 · 65C05 · 65C40 · 65C60 · 62F15 · 15A69 · 15A23

1 Introduction

Exploration of high-dimensional probability distributions is a key task in statistical physics, machine learning, uncertainty quantification, econometrics, and beyond. In many practical scenarios, high-dimensional random variables of interest follow *intractable* probability measures that

T. Cui
School of Mathematics, Monash University, Victoria 3800, Australia
E-mail: tiangang.cui@monash.edu

S. Dolgov
Department of Mathematical Sciences, University of Bath, Bath, BA2 7AY, UK
E-mail: s.dolgov@bath.ac.uk

exhibit nonlinear interactions and concentrate in some sub-manifolds. This way, one cannot directly simulate the random variables of interest but may be able to evaluate the unnormalised density function pointwise. Various approaches have been proposed to characterise intractable probability measures using some tractable probability measures where independent and identically distributed random variables can be drawn from. These include the Markov chain Monte Carlo (MCMC) methods [34, 51] that generate a Markov chain of random variables converging to the target probability measure; importance sampling and/or sequential Monte Carlo [29, 46] that characterise the target probability measures using weighted samples drawn from some tractable probability measures; variational methods [4, 28] that minimise some divergence, often the Kullback-Leibler divergence, of the target probability measure from a reference measure in some class of tractable probability measures; and many others.

The recent development of the *transport map* idea, e.g., [37, 41, 48], offers new insights in designing potent computational methods for characterising intractable high-dimensional random variables. Suppose we have an intractable target probability measure ν_π with the unnormalised density function $\pi(\mathbf{x})$ over a parameter space $\mathcal{X} \subseteq \mathbb{R}^d$, for example, the posterior measure in a Bayesian inference problem. Given a tractable reference probability measure μ defined over $\mathcal{U} \subseteq \mathbb{R}^d$ that we can simulate, e.g., a uniform or a Gaussian, one aims to construct a measurable mapping, $T: \mathcal{U} \mapsto \mathcal{X}$, such that the pushforward of μ , denoted by $T_\# \mu$, is a close approximation to ν_π . The mapping T can be used to either accelerate classical sampling methods such as MCMC (cf. [48]) or to improve the efficiency of high-order quadrature methods by mapping quadrature points (usually defined with respect to some tractable reference measures) to the support of the intractable target measure (cf. [14]).

There exist several ways to realise such mappings. One family of methods identifies the mapping T in some parametrised class of functions by solving an optimisation problem so that T minimises the Kullback-Leibler divergence of the target ν_π from the pushforward $T_\# \mu$. Some notable examples include the polynomial-based construction used in [3, 41, 48] and normalising flows [33, 31, 47, 50] that employ (invertible) neural networks. These methods often employ a mapping T with a triangular structure such that the Jacobian and the inverse of T can be evaluated in a computationally efficient manner. We also want to mention the Stein variational gradient descent method [35] and its Newton variant [12], which minimises the Kullback-Leibler divergence of the target ν_π from the empirical measure defined by a set of particles. This framework iteratively constructs a composition of mappings $T_{k+1} \circ T_k \circ \dots \circ T_1$, which are taken from some reproducing kernel Hilbert space, to push the particle set towards the target measure. Another recent development is the tensor-train (TT) based construction [14] that bypasses the variational formulation. Instead of defining a mapping by minimising some divergence of ν_π from $T_\# \mu$, the TT-based approach realises the mapping T via a separable TT factorisation [45] of the density function of ν_π . Since the separable tensor factorisation enables the marginalisation of the target density at a computational cost scaling linearly in the dimension of the random variables, it offers a computationally viable way to approximating marginal and conditional density functions of the target measure. In turn, the cumulative distribution functions (CDFs) of the marginals and conditionals define the Rosenblatt transport¹ that can couple the target measure with the uniform reference measure.

This work significantly generalises the TT-based approach of [14]. Firstly, we introduce the monotonicity- and smoothness-preserving construction of the inverse Rosenblatt transport (IRT) using the functional form of the TT factorisation [2, 22, 24]. More importantly, we propose a nested Rosenblatt transport with several layers that enables us to tackle random variables with

¹ This is also referred to as the Knothe-Rosenblatt rearrangement. It was independently proposed by Rosenblatt [53] for statistical purposes and by Knothe [30] for proving the isoperimetric inequality. The setup of the TT-based approach closely follows the original work of Rosenblatt.

concentrate probability measures and nonlinear interactions. To begin, in Section 2 we present the relevant background of the inverse Rosenblatt transport and the FTT factorisation of multivariate functions, followed by the FTT-based construction of the inverse Rosenblatt transport. Next, we present a monotonicity-preserving construction of the inverse Rosenblatt transport based on the FTT factorisation of the squared root of the target density, and derive error bounds on various statistical divergences within the f -divergence family (Section 3). The resulting *squared inverse Rosenblatt transport* (SIRT) serves as a basis for further developments of the FTT-based transport maps. The associated error bounds are useful for bounding the statistical efficiency of posterior characterisation algorithms such as MCMC and importance sampling.

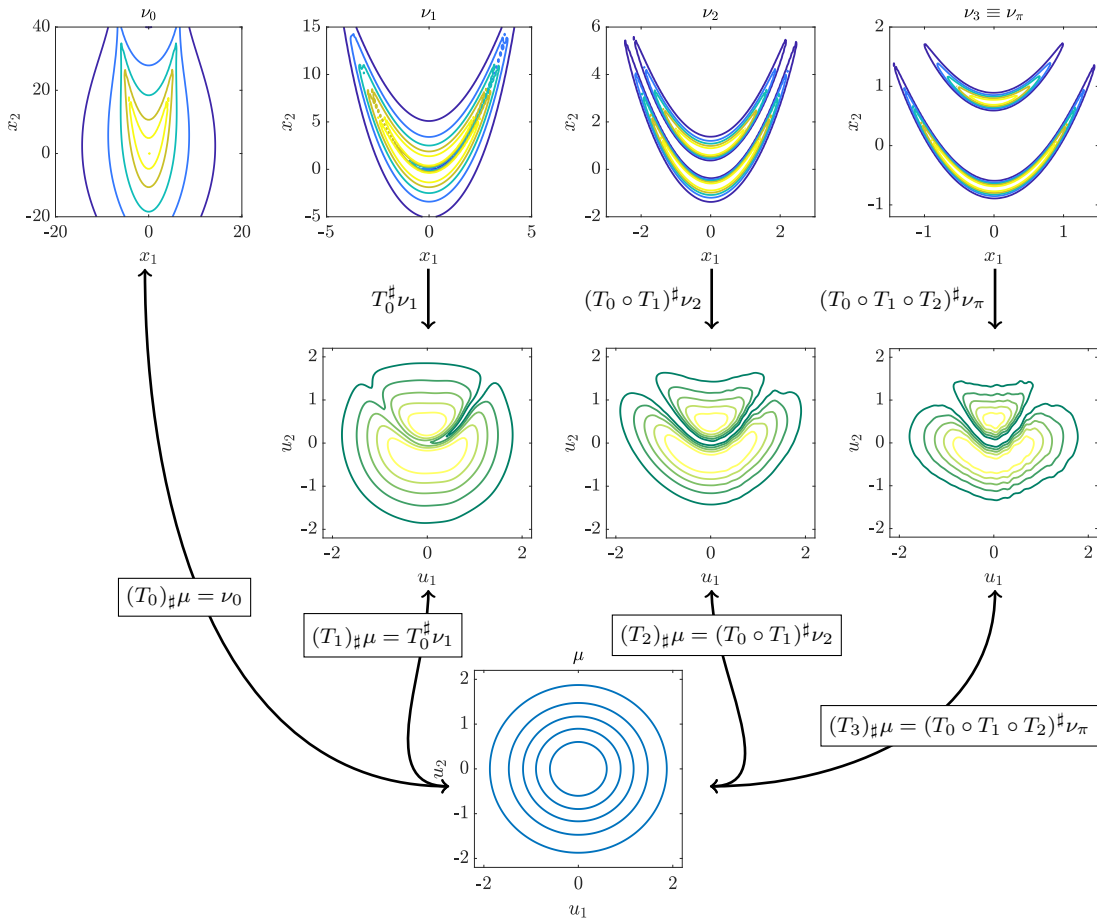


Fig. 1: Illustration of DIRT. Top row shows a sequence of bridging measures towards the target measure ν_π . Each layer of DIRT identifies an incremental mapping that couples the reference measure (bottom row) with the pullback of the bridging measure under existing composition of mappings (middle row), which admits a simpler structure for constructing TT factorisation.

The FTT factorisation works best when the correlations between random variables are *local*, i.e., the correlation decays with the distance between the indices of the variables. In the extreme case of independent random variables, the joint density factorises into the product of

marginal densities exactly. However, high-dimensional random variables of interest often have concentrated density functions and exhibits complicated nonlinear interactions, which cause a significant challenge for constructing the FTT factorisation. In such cases, one may need a FTT with high ranks to approximate the target probability density with sufficient accuracy, which in turn requires a rather large number of target density evaluations during the FTT construction. Inspired by deep neural networks, in Section 4 we present a multi-layer *deep inverse Rosenblatt transport* (DIRT) to circumvent this challenge by building a composition of monotonic mappings guided by a sequence of bridging measures with increasing complexity. See Figure 1 for an illustration of this idea. At each layer of DIRT, we aim to obtain a composition of inverse Rosenblatt transports, denoted by $T_0 \circ T_1 \circ \dots \circ T_k$, such that the pushforward of the reference measure under this composition is a close approximation of the k -th bridging measure ν_k . The existing composition $T_0 \circ T_1 \circ \dots \circ T_k$ offers a nonlinear transformation of coordinates that can effectively capture the correlations and support of the next bridging measure ν_{k+1} . As shown in Figure 1, the density of the pullback measure, $(T_0 \circ T_1 \circ \dots \circ T_k)^\# \nu_{k+1}$, can have a much simpler structure for building the FTT factorisation compared with the density of ν_{k+1} . This way, we can then factorise the density of $(T_0 \circ T_1 \circ \dots \circ T_k)^\# \nu_{k+1}$ to define the incremental mapping T_{k+1} such that $(T_{k+1})^\# \mu = (T_0 \circ T_1 \circ \dots \circ T_k)^\# \nu_{k+1}$. In Section 4, we also discuss strategies that can embed *general reference measures* rather than the uniform reference measure in DIRT to avoid complicated boundary layers.

The proposed DIRT has a similar structure to the compositions of mappings defined by methods such as the lazy maps [3] and the Stein variational gradient descent [35], in which the increment mappings are obtained by a greedy optimisation strategy. In contrast to the greedy strategy, the usage of bridging measures allows DIRT to independently construct FTT factorisations in different layers with arbitrary accuracy. Moreover, we can show that the DIRT construction is robust to FTT approximation errors in various statistical divergences, in the sense that the error bounds on a range of divergences is a linear combination of errors of FTT factorisations involved in the DIRT construction process.

The layered construction of DIRT is capable to characterise random variables with concentrated density functions. In Section 5, we integrate DIRT into existing MCMC and importance sampling methods, in which DIRT can be used as a proposal mechanism, to further reduce the estimation and sampling bias due to approximation errors of FTTs. In Section 6, we apply DIRT to four Bayesian inverse problems constrained by systems of ordinary differential equations (ODEs) and partial differential equations (PDEs). Using a predator-prey dynamical system (Section 6.1), we benchmark the impact of various tuning parameters of the FTT factorisation such as the TT rank, the number of collocation points and the choice of the reference measure on the accuracy of the DIRT. On a commonly used elliptic PDE example (Section 6.3), we are able to compare the single layered SIRT with DIRT, in which DIRT shows a clear advantage in both the computational efficiency and the accuracy compared to the single-layered counterpart. In the same example, we also demonstrate the efficacy of the FTT with the spectral Fourier basis compared to the piecewise-linear basis. The new DIRT scheme allows us to tackle concentrated posterior measures that were inaccessible previously due to increasing number of measurements and decreasing measurement noises. Moreover, we can vary the discretisation of the underlying ODE or PDE models from layer to layer to accelerate the DIRT construction. On an example involving a computationally expensive parabolic PDE (Section 6.4), we use models with increasingly refined grids to construct DIRT that is otherwise computationally infeasible to build. This multilevel construction shares similarities with the multi-fidelity preconditioning strategy of [49], except that our DIRT construction is based on FTT rather than optimisation and the multilevel models are blended into the bridging densities.

2 Background

In this section, we first introduce some notations and assumptions used throughout the paper. Then, we review the inverse Rosenblatt transport method that offers an algebraically exact transformation from the reference measure to the target measure. We will also discuss the role of the FTT decomposition in the numerical construction of the (approximate) inverse Rosenblatt transport.

2.1 Notations

We consider probability measures that are absolutely continuous with respect to the Lebesgue measure. Suppose a mapping $S : \mathcal{X} \mapsto \mathcal{U}$ is a diffeomorphism and a probability measure ν has a density $p(\mathbf{x})$, the pushforward of ν under S , denoted by $S_{\#}\nu$, has the density:

$$S_{\#}p(\mathbf{u}) = (p \circ S^{-1})(\mathbf{u}) |\nabla_{\mathbf{u}} S^{-1}(\mathbf{u})|. \quad (1)$$

Similarly, given a probability measure λ with a density $q(\mathbf{u})$, the pullback of λ under S , denoted by $S^{\#}\lambda$, has the density:

$$S^{\#}q(\mathbf{x}) = (q \circ S)(\mathbf{x}) |\nabla_{\mathbf{x}} S(\mathbf{x})|. \quad (2)$$

The short hand $\mathbf{X} \sim \nu$ is used to refer a random variable \mathbf{X} with the law ν . For a ν -integrable function $q : \mathcal{X} \mapsto \mathbb{R}$, the expectation of q is denoted by $\nu(q) = \int q(\mathbf{x})\nu(d\mathbf{x})$.

We assume the parameter space \mathcal{X} and the reference space \mathcal{U} can be expressed as Cartesian products $\mathcal{X} = \mathcal{X}_1 \times \mathcal{X}_2 \times \cdots \times \mathcal{X}_d$ and $\mathcal{U} = \mathcal{U}_1 \times \mathcal{U}_2 \times \cdots \times \mathcal{U}_d$ respectively, where $\mathcal{X}_k \subseteq \mathbb{R}$ and $\mathcal{U}_k = [0, 1]$. Using product-form Lebesgue measurable weighting functions $\lambda(\mathbf{x}) = \prod_{i=1}^d \lambda_i(\mathbf{x}_i)$ and $\omega(\mathbf{u}) = \prod_{i=1}^d \omega_i(\mathbf{u}_i)$, we define weighted L^p norms

$$\|f\|_{L^p_{\lambda}(\mathcal{X})} = \left(\int_{\mathcal{X}} |f(\mathbf{x})|^p \lambda(\mathbf{x}) d\mathbf{x} \right)^{\frac{1}{p}} \quad \text{and} \quad \|g\|_{L^p_{\omega}(\mathcal{U})} = \left(\int_{\mathcal{U}} |g(\mathbf{u})|^p \omega(\mathbf{u}) d\mathbf{u} \right)^{\frac{1}{p}},$$

on \mathcal{X} and \mathcal{U} , respectively. We use the expression $f^p(\mathbf{x})$ to denote the p -th power of $f(\mathbf{x})$ for $p > 0$.

For a vector $\mathbf{x} \in \mathbb{R}^d$ and an index $k \in \mathbb{N}$ such that $1 < k < d$, we express the first $k - 1$ coordinates and the last $d - k$ coordinates of \mathbf{x} as

$$\mathbf{x}_{<k} \equiv [\mathbf{x}_1, \dots, \mathbf{x}_{k-1}]^{\top}, \quad \text{and} \quad \mathbf{x}_{>k} \equiv [\mathbf{x}_{k+1}, \dots, \mathbf{x}_d]^{\top},$$

respectively. Similarly, we write $\mathbf{x}_{\leq k} = (\mathbf{x}_{<k}, \mathbf{x}_k)$, $\mathbf{x}_{\geq k} = (\mathbf{x}_k, \mathbf{x}_{>k})$, $\mathbf{x}_{\leq 1} = \mathbf{x}_1$, and $\mathbf{x}_{\geq d} = \mathbf{x}_d$. For any non-negative function $\pi \in L^1_{\lambda}(\mathcal{X})$, we define its marginal functions as

$$\pi_{\leq k}(\mathbf{x}_{\leq k}) \equiv \int \pi(\mathbf{x}_{\leq k}, \mathbf{x}_{>k}) \left(\prod_{i=k+1}^d \lambda_i(\mathbf{x}_i) \right) d\mathbf{x}_{>k}, \quad \text{for } 1 \leq k < d, \quad (3)$$

with $\pi_{\leq d}(\mathbf{x}_{\leq d}) = \pi(\mathbf{x})$. The marginal functions should not be confused with $\pi_1(\mathbf{x})$, $\pi_2(\mathbf{x})$, ..., $\pi_k(\mathbf{x})$ where the subscript indexes a sequence of functions on \mathcal{X} .

2.2 Inverse Rosenblatt transport

We start with a d -dimensional uniform reference probability measure, μ_{uni} , defined in a unit hypercube $\mathcal{U} = [0, 1]^d$, which has the density $f_{\text{uni}}(\mathbf{u}) = 1$. We aim to characterise a target probability measure ν_π with the probability density function (PDF)

$$f_{\mathbf{X}}(\mathbf{x}) = \frac{1}{z} \pi(\mathbf{x}) \lambda(\mathbf{x}) \quad \text{and} \quad z = \int_{\mathcal{X}} \pi(\mathbf{x}) \lambda(\mathbf{x}) d\mathbf{x}. \quad (4)$$

Here, $\pi \in L^1_\lambda(\mathcal{X})$ is the unnormalised density function (with respect to the weight λ) that is non-negative, i.e., $\pi(\mathbf{x}) \geq 0, \forall \mathbf{x} \in \mathcal{X}$, and z is the normalising constant that is often unknown.

Let $\mathbf{X} := (\mathbf{X}_1, \dots, \mathbf{X}_d)$ be the target d -dimensional random variable with law ν_π and \mathbf{U} be the reference d -dimensional random variable with law μ_{uni} . The *Rosenblatt transport* offers a viable way to constructing a map $F: \mathbb{R}^d \mapsto \mathbb{R}^d$ such that $F(\mathbf{X}) = \mathbf{U}$. As explained in [7, 56, 60], the principle of the Rosenblatt transport is the following. For $1 \leq k \leq d$, we denote the marginal PDF of the k -dimensional random variable $\mathbf{X}_{\leq k} := (\mathbf{X}_1, \dots, \mathbf{X}_k)$ by

$$f_{\mathbf{X}_{\leq k}}(\mathbf{x}_{\leq k}) = \frac{1}{z} \pi_{\leq k}(\mathbf{x}_{\leq k}) \left(\prod_{i=1}^k \lambda_i(\mathbf{x}_i) \right)$$

and the PDF of the conditional random variable $\mathbf{X}_k | \mathbf{X}_{<k}$ by

$$f_{\mathbf{X}_k | \mathbf{X}_{<k}}(\mathbf{x}_k | \mathbf{x}_{<k}) = \frac{f_{\mathbf{X}_{\leq k}}(\mathbf{x}_{<k}, \mathbf{x}_k)}{f_{\mathbf{X}_{<k}}(\mathbf{x}_{<k})} = \frac{\pi_{\leq k}(\mathbf{x}_{<k}, \mathbf{x}_k)}{\pi_{<k}(\mathbf{x}_{<k})} \lambda_k(\mathbf{x}_k).$$

This way, the CDF of \mathbf{X}_1 and the conditional CDF of $\mathbf{X}_k | \mathbf{X}_{<k}$ can be expressed as

$$F_{\mathbf{X}_1}(\mathbf{x}_1) = \int_{-\infty}^{\mathbf{x}_1} f_{\mathbf{X}_1}(\mathbf{x}_1) d\mathbf{x}_1 \quad \text{and} \quad F_{\mathbf{X}_k | \mathbf{X}_{<k}}(\mathbf{x}_k | \mathbf{x}_{<k}) = \int_{-\infty}^{\mathbf{x}_k} f_{\mathbf{X}_k | \mathbf{X}_{<k}}(\mathbf{x}_k | \mathbf{x}_{<k}) d\mathbf{x}_k, \quad (5)$$

respectively. Under mild assumptions (cf. [7]), the following sequence of transformations

$$\begin{cases} \mathbf{u}_1 & \doteq \Pr[\mathbf{X}_1 \leq \mathbf{x}_1] & = F_{\mathbf{X}_1}(\mathbf{x}_1) \\ \vdots & & \\ \mathbf{u}_k & \doteq \Pr[\mathbf{X}_k \leq \mathbf{x}_k | \mathbf{X}_{<k} = \mathbf{x}_{<k}] & = F_{\mathbf{X}_k | \mathbf{X}_{<k}}(\mathbf{x}_k | \mathbf{x}_{<k}) \\ \vdots & & \\ \mathbf{u}_d & \doteq \Pr[\mathbf{X}_d \leq \mathbf{x}_d | \mathbf{X}_{<d} = \mathbf{x}_{<d}] & = F_{\mathbf{X}_d | \mathbf{X}_{<d}}(\mathbf{x}_d | \mathbf{x}_{<d}) \end{cases} \quad (6)$$

defines uniquely a monotonically increasing map $F: \mathcal{X} \mapsto \mathcal{U}$ in the form of

$$F(\mathbf{x}) = [F_{\mathbf{X}_1}(\mathbf{x}_1), \dots, F_{\mathbf{X}_k | \mathbf{X}_{<k}}(\mathbf{x}_k | \mathbf{x}_{<k}), \dots, F_{\mathbf{X}_d | \mathbf{X}_{<d}}(\mathbf{x}_d | \mathbf{x}_{<d})]^\top, \quad (7)$$

such that the random variable $\mathbf{U} = F(\mathbf{X})$ is uniformly distributed in the unit hypercube $[0, 1]^d$. Since the k -th component of F is a scalar valued function depending on only the first k variables, that is, $F_{\mathbf{X}_k | \mathbf{X}_{<k}}: \mathbb{R}^k \mapsto \mathbb{R}$, the map F has a *lower-triangular* form. Furthermore, the map F (as well as its inverse) is almost surely differentiable and satisfies

$$F^\# f_{\text{uni}}(\mathbf{x}) = (f_{\text{uni}} \circ F)(\mathbf{x}) |\nabla_{\mathbf{x}} F(\mathbf{x})| = |\nabla_{\mathbf{x}} F(\mathbf{x})| = f_{\mathbf{X}}(\mathbf{x}),$$

ν_π -almost surely.

Suppose one can compute the Rosenblatt transport. Then, it provides a viable way to characterising the target measure. One can first generate uniform random variables $\mathbf{U} \sim \mu_{\text{uni}}$ and then applying the *inverse Rosenblatt transport* (IRT)

$$\mathbf{X} = F^{-1}(\mathbf{U})$$

to obtain a corresponding target random variable $\mathbf{X} \sim \nu_\pi$. The inverse Rosenblatt transport $T \equiv F^{-1} : \mathcal{U} \mapsto \mathcal{X}$ is also *lower-triangular* and can be constructed by successively inverting the Rosenblatt transport for $k = 1, \dots, d$:

$$\mathbf{x} = T(\mathbf{u}) \equiv \left[F_{\mathbf{X}_1}^{-1}(\mathbf{u}_1), \dots, F_{\mathbf{X}_k | \mathbf{X}_{<k}}^{-1}(\mathbf{u}_k | \mathbf{x}_{<k}), \dots, F_{\mathbf{X}_d | \mathbf{X}_{<d}}^{-1}(\mathbf{u}_d | \mathbf{x}_{<d}) \right]^\top. \quad (8)$$

The evaluation of each $F_{\mathbf{X}_k | \mathbf{X}_{<k}}^{-1}(\mathbf{u}_k | \mathbf{x}_{<k})$ requires inverting only a scalar valued monotonic function $\mathbf{u}_k = F_{\mathbf{X}_k | \mathbf{X}_{<k}}(\mathbf{x}_k | \mathbf{x}_{<k})$, where $\mathbf{x}_{<k}$ is already determined in the first $k-1$ steps. Using the change-of-variables formula, the expectation of a function $h : \mathcal{X} \mapsto \mathbb{R}$ can be expressed as

$$\nu_\pi(h) = \mu_{\text{uni}}(h \circ T).$$

This way, the expectation over the intractable target probability measure can be expressed as the expectation over a reference uniform probability measure, and thus many efficient high-dimensional quadrature methods such as sparse grids [6] and quasi Monte Carlo [13] apply.

2.3 Functional tensor-train

For high-dimensional target measures, it may be not computationally feasible to compute the marginal densities $\pi_{\leq k}$, and hence the marginal and the conditional CDFs in (5) for building the inverse Rosenblatt transport. To overcome this challenge, a recent work [14] employed the TT decomposition [45] to factorise the density of the target measure in a separable form, which leads to a computationally scalable method for building the inverse Rosenblatt transport. Here we first discuss the basics of the TT decomposition of a multivariate function.

Since multivariate functions can be viewed as continuous analogues of tensors (cf. [24]), one can decompose the unnormalised density function using FTT [2, 22]. Given a multivariate function $h : \mathcal{X} \mapsto \mathbb{R}$, where $\mathcal{X} = \mathcal{X}_1 \times \mathcal{X}_2 \times \dots \times \mathcal{X}_d$, the FTT approximates $h(\mathbf{x})$ as

$$h(\mathbf{x}) \approx \tilde{h}(\mathbf{x}) \equiv \sum_{\alpha_0=1}^{r_0} \sum_{\alpha_1=1}^{r_1} \dots \sum_{\alpha_d=1}^{r_d} \mathcal{H}_1^{(\alpha_0, \alpha_1)}(\mathbf{x}_1) \dots \mathcal{H}_k^{(\alpha_{k-1}, \alpha_k)}(\mathbf{x}_k) \dots \mathcal{H}_d^{(\alpha_{d-1}, \alpha_d)}(\mathbf{x}_d), \quad (9)$$

with $r_0 = r_d = 1$, where the summation ranges r_0, r_1, \dots, r_d are called *TT ranks*. Each univariate function $\mathcal{H}_k^{(\alpha_{k-1}, \alpha_k)}(\mathbf{x}_k) : \mathcal{X}_k \mapsto \mathbb{R}$ is represented as a linear combination of a set of n_k basis functions $\{\phi_k^{(1)}(\mathbf{x}_k), \dots, \phi_k^{(n_k)}(\mathbf{x}_k)\}$. This way, we have

$$\mathcal{H}_k^{(\alpha_{k-1}, \alpha_k)}(\mathbf{x}_k) = \sum_{i=1}^{n_k} \phi_k^{(i)}(\mathbf{x}_k) \mathcal{A}_k[\alpha_{k-1}, i, \alpha_k], \quad (10)$$

where $\mathcal{A}_k \in \mathbb{R}^{r_{k-1} \times n_k \times r_k}$ is a coefficient tensor. Examples of the basis functions include piecewise polynomials, orthogonal functions, radial basis functions, etc. In general, the FTT decomposition $\tilde{h}(\mathbf{x})$ is only an approximation to the original function $h(\mathbf{x})$ because of truncated TT ranks and sets of basis functions used for representing each $\mathcal{H}_k^{(\alpha_{k-1}, \alpha_k)}(\mathbf{x}_k)$.

Remark 1 For each k , grouping all the univariate functions $\mathcal{H}_k^{(\alpha_{k-1}, \alpha_k)}(\mathbf{x}_k)$, we have a matrix valued function $\mathcal{H}_k(\mathbf{x}_k) : \mathcal{X}_k \mapsto \mathbb{R}^{r_{k-1} \times r_k}$ that is commonly referred to as the *k-th TT core*. This way, the FTT decomposition can also be expressed in the matrix form

$$\tilde{h}(\mathbf{x}) = \mathcal{H}_1(\mathbf{x}_1) \dots \mathcal{H}_k(\mathbf{x}_k) \dots \mathcal{H}_d(\mathbf{x}_d). \quad (11)$$

We follow the MATLAB notation to denote vector-valued functions consisting of the α_k -th column and α_{k-1} -th row of $\mathcal{H}_k(\mathbf{x}_k)$ by $\mathcal{H}_k^{(:,\alpha_k)}(\mathbf{x}_k) : \mathcal{X}_k \mapsto \mathbb{R}^{r_{k-1} \times 1}$ and $\mathcal{H}_k^{(\alpha_{k-1},:)}(\mathbf{x}_k) : \mathcal{X}_k \mapsto \mathbb{R}^{1 \times r_k}$, respectively. In some situations, it is convenient to represent the FTT decomposition with grouped coordinates. For example, we can write the FTT as the functional analogue of the compact singular value decomposition (SVD):

$$\tilde{h}(\mathbf{x}) = \sum_{\alpha_k=1}^{r_k} \mathcal{H}_{\leq k}^{(\alpha_k)}(\mathbf{x}_{\leq k}) \mathcal{H}_{> k}^{(\alpha_k)}(\mathbf{x}_{> k}), \quad (12)$$

where

$$\mathcal{H}_{\leq k}^{(\alpha_k)}(\mathbf{x}_{\leq k}) = \mathcal{H}_1(\mathbf{x}_1) \cdots \mathcal{H}_{k-1}(\mathbf{x}_{k-1}) \mathcal{H}_k^{(:,\alpha_k)}(\mathbf{x}_k) : \mathcal{X}_1 \times \cdots \times \mathcal{X}_k \mapsto \mathbb{R}, \quad (13)$$

$$\mathcal{H}_{> k}^{(\alpha_k)}(\mathbf{x}_{> k}) = \mathcal{H}_{k+1}^{(\alpha_k,:)}(\mathbf{x}_{k+1}) \mathcal{H}_{k+2}(\mathbf{x}_{k+2}) \cdots \mathcal{H}_d(\mathbf{x}_d) : \mathcal{X}_{k+1} \times \cdots \times \mathcal{X}_d \mapsto \mathbb{R}. \quad (14)$$

Given a multivariate function, its FTT decomposition can be computed using alternating linear schemes such as the classical alternating least squares method (cf. [32, 43]), density matrix renormalization group methods [45, 26, 61], and the alternating minimal energy method [15] together with the cross approximation [20, 21, 19, 36] or the empirical interpolation [1, 8]. In Appendix 8.1, we detail the cross algorithm used for constructing the FTT decomposition.

2.4 A FTT-based inverse Rosenblatt transport

Using the FTT previously discussed, now we review the TT-based construction of the inverse Rosenblatt transport [14]. Suppose one has the (approximate) FTT decomposition $\tilde{\pi}(\mathbf{x})$ of the unnormalised target density $\pi(\mathbf{x})$ in the form of

$$\tilde{\pi}(\mathbf{x}_1, \mathbf{x}_2, \dots, \mathbf{x}_d) = \mathcal{F}_1(\mathbf{x}_1) \cdots \mathcal{F}_k(\mathbf{x}_k) \cdots \mathcal{F}_d(\mathbf{x}_d),$$

where $\mathcal{F}_k(\mathbf{x}_k) : \mathcal{X}_k \mapsto \mathbb{R}^{r_{k-1} \times r_k}$ is the k -th TT core. Then, we can approximate the target PDF by

$$\tilde{f}_{\mathbf{X}}(\mathbf{x}) = \frac{1}{\tilde{c}} \tilde{\pi}(\mathbf{x}) \lambda(\mathbf{x}), \quad \text{where } \tilde{c} = \int_{\mathcal{X}} \tilde{\pi}(\mathbf{x}) \lambda(\mathbf{x}) d\mathbf{x}. \quad (15)$$

Proposition 1 *For $k < d$, the k -th marginal PDF is given by*

$$\tilde{f}_{\mathbf{X}_{\leq k}}(\mathbf{x}_{\leq k}) = \frac{1}{\tilde{c}} \tilde{\pi}_{\leq k}(\mathbf{x}_{\leq k}) \left(\prod_{i=1}^k \lambda_i(\mathbf{x}_i) \right),$$

where $\tilde{\pi}_{\leq k}(\mathbf{x}_{\leq k}) = \mathcal{F}_1(\mathbf{x}_1) \cdots \mathcal{F}_k(\mathbf{x}_k) \bar{\mathcal{F}}_{k+1} \cdots \bar{\mathcal{F}}_d$, $\tilde{c} = \bar{\mathcal{F}}_1 \cdots \bar{\mathcal{F}}_d$, and the matrices $\bar{\mathcal{F}}_k$ are the integrated TT cores

$$\bar{\mathcal{F}}_k = \int_{\mathcal{X}_k} \mathcal{F}_k(\mathbf{x}_k) \lambda_k(\mathbf{x}_k) d\mathbf{x}_k \in \mathbb{R}^{r_{k-1} \times r_k}, \quad \text{for } k = 1, \dots, d.$$

Proof The marginal function of $\tilde{\pi}(\mathbf{x})$ can be expressed by

$$\tilde{\pi}_{\leq k}(\mathbf{x}_{\leq k}) = \int_{\mathcal{X}_{> k}} \mathcal{F}_1(\mathbf{x}_1) \cdots \mathcal{F}_d(\mathbf{x}_d) \left(\prod_{i=k+1}^d \lambda_i(\mathbf{x}_i) \right) d\mathbf{x}_{> k}.$$

Using the separable form of the tensor–train, the marginal density then has the form

$$\begin{aligned}\tilde{\pi}_{\leq k}(\mathbf{x}_{\leq k}) &= \mathcal{F}_1(\mathbf{x}_1) \cdots \mathcal{F}_k(\mathbf{x}_k) \left(\int_{\mathcal{X}_{k+1}} \mathcal{F}_{k+1}(\mathbf{x}_{k+1}) \lambda_{k+1}(\mathbf{x}_{k+1}) d\mathbf{x}_{k+1} \right) \cdots \left(\int_{\mathcal{X}_d} \mathcal{F}_d(\mathbf{x}_d) \lambda_d(\mathbf{x}_d) d\mathbf{x}_d \right) \\ &= \mathcal{F}_1(\mathbf{x}_1) \cdots \mathcal{F}_k(\mathbf{x}_k) \bar{\mathcal{F}}_{k+1} \cdots \bar{\mathcal{F}}_d.\end{aligned}$$

Since $\tilde{c} = \int_{\mathcal{X}} \tilde{f}(\mathbf{x}) \lambda(\mathbf{x}) d\mathbf{x}$, we have $\tilde{c} = \bar{\mathcal{F}}_1 \cdots \bar{\mathcal{F}}_d$ using a similar argument.

The above proposition leads to the marginal PDF $\tilde{f}_{\mathbf{X}_1} = \frac{1}{\tilde{c}} \tilde{\pi}_{\leq 1}(\mathbf{x}_1) \lambda_1(\mathbf{x}_1)$ and the sequence of conditional probability densities

$$\tilde{f}_{\mathbf{X}_k | \mathbf{X}_{<k}}(\mathbf{x}_k | \mathbf{x}_{<k}) = \frac{\tilde{\pi}_{\leq k}(\mathbf{x}_{<k}, \mathbf{x}_k)}{\tilde{\pi}_{<k}(\mathbf{x}_{<k})} \lambda_k(\mathbf{x}_k), \quad k = 2, \dots, d. \quad (16)$$

This leads to the CDF and the sequence of conditional CDFs

$$\tilde{F}_{\mathbf{X}_1}(\mathbf{x}_1) = \int_{-\infty}^{\mathbf{x}_1} \tilde{f}_{\mathbf{X}_1} d\mathbf{x}'_1 \quad \text{and} \quad \tilde{F}_{\mathbf{X}_k | \mathbf{X}_{<k}}(\mathbf{x}_k | \mathbf{x}_{<k}) = \int_{-\infty}^{\mathbf{x}_k} \tilde{f}_{\mathbf{X}_k | \mathbf{X}_{<k}}(\mathbf{x}_k | \mathbf{x}_{<k}) d\mathbf{x}'_k, \quad (17)$$

for $k = 2, \dots, d$, and hence the Rosenblatt transport $\mathbf{U} = \tilde{F}(\mathbf{X})$. This equivalently defines the inverse Rosenblatt transport $\tilde{T} = \tilde{F}^{-1}$. This way, by drawing a reference random variable $\mathbf{U} \sim \mu_{\text{uni}}$ and evaluating $\mathbf{X} = \tilde{T}(\mathbf{U})$, we obtain an approximate target random variable $\mathbf{X} \sim \tilde{T}_{\#} \mu_{\text{uni}}$. Note that the pushforward measure $\tilde{T}_{\#} \mu_{\text{uni}}$ has the density $\tilde{f}_{\mathbf{X}}(\mathbf{x})$.

To estimate the numerical complexity, let us introduce the maximal number of basis functions $n = \max_{k=1, \dots, d} n_k$, TT rank $r = \max_{k=0, \dots, d} r_k$, and suppose we need to draw N samples from $\tilde{\pi}(\mathbf{x})$. Note that we can precompute $\bar{\mathcal{F}}_{k+1} \cdots \bar{\mathcal{F}}_d$ with the total cost of $\mathcal{O}(dnr^2)$ operations, before any sampling starts. Similarly, the conditioning requires the interpolation of $\mathcal{F}_1(\mathbf{x}_1) \cdots \mathcal{F}_{k-1}(\mathbf{x}_{k-1})$ at the current sample coordinates, which can be built up sequentially. Each univariate interpolation needs $\mathcal{O}(nr^2)$ operations in general, but for a piecewise interpolation this can be reduced to $\mathcal{O}(r^2)$ operations per sample per coordinate. Finally, the assembling of the conditional density requires the multiplication of N vectors $\mathcal{F}_1(\mathbf{x}_1) \cdots \mathcal{F}_{k-1}(\mathbf{x}_{k-1}) \in \mathbb{R}^{r_{k-1}}$ with a vector-valued function $\mathcal{F}_k(\mathbf{x}_k) \bar{\mathcal{F}}_{k+1} \cdots \bar{\mathcal{F}}_d \in \mathbb{R}^{r_{k-1}}$. The total complexity is therefore $\mathcal{O}(dnr^2 + Ndr^2 + Ndnr)$ [14].

Constructing the inverse Rosenblatt transport using the FTT decomposition of the target density faces several challenges. First, the density function $\pi(\mathbf{x})$ is non-negative, however, its truncated FTT decomposition $\tilde{\pi}(\mathbf{x})$ can have negative values—a discrete analogue is that the truncated SVD of a matrix filled with non-negative entries can be negative. This leads to a critical issue: if the set $\{\mathbf{x} \in \mathcal{X} \mid \tilde{\pi}(\mathbf{x}) < 0\}$ has non-zero measure under ν_{π} , then the Rosenblatt transport constructed from $\tilde{\pi}(\mathbf{x})$ loses monotonicity. A simple way to circumvent this is to take the modulus of the univariate density $\tilde{f}_{\mathbf{X}_k | \mathbf{X}_{<k}}(\mathbf{x}_k | \mathbf{x}_{<k})$ before computing the CDF [14]. However, this may degrade the smoothness of the PDF and consequently the order of convergence of quadrature and interpolation. Second, the construction of the FTT decomposition (cf. Section 8.1) requires evaluating the target density at parameter points where the target density is significant. In practice, the high probability region of a high-dimensional target density, e.g., the posterior in the Bayesian inference context, can be hard to characterise. Thus, it can be challenging to construct the FTT decomposition for approximating the target density directly. In the next section, we generalise the FTT-based construction of the inverse Rosenblatt transport by tackling the aforementioned challenges.

3 Squared inverse Rosenblatt transport

We first introduce the SIRT to overcome the negativity issue outlined above. Instead of directly decomposing the unnormalised target density $\pi(\mathbf{x})$, we first obtain the (approximate) FTT decomposition $\tilde{g}(\mathbf{x})$ of the square root of $\pi(\mathbf{x})$ in the form of

$$\sqrt{\pi}(\mathbf{x}) \approx \tilde{g}(\mathbf{x}) = \mathcal{G}_1(\mathbf{x}_1) \cdots \mathcal{G}_k(\mathbf{x}_k) \cdots \mathcal{G}_d(\mathbf{x}_d), \quad (18)$$

where $\mathcal{G}_k(\mathbf{x}_k) : \mathcal{X}_k \mapsto \mathbb{R}^{r_{k-1} \times r_k}$ is the k -th TT core. This leads to an alternative approximation to the target PDF:

$$\hat{f}_{\hat{\mathbf{X}}}(\mathbf{x}) = \frac{1}{\hat{z}} \hat{\pi}(\mathbf{x}) \lambda(\mathbf{x}), \quad \text{where} \quad \hat{\pi}(\mathbf{x}) = \tilde{g}^2(\mathbf{x}) \quad \text{and} \quad \hat{z} = \int_{\mathcal{X}} \tilde{g}^2(\mathbf{x}) \lambda(\mathbf{x}) d\mathbf{x}. \quad (19)$$

Similar to the process discussed in Section 2.4, we can obtain the SIRT, $\hat{\mathbf{X}} = \hat{T}(\mathbf{U})$, by constructing the sequence of marginal functions $\hat{\pi}_{\leq k}(\mathbf{x}_{\leq k}) = \int_{\mathcal{X}} \hat{\pi}(\mathbf{x}) \prod_{i=k+1}^d \lambda_i(\mathbf{x}_i) d\mathbf{x}_{>k}$ for $k = 1, \dots, d-1$ and computing the normalising constant \hat{z} . Given a reference random variable $\mathbf{U} \sim \mu_{\text{uni}}$, we can evaluate $\hat{\mathbf{X}} = \hat{T}(\mathbf{U})$ to obtain an approximate target random variable $\hat{\mathbf{X}} \sim \hat{T}_{\#} \mu_{\text{uni}}$, which has the PDF $\hat{f}_{\hat{\mathbf{X}}}(\mathbf{x})$. Since the function $\hat{\pi}(\mathbf{x})$ is non-negative by construction, we can *preserve the smoothness and monotonicity* in the resulting SIRT \hat{T} .

3.1 Marginal functions and conditional PDFs

We represent each TT core of the decomposition in (18) as

$$\mathcal{G}_k^{(\alpha_{k-1}, \alpha_k)}(\mathbf{x}_k) = \sum_{i=1}^{n_k} \phi_k^{(i)}(\mathbf{x}_k) \mathcal{A}_k[\alpha_{k-1}, i, \alpha_k], \quad k = 1, \dots, d, \quad (20)$$

where $\{\phi_k^{(i)}(\mathbf{x}_k)\}_{i=1}^{n_k}$ are the basis functions for the k -th coordinate and $\mathcal{A}_k \in \mathbb{R}^{r_{k-1} \times n_k \times r_k}$ is the associated k -th coefficient tensor. For the k -th set of basis functions, we define the mass matrix $\mathbf{M}_k \in \mathbb{R}^{n_k \times n_k}$ by

$$\mathbf{M}_k[i, j] = \int_{\mathcal{X}_k} \phi_k^{(i)}(\mathbf{x}_k) \phi_k^{(j)}(\mathbf{x}_k) \lambda(\mathbf{x}_k) d\mathbf{x}_k, \quad \text{for} \quad i = 1, \dots, n_k, j = 1, \dots, n_k. \quad (21)$$

Then, we can represent the marginal functions by

$$\hat{\pi}_1(\mathbf{x}_1) = \sum_{\ell_1=1}^{r_1} \left(\mathcal{L}_1^{(\alpha_0, \ell_1)}(\mathbf{x}_1) \right)^2, \quad (22)$$

$$\hat{\pi}_{\leq k}(\mathbf{x}_{\leq k}) = \sum_{\ell_k=1}^{r_k} \left(\mathcal{G}_{<k}^{(\alpha_{k-1})}(\mathbf{x}_{<k}) \mathcal{L}_k^{(\alpha_{k-1}, \ell_k)}(\mathbf{x}_k) \right)^2, \quad k = 2, \dots, d, \quad (23)$$

where $\alpha_0 = 1$ and

$$\mathcal{G}_{<k}^{(\alpha_{k-1})}(\mathbf{x}_{<k}) = \mathcal{G}_1(\mathbf{x}_1) \cdots \mathcal{G}_{k-1}^{(\cdot, \alpha_{k-1})}(\mathbf{x}_{k-1}) : \mathcal{X}_{<k} \mapsto \mathbb{R}, \quad (24)$$

$$\mathcal{L}_k^{(\alpha_{k-1}, \ell_k)}(\mathbf{x}_k) = \sum_{i=1}^{n_k} \phi_k^{(i)}(\mathbf{x}_k) \mathcal{B}_k[\alpha_{k-1}, i, \ell_k] : \mathcal{X}_k \mapsto \mathbb{R}, \quad (25)$$

for a coefficient tensor $\mathcal{B}_k \in \mathbb{R}^{r_{k-1} \times n_k \times r_k}$ that is recursively defined as follows.

Proposition 2 Starting with the last coordinate $k = d$, we set $\mathbf{B}_d = \mathbf{A}_d$. Suppose for the first k dimensions ($k > 1$), we have a coefficient tensor $\mathbf{B}_k \in \mathbb{R}^{r_{k-1} \times n_k \times r_k}$ that defines a marginal function $\hat{\pi}_{\leq k}(\mathbf{x}_{\leq k})$ as in (23). The following procedure can be used to obtain the coefficient tensor $\mathbf{B}_{k-1} \in \mathbb{R}^{r_{k-2} \times n_{k-1} \times r_{k-1}}$ for defining the next marginal function $\hat{\pi}_{< k}(\mathbf{x}_{< k})$:

1. Use the Cholesky factorisation of the mass matrix, $\mathbf{L}_k \mathbf{L}_k^\top = \mathbf{M}_k \in \mathbb{R}^{n_k \times n_k}$, to construct a tensor $\mathbf{C}_k \in \mathbb{R}^{r_{k-1} \times n_k \times r_k}$:

$$\mathbf{C}_k[\alpha_{k-1}, \tau, \ell_k] = \sum_{i=1}^{n_k} \mathbf{B}_k[\alpha_{k-1}, i, \ell_k] \mathbf{L}_k[i, \tau]. \quad (26)$$

2. Unfold \mathbf{C}_k along the first coordinate [32] to obtain a matrix $\mathbf{C}_k^{(R)} \in \mathbb{R}^{r_{k-1} \times (n_k r_k)}$ and compute the thin QR factorisation

$$\mathbf{Q}_k \mathbf{R}_k = (\mathbf{C}_k^{(R)})^\top, \quad (27)$$

where $\mathbf{Q}_k \in \mathbb{R}^{(n_k r_k) \times r_{k-1}}$ is semi-orthogonal and $\mathbf{R}_k \in \mathbb{R}^{r_{k-1} \times r_{k-1}}$ is upper-triangular.

3. Compute the new coefficient tensor

$$\mathbf{B}_{k-1}[\alpha_{k-2}, i, \ell_{k-1}] = \sum_{\alpha_{k-1}=1}^{r_{k-1}} \mathbf{A}_{k-1}[\alpha_{k-2}, i, \alpha_{k-1}] \mathbf{R}_k[\ell_{k-1}, \alpha_{k-1}]. \quad (28)$$

Furthermore, at index $k = 1$, the unfolded \mathbf{C}_1 along the first coordinate is a row vector $\mathbf{C}_1^{(R)} \in \mathbb{R}^{1 \times (n_1 r_1)}$. Thus, the thin QR factorisation $\mathbf{Q}_1 \mathbf{R}_1 = (\mathbf{C}_1^{(R)})^\top$ produces a scalar $\mathbf{R}_1 \in \mathbb{R}$ and the normalising constant $\hat{z} = \int_{\mathcal{X}_1} \hat{\pi}_{\leq 1}(\mathbf{x}_1) \lambda_1(\mathbf{x}_1) d\mathbf{x}_1$ can be obtain by $\hat{z} = \mathbf{R}_1^2 = \|\mathbf{C}_1^{(R)}\|^2$.

Proof See Appendix 8.2.

Proposition 3 The marginal PDF of $\hat{\mathbf{X}}_1$ can be expressed as

$$\hat{f}_{\hat{\mathbf{X}}_1}(\mathbf{x}_1) = \sum_{\ell_1=1}^{r_1} \left(\sum_{i=1}^{n_1} \phi_1^{(i)}(\mathbf{x}_1) \mathbf{D}_1[i, \ell_1] \right)^2 \lambda_1(\mathbf{x}_1), \quad \text{where } \mathbf{D}_1[i, \ell_1] = \frac{1}{\hat{z}} \mathbf{B}_1[\alpha_0, i, \ell_1], \quad (29)$$

and $\alpha_0 = 1$. For $k > 1$ and a given $\mathbf{x}_{< k}$, the conditional PDF of $\hat{\mathbf{X}}_k | \hat{\mathbf{X}}_{< k}$ can be expressed as

$$\hat{f}_{\hat{\mathbf{X}}_k | \hat{\mathbf{X}}_{< k}}(\mathbf{x}_k | \mathbf{x}_{< k}) = \sum_{\ell_k=1}^{r_k} \left(\sum_{i=1}^{n_k} \phi_k^{(i)}(\mathbf{x}_k) \mathbf{D}_k[i, \ell_k] \right)^2 \lambda_k(\mathbf{x}_k) \quad (30)$$

where $\mathbf{D}_k \in \mathbb{R}^{n_k \times r_k}$ is given by

$$\mathbf{D}_k[i, \ell_k] = \frac{1}{\hat{\pi}_{< k}(\mathbf{x}_{< k})} \sum_{\alpha_{k-1}=1}^{r_{k-1}} \mathcal{G}_{< k}^{(\alpha_{k-1})}(\mathbf{x}_{< k}) \mathbf{B}_k[\alpha_{k-1}, i, \ell_k].$$

Proof The above results directly follow from the definition of conditional PDF and the marginal functions in (22) and (23).

Note that the product $\mathcal{G}_1(\mathbf{x}_1) \cdots \mathcal{G}_{k-1}(\mathbf{x}_{k-1})$ requires $k-1$ univariate interpolations and $k-2$ products of matrices per sample, that is the same operations as in the standard inverse Rosenblatt transport. The QR decomposition (27) and the construction of the coefficient tensors (28) need $\mathcal{O}(dnr^3)$ operations, but these are pre-processing steps that are independent of the number of samples. However, in contrast to the vector-valued function $\mathcal{F}_k(\mathbf{x}_k) \bar{\mathcal{F}}_{k+1} \cdots \bar{\mathcal{F}}_d \in \mathbb{R}^{r_{k-1}}$, in evaluating the PDF $\hat{f}_{\hat{\mathbf{X}}}$, we need to multiply the matrix-valued function $\mathcal{L}_k(\mathbf{x}_k) \in \mathbb{R}^{r_{k-1} \times r_k}$ for each sample. Thus, the leading term of the complexity becomes $\mathcal{O}(Ndnr^2)$, one order of r or n higher than the complexity of the standard inverse Rosenblatt transport. However, for small r and n this is well compensated by a smoother map, which will be crucial in Section 4.

3.2 Implementation of CDFs

To evaluate the SIRT, one has to first construct the marginal CDF of $\hat{\mathbf{X}}_1$ and the conditional CDFs of $\hat{\mathbf{X}}_k | \hat{\mathbf{X}}_{<k}$ for $k > 1$, and then inverts the CDFs (see (8)). Here we discuss the computation and the inversion of CDFs, which are based on pseudo-spectral methods, for problems with bounded domains and extensions to problems with unbounded domains. We refer the readers to [5, 55, 59] and references therein for a more details.

3.2.1 Bounded domain with polynomial basis

For a bounded parameter space $\mathcal{X} \subset \mathbb{R}^d$, we consider the weighting function $\lambda(\mathbf{x}) = 1$. Since \mathcal{X} can be expressed as a Cartesian product, without loss of generality, here we discuss the CDF of a one-dimensional random variable Z with PDF

$$\hat{f}_Z(\zeta) = \sum_{\ell=1}^r \left(\sum_{i=1}^n \phi^{(i)}(\zeta) \mathbf{D}[i, \ell] \right)^2, \quad (31)$$

where $\{\phi^{(i)}(\zeta)\}_{i=1}^n$ are the basis functions, $\mathbf{D} \in \mathbb{R}^{n \times r}$ is a coefficient matrix, and $\zeta \in [-1, 1]$. Here $\hat{f}_Z(\zeta)$ can be either the marginal PDF or the conditional PDFs defined in Proposition 3 with a suitable linear change of coordinate.

We first consider a polynomial basis, $\phi^{(i)}(z) \in \mathbb{P}_{n-1}$ for $i = 1, \dots, n$, where \mathbb{P}_{n-1} is a vector space of polynomials of degree at most $n-1$ defined on $[-1, 1]$. Thus, the PDF $\hat{f}_Z(\zeta)$ can be represented exactly in \mathbb{P}_{2n-2} . To enable fast computation of the CDF, we choose the Chebyshev polynomials of the second kind

$$p_m(\zeta) = \frac{\sin((m+1)\cos^{-1}(\zeta))}{\sin(\cos^{-1}(\zeta))}, \quad m = 0, 1, \dots, 2n-2,$$

as the basis of \mathbb{P}_{2n-2} . Using the roots of $p_{2n-1}(\zeta)$, we can define the set of collocation points

$$\{\zeta_m\}_{m=1}^{2n-1}, \quad \text{where } \zeta_m = \cos\left(\frac{m\pi}{2n}\right).$$

This way, by evaluating $\hat{f}_Z(\zeta)$ on the collocation points, which needs $\mathcal{O}(nr)$ operations, one can apply the collocation method (Chapter 4 of [5]) to represent $\hat{f}_Z(\zeta)$ using the Chebyshev basis:

$$\hat{f}_Z(\zeta) = \sum_{m=0}^{2n-2} a_m p_m(\zeta), \quad (32)$$

where the coefficients $\{a_m\}_{m=0}^{2n-2}$ can be computed by the fast Fourier transform with $\mathcal{O}(n \log(n))$ operations. Then, one can express the CDF of Z as

$$F_Z(\zeta) = \int_{-1}^{\zeta} \hat{f}_Z(\zeta') d\zeta' = \sum_{m=0}^{2n-2} \frac{a_m}{m+1} (t_{m+1}(\zeta) - t_{m+1}(-1)), \quad (33)$$

where $t_m(\zeta) = \cos(m \cos^{-1}(\zeta))$ is the Chebyshev polynomial of the first kind of degree m . A random variable Z can be generated by drawing a uniform random variable U and evaluating $Z = F_Z^{-1}(U)$ by solving the root finding problem $F_Z(Z) = U$.

Remark 2 The PDF in (31) is non-negative for $\forall \zeta \in [-1, 1]$ by construction and can be represented exactly in \mathbb{P}_{2n-2} with the polynomial basis. Thus, its Chebyshev representation in (32) is also non-negative. This way, the resulting CDF in (33) is monotonic, and thus the solution to the inverse CDF equation, $F_Z(Z) = U$, admits a unique solution.

Remark 3 One can also employ piecewise Lagrange polynomials as a basis to enable hp-adaptivity. With piecewise Lagrange polynomials, the above-mentioned technique can also be used to obtain the piecewise definition of the CDF.

Since $F_Z(Z) = U$ has a unique solution and F_Z is monotone and bounded between $[0, 1]$, it requires usually only a few iterations to apply the root finding methods, such as the regula falsi method and the Newton's method, to solve $F_Z(Z) = U$ with an accuracy close to machine precision. Overall, the construction of the CDF needs $\mathcal{O}(nr + n \log(n))$ operations, and the inversion of the CDF function needs $\mathcal{O}(cn)$ operations, where $\mathcal{O}(n)$ is the cost of evaluating the CDF and c is the number of iterations required by the root finding method. In comparison, building the matrix \mathbf{D} requires $\mathcal{O}(nr^2)$ operations (cf. Proposition 3).

3.2.2 Bounded domain with Fourier basis

If the Fourier transform of the PDF of Z , which is the characteristic function, is band-limited in the frequency domain, then one may choose the sine and cosine Fourier series as the basis for representing the PDF in (31). In this case, the above strategy can also be applied. Recall the Fourier basis with an even cardinality n

$$\{1, \dots, \sin(m\pi\zeta), \cos(m\pi\zeta), \dots, \cos(n\pi\zeta/2)\}, \quad m = 1, \dots, n/2 - 1,$$

which consists of $n/2 - 1$ sine functions and $n/2 + 1$ cosine functions. The PDF $\hat{f}_Z(\zeta)$ defined in (31) yields an exact representation using the Fourier basis with cardinality $2n$. This way, one can represent $\hat{f}_Z(\zeta)$ as

$$\hat{f}_Z(\zeta) = a_0 + \sum_{m=1}^n a_m \cos(m\pi\zeta) + \sum_{m=1}^{n-1} b_m \sin(m\pi\zeta),$$

where the coefficients, a_m and b_m , are obtained by evaluating $\hat{f}_Z(\zeta)$ on the collocation points

$$\{\zeta_m\}_{m=1}^{2n}, \quad \text{where } \zeta_m = \frac{m}{n} - 1,$$

and applying the rectangular rule. This leads to the CDF

$$F_Z(\zeta) = \int_{-1}^{\zeta} \hat{f}_Z(\zeta') d\zeta' = a_0(\zeta + 1) + \sum_{m=1}^n \frac{a_m}{m\pi} \sin(m\pi\zeta) - \sum_{m=1}^{n-1} \frac{b_m}{m\pi} (\cos(m\pi\zeta) - \cos(m\pi)).$$

The construction and the inversion of the CDF using the Fourier basis cost a similar amount of operations compared to the polynomial basis.

3.2.3 Unbounded domain

Given an unbounded domain, the simplest approach is to truncate the domain at the tail of the PDF. With the domain truncation, the above-mentioned implementations based on Chebyshev and Fourier basis can be applied directly. Although the function approximation error induced by the domain truncation can be bounded, using the resulting SIRT for computing expectations may lead to a biased estimator.

One can also consider basis functions that are intrinsic to an unbounded domain. For the domain $\mathcal{X}_k = (0, \infty)$, one can employ the Laguerre polynomials as the basis. This equips \mathcal{X}_k with a natural exponential weighting function $\lambda_k(\mathbf{x}_k) = \exp(-\mathbf{x}_k)$. The collocation method using higher order Laguerre polynomials can be applied again to obtain the exact representation of the CDF. Similarly, for $\mathcal{X}_k = (-\infty, \infty)$, the Hermite polynomials can be used as a basis, which equips \mathcal{X}_k with a Gaussian weighting function $\lambda_k(\mathbf{x}_k) = \exp(-\frac{1}{2}\mathbf{x}_k^2)$. Although one can apply the collocation method to obtain an algebraically exact representation of the CDF, the resulting CDF involves error functions, complementary error functions, and imaginary error functions. Those functions have to be approximated numerically. Thus, the computational cost of computing the CDF can be high, and it may be hard to guarantee the monotonicity and uniqueness of the inverse CDF solution at the tails. Using other bases such as the Whittaker cardinal functions for $\mathcal{X}_k = (-\infty, \infty)$ may face a similar challenge.

Remark 4 In a situation where the squared form of the PDF in (31) can be computed but it is challenging to invert the CDF function, one can employ the rejection sampling [51] to generate random variables. In this situation, our FTT approximation can still be used to draw conditional samples. However, this approach may not lead to the deterministic inverse Rosenblatt transport.

3.2.4 Change of coordinate

One can also apply a diffeomorphic mapping to change the coordinate of an unbounded domain \mathcal{X} to a bounded one, e.g., $\mathcal{Z} = [-1, 1]^d$, followed by application of the Chebyshev polynomials or Fourier series. Given a PDF $f_{\mathbf{X}}(\mathbf{x})$ of a random variable $\mathbf{X} \in \mathcal{X}$, suppose we have a diffeomorphic mapping $R: \mathcal{X} \mapsto \mathcal{Z}$ and let $q(\mathbf{x}) = |\nabla R(\mathbf{x})| \geq 0$. For any Borel set $\mathcal{B}_X \subseteq \mathcal{X}$, we have

$$\mathbb{P}[\mathbf{X} \in \mathcal{B}_X] = \int_{\mathcal{B}_X} f_{\mathbf{X}}(\mathbf{x}) d\mathbf{x} = \int_{\mathcal{B}_Z} (f_{\mathbf{X}} \circ R^{-1})(\zeta) |\nabla R^{-1}(\zeta)| d\zeta = \int_{\mathcal{B}_Z} \frac{(f_{\mathbf{X}} \circ R^{-1})(\zeta)}{(q \circ R^{-1})(\zeta)} d\zeta,$$

where $\mathcal{B}_Z = R(\mathcal{B}_X)$. Thus, one can draw a random variable \mathbf{Z} with PDF

$$f_{\mathbf{Z}}(\zeta) = \frac{(f_{\mathbf{X}} \circ R^{-1})(\zeta)}{(q \circ R^{-1})(\zeta)},$$

and apply the mapping $\mathbf{X} = R(\mathbf{Z})$ to obtain a random variable X . With the change of the coordinate $\zeta = R(\mathbf{x})$, one needs to build the FTT to approximate $\sqrt{f_{\mathbf{Z}}}(\zeta)$ and construct the corresponding SIRT to simulate the random variable \mathbf{Z} . To avoid singularities at the boundary of \mathcal{Z} , one can choose a mapping R such that the function $q(\mathbf{x})$ decays slower than $f_{\mathbf{Z}}(\zeta)$.

3.3 SIRT error

Since the SIRT enables us to generate i.i.d. samples from the probability measure $\hat{T}_{\sharp} \mu_{\text{uni}}$, it can be used to define either Metropolis independence samplers or importance sampling schemes. Based on certain assumptions on the FTT approximation \tilde{g} , here we establish error bounds for

the TV distance, the Hellinger distance, and the χ^2 -divergence of the target measure ν_π from $\hat{T}_\# \mu_{\text{uni}}$. These divergences play a vital role in analysing the convergence of Metropolis-Hastings methods and the efficiency of importance sampling.

Proposition 4 *Given a FTT approximation to the square root of the unnormalised target density, i.e., $\tilde{g} \approx \sqrt{\pi}$, suppose that the error of \tilde{g} satisfies*

$$\|\tilde{g} - \sqrt{\pi}\|_{L_\lambda^2(\mathcal{X})} \leq \epsilon. \quad (34)$$

Then, the approximate normalising constant \hat{z} satisfies $|\sqrt{z} - \sqrt{\hat{z}}| \leq \epsilon$.

Proof The normalising constants z and \hat{z} satisfy

$$|z - \hat{z}| = \left| \int_{\mathcal{X}} (\pi(\mathbf{x}) - \tilde{g}(\mathbf{x})^2) \lambda(\mathbf{x}) d\mathbf{x} \right| \leq \|\pi - \tilde{g}^2\|_{L_\lambda^1(\mathcal{X})}. \quad (35)$$

Applying the Hölder's inequality (with $p = q = 2$) and the Minkowski inequality, the right hand side of the above inequality also satisfies

$$\begin{aligned} \|\pi - \tilde{g}^2\|_{L_\lambda^1(\mathcal{X})} &= \|(\sqrt{\pi} - \tilde{g})(\sqrt{\pi} + \tilde{g})\|_{L_\lambda^1(\mathcal{X})} \\ &\leq \|\sqrt{\pi} - \tilde{g}\|_{L_\lambda^p(\mathcal{X})} \|\sqrt{\pi} + \tilde{g}\|_{L_\lambda^q(\mathcal{X})} \\ &\leq \epsilon (\|\sqrt{\pi}\|_{L_\lambda^2(\mathcal{X})} + \|\tilde{g}\|_{L_\lambda^2(\mathcal{X})}) \\ &= \epsilon (\sqrt{z} + \sqrt{\hat{z}}). \end{aligned} \quad (36)$$

Since both z and \hat{z} are positive, we have $|z - \hat{z}| = |\sqrt{\hat{z}} - \sqrt{z}| (\sqrt{z} + \sqrt{\hat{z}})$. Substituting this identity and the inequality in (36) into (35), the result follows.

Theorem 1 *Suppose the error of a FTT approximation $\tilde{g} \approx \sqrt{\pi}$ satisfies (34). The Hellinger distance between ν_π and $\hat{T}_\# \mu_{\text{uni}}$ satisfies*

$$D_{\text{H}}(\nu_\pi \| \hat{T}_\# \mu_{\text{uni}}) \leq \sqrt{\frac{2}{z}} \epsilon. \quad (37)$$

Proof Since the target measure ν_π and the approximate measure $\hat{T}_\# \mu_{\text{uni}}$ respectively have the densities $\frac{1}{z} \pi(\mathbf{x}) \lambda(\mathbf{x})$ and $\frac{1}{\hat{z}} \tilde{g}(\mathbf{x})^2 \lambda(\mathbf{x})$, the squared Hellinger distance satisfies

$$D_{\text{H}}^2(\nu_\pi \| \hat{T}_\# \mu_{\text{uni}}) = \frac{1}{2} \int_{\mathcal{X}} \left(\frac{\sqrt{\pi}(\mathbf{x})}{\sqrt{z}} - \frac{\tilde{g}(\mathbf{x})}{\sqrt{\hat{z}}} \right)^2 \lambda(\mathbf{x}) d\mathbf{x}$$

This leads to the inequality

$$\begin{aligned} D_{\text{H}}^2(\nu_\pi \| \hat{T}_\# \mu_{\text{uni}}) &= \frac{1}{2z} \|\sqrt{\pi} - \tilde{g} + \tilde{g} - \tilde{g} \sqrt{z/\hat{z}}\|_{L_\lambda^2(\mathcal{X})}^2 \\ &\leq \frac{1}{2z} \left(\|\sqrt{\pi} - \tilde{g}\|_{L_\lambda^2(\mathcal{X})} + \|\tilde{g}\|_{L_\lambda^2(\mathcal{X})} |1 - \sqrt{z/\hat{z}}| \right)^2. \end{aligned} \quad (38)$$

Applying Proposition 4 and $\|\tilde{g}\|_{L_\lambda^2(\mathcal{X})}^2 = \hat{z}$, the above inequality can be further reduced to

$$D_{\text{H}}^2(\nu_\pi \| \hat{T}_\# \mu_{\text{uni}}) \leq \frac{1}{2z} \left(\epsilon + |\sqrt{\hat{z}} - \sqrt{z}| \right)^2 \leq \frac{2\epsilon^2}{z}.$$

Thus, we have $D_{\text{H}}(\nu_\pi \| \hat{T}_\# \mu_{\text{uni}}) \leq \sqrt{\frac{2}{z}} \epsilon$.

Corollary 1 *Suppose the error of a given FTT approximation $\tilde{g} \approx \sqrt{\pi}$ satisfies (34). The total variation distance between ν_π and $\hat{T}_\# \mu_{\text{uni}}$ satisfies*

$$D_{\text{TV}}(\nu_\pi \| \hat{T}_\# \mu_{\text{uni}}) \leq \frac{2\epsilon}{\sqrt{z}}. \quad (39)$$

Proof The result directly follows from the inequality $D_{\text{TV}} \leq \sqrt{2}D_{\text{H}}$ and Theorem 1.

Proposition 5 *Given two probability measures ν_π and $\hat{\nu}_\pi$ and a function h with finite second moments with respect to ν_π and $\hat{\nu}_\pi$. Then*

$$|\nu_\pi(h) - \hat{\nu}_\pi(h)| \leq \sqrt{2} (\nu_\pi(h^2))^{\frac{1}{2}} + \hat{\nu}_\pi(h^2)^{\frac{1}{2}} D_{\text{H}}(\nu_\pi \| \hat{\nu}_\pi).$$

Proof Suppose ν_π and $\hat{\nu}_\pi$ respectively have density functions $f_{\mathbf{X}}(\mathbf{x})$ and $\hat{f}_{\hat{\mathbf{X}}}(\mathbf{x})$ with respect to the Lebesgue measure. We have the following inequality

$$\begin{aligned} |\nu_\pi(h) - \hat{\nu}_\pi(h)| &= \left| \int_{\mathcal{X}} h(\mathbf{x})(f_{\mathbf{X}}(\mathbf{x}) - \hat{f}_{\hat{\mathbf{X}}}(\mathbf{x})) d\mathbf{x} \right| \\ &= \left| \int_{\mathcal{X}} h(\mathbf{x})(f_{\hat{\mathbf{X}}}^{\frac{1}{2}}(\mathbf{x}) + \hat{f}_{\hat{\mathbf{X}}}^{\frac{1}{2}}(\mathbf{x}))(f_{\hat{\mathbf{X}}}^{\frac{1}{2}}(\mathbf{x}) - \hat{f}_{\hat{\mathbf{X}}}^{\frac{1}{2}}(\mathbf{x})) d\mathbf{x} \right| \\ &\leq \left(\int_{\mathcal{X}} (h(\mathbf{x})f_{\hat{\mathbf{X}}}^{\frac{1}{2}}(\mathbf{x}) + h(\mathbf{x})\hat{f}_{\hat{\mathbf{X}}}^{\frac{1}{2}}(\mathbf{x}))^2 d\mathbf{x} \right)^{\frac{1}{2}} \left(\int_{\mathcal{X}} (f_{\hat{\mathbf{X}}}^{\frac{1}{2}}(\mathbf{x}) - \hat{f}_{\hat{\mathbf{X}}}^{\frac{1}{2}}(\mathbf{x}))^2 d\mathbf{x} \right)^{\frac{1}{2}} \\ &\leq \sqrt{2} \left(\left(\int_{\mathcal{X}} h(\mathbf{x})^2 f_{\mathbf{X}}(\mathbf{x}) d\mathbf{x} \right)^{\frac{1}{2}} + \left(\int_{\mathcal{X}} h(\mathbf{x})^2 \hat{f}_{\hat{\mathbf{X}}}(\mathbf{x}) d\mathbf{x} \right)^{\frac{1}{2}} \right) D_{\text{H}}(\nu_\pi \| \hat{\nu}_\pi). \end{aligned}$$

Thus, the result follows.

Corollary 2 *Suppose the error of a given FTT approximation $\tilde{g} \approx \sqrt{\pi}$ satisfies (34). We assume*

$$\sup_{\mathbf{x} \in \mathcal{X}} \frac{\pi(\mathbf{x})}{\tilde{g}^2(\mathbf{x})} = c_1 < \infty. \quad (40)$$

The χ^2 -divergence of ν_π from $\hat{T}_\# \mu_{\text{uni}}$ satisfies

$$D_{\chi^2}(\nu_\pi \| \hat{T}_\# \mu_{\text{uni}}) \leq \left(\nu_\pi(\pi^2/\tilde{g}^4)^{\frac{1}{2}} + (\hat{T}_\# \mu_{\text{uni}})(\pi^2/\tilde{g}^4)^{\frac{1}{2}} \right) \frac{2\hat{z}}{z\sqrt{z}} \epsilon. \quad (41)$$

Proof Given the bound in (40), the ratio between $f_{\mathbf{X}}(\mathbf{x})$ and $\hat{f}_{\hat{\mathbf{X}}}(\mathbf{x})$ satisfies

$$\sup_{\mathbf{x} \in \mathcal{X}} \frac{f_{\mathbf{X}}(\mathbf{x})}{\hat{f}_{\hat{\mathbf{X}}}(\mathbf{x})} = \frac{\hat{z}}{z} \sup_{\mathbf{x} \in \mathcal{X}} \frac{\pi(\mathbf{x})}{\tilde{g}^2(\mathbf{x})} = \frac{\hat{z}}{z} c_1 < \infty. \quad (42)$$

This way, ν_π is absolutely continuous with respect to $\hat{T}_\# \mu_{\text{uni}}$. Thus, the χ^2 -divergence of ν_π from $\hat{T}_\# \mu_{\text{uni}}$ can be expressed as

$$\begin{aligned} D_{\chi^2}(\nu_\pi \| \hat{T}_\# \mu_{\text{uni}}) &= \int_{\mathcal{X}} \left(\frac{f_{\mathbf{X}}(\mathbf{x})}{\hat{f}_{\hat{\mathbf{X}}}(\mathbf{x})} \right)^2 \hat{f}_{\hat{\mathbf{X}}}(\mathbf{x}) d\mathbf{x} - 1 \\ &= \nu_\pi(f_{\mathbf{X}}/\hat{f}_{\hat{\mathbf{X}}}) - (\hat{T}_\# \mu_{\text{uni}})(f_{\mathbf{X}}/\hat{f}_{\hat{\mathbf{X}}}) \\ &= \frac{\hat{z}}{z} \left(\nu_\pi(\pi/\tilde{g}^2) - (\hat{T}_\# \mu_{\text{uni}})(\pi/\tilde{g}^2) \right). \end{aligned}$$

The bound in (40) also implies that the expectations $\nu_\pi(\pi^2/\tilde{g}^4)$ and $(\hat{T}_\# \mu_{\text{uni}})(\pi^2/\tilde{g}^4)$ are finite. Therefore, the result follows from Proposition 5.

Remark 5 The TV distance, Hellinger distance, and χ^2 -divergence of the target measure ν_π from the pushforward of the reference μ_{uni} under the SIRT \hat{T} are linear in the approximation error of the FTT. Note that $\sqrt{z} = \|\sqrt{\pi}\|_{L_\lambda^2(\mathcal{X})}$. Suppose the relative error of \tilde{g} satisfies

$$\|\tilde{g} - \sqrt{\pi}\|_{L_\lambda^2(\mathcal{X})} / \|\sqrt{\pi}\|_{L_\lambda^2(\mathcal{X})} \leq \tau,$$

then the TV distance, Hellinger distance, and χ^2 -divergence of ν_π from $\hat{T}_\# \mu_{\text{uni}}$ respectively satisfy

$$D_{\text{H}}(\nu_\pi \| \hat{T}_\# \mu_{\text{uni}}) \leq \sqrt{2} \tau, \quad D_{\text{TV}}(\nu_\pi \| \hat{T}_\# \mu_{\text{uni}}) < 2\tau,$$

and

$$D_{\chi^2}(\nu_\pi \| \hat{T}_\# \mu_{\text{uni}}) \leq \left(\nu_\pi(\pi^2 / \tilde{g}^4)^{\frac{1}{2}} + (\hat{T}_\# \mu_{\text{uni}})(\pi^2 / \tilde{g}^4)^{\frac{1}{2}} \right) \frac{2\hat{z}}{z} \tau.$$

Remark 6 The bound in (40) is also essential to ensure the uniform ergodicity of the Metropolis independent algorithm and the convergence of importance sampling schemes defined by the SIRT. See Section 5 for further details. One can add a small positive constant $\gamma > 0$ to the FTT factorisation \tilde{g} to ensure the condition in (40). The resulting unnormalised density function $(\tilde{g}^2 + \gamma)\lambda$ is still integrable, since $\int_{\mathcal{X}} \lambda(\mathbf{x}) d\mathbf{x} < \infty$.

4 Deep inverse Rosenblatt transport

In many practical applications, probability densities can be concentrated to a small region of the parameter space or have complicated correlation structures. For example, posterior densities in Bayesian inference problems with informative data often occupy a relatively small region of the parameter space and demonstrate complicated nonlinear interactions in some sub-manifold, see [10, 11, 18, 48] for detailed examples. In this situation, straightforward approximation of a complicated density function in a FTT decomposition may require rather large ranks. As the number of function evaluations needed in constructing FTT decompositions grows quadratically with the ranks, such direct factorisation of the target densities with complicated structures may become infeasible.

Example 1 Consider a d -dimensional multivariate normal distribution with the unnormalised density $\pi(\mathbf{x}) = \exp(-\frac{1}{2}\mathbf{x}^\top \mathbf{C}^{-1}\mathbf{x})$. If the covariance matrix $\mathbf{C} \in \mathbb{R}^{d \times d}$ is diagonal, the joint density factorises into a product of marginal densities, that is a FTT decomposition with ranks 1. This corresponds to zero-rank *off-diagonal* blocks $\mathbf{C}[1:k, (k+1):d]$, $k = 1, \dots, d-1$. However, the FTT ranks of a correlated normal density $\pi(\mathbf{x})$ may grow *exponentially* in the rank of the off-diagonal blocks of \mathbf{C} [52].

Inspired by deep neural networks, we design a DIRT framework to construct a *composition* of monotonic mappings in the SIRT format that can characterise concentrated probability densities with complicated correlation structures. The construction of DIRT is guided by a sequence of bridging probability measures $\nu_0, \nu_1, \dots, \nu_L$, where $\nu_L = \nu_\pi$ is the target measure. Each bridging measure ν_k has the corresponding PDF

$$f_{\mathbf{X}^k}(\mathbf{x}) = \frac{1}{z_k} \pi_k(\mathbf{x}) \lambda(\mathbf{x}), \quad \text{where } z_k = \int_{\mathcal{X}} \pi_k(\mathbf{x}) \lambda(\mathbf{x}) d\mathbf{x}. \quad (43)$$

Here $\pi_0(\mathbf{x})$ is the unnormalised initial density, $\pi_L(\mathbf{x}) = \pi(\mathbf{x})$ is the unnormalised target density, and the superscript k indexes the random variable $\mathbf{X}^k \in \mathcal{X}$, $\mathbf{X}^k \sim \nu_k$. Our goal is to construct a composition of mappings $T_0 \circ T_1 \circ \dots \circ T_k$ such that the pushforward of the reference measure

under this composition matches the k -th bridging measure, i.e., $(T_0 \circ T_1 \circ \dots \circ T_k)_\# \mu = \nu_k$. This way, by gradually increasing the complexity in the geometry and/or the computational cost of the densities of the bridging measures, it becomes computationally feasible to construct FTT and the corresponding SIRT at each layer of the composition.

Assumption 2 Denoting the ratio between two unnormalised densities by

$$r_{k,j}(\mathbf{x}) = \frac{\pi_k(\mathbf{x})}{\pi_j(\mathbf{x})}, \quad (44)$$

we assume that for each pair of $j < k$, the ratio $r_{k,j}(\mathbf{x})$ is finite such that

$$\sup_{\mathbf{x} \in \mathcal{X}} r_{k,j}(\mathbf{x}) = c_{k,j} < \infty, \quad \forall j < k. \quad (45)$$

In practice, there are many ways to choose the bridging measures. For example, one can consider *tempered* distributions [17, 27, 38, 42, 58] where $\pi_k(\mathbf{x}) = \pi(\mathbf{x})^{\beta_k}$ for a suitable chosen set of powers (*reciprocal temperatures*) $0 \leq \beta_0 < \dots < \beta_L = 1$; and for problems involving computationally expensive PDE models, one can employ a hierarchy of models with different grid resolutions to reduce the computational cost for building the DIRT. In the rest of this section, we will present the recursive construction of DIRT and provide error analysis.

4.1 Recursive construction

In the initial step ($k = 0$), we compute a FTT $\tilde{g}_0(\mathbf{x})$ that approximates $\sqrt{\pi_0}$ and construct the corresponding SIRT $\hat{\mathbf{X}}^0 = \hat{T}_0(\mathbf{U})$ so that the reference random variable $\mathbf{U} \sim \mu_{\text{uni}}$ and $\hat{\mathbf{X}}^0 \sim (\hat{T}_0)_\# \mu_{\text{uni}}$ with the PDF

$$\hat{f}_{\hat{\mathbf{X}}^0}(\mathbf{x}) = \frac{1}{\hat{z}_0} \tilde{g}_0^2(\mathbf{x}) \lambda(\mathbf{x}), \quad \text{where} \quad \hat{z}_0 = \int_{\mathcal{X}} \tilde{g}_0^2(\mathbf{x}) \lambda(\mathbf{x}) d\mathbf{x}. \quad (46)$$

Note that $\hat{f}_{\hat{\mathbf{X}}^0}(\mathbf{x})$ is an approximation to $f_{\mathbf{X}^0}(\mathbf{x})$.

Remark 7 We can replace the uniform reference measure μ_{uni} with a general product-form probability measure μ that has the PDF $f_{\mathbf{U}}(\mathbf{u}) = \prod_{k=1}^d f_{\mathbf{U}_k}(\mathbf{u}_k)$ with support in $\mathcal{U} = \mathcal{U}_1 \times \mathcal{U}_2 \times \dots \times \mathcal{U}_d$. One can construct a mapping

$$R(\mathbf{u}) = \left[F_{\mathbf{U}_1}(\mathbf{u}_1), \dots, F_{\mathbf{U}_k}(\mathbf{u}_k), \dots, F_{\mathbf{U}_d}(\mathbf{u}_d) \right]^\top,$$

where $F_{\mathbf{U}_k}(\mathbf{u}_k)$ is the CDF of \mathbf{U}_k , such that $R_\# \mu = \mu_{\text{uni}}$. Then, the composition of mappings $\hat{T}_0 \circ R : \mathcal{U} \mapsto \mathcal{X}$ is lower-triangular and $(\hat{T}_0 \circ R)_\# \mu$ has the density $\hat{f}_{\hat{\mathbf{X}}^0}(\mathbf{x})$. We initialise the DIRT by $\bar{T}_0 = \hat{T}_0 \circ R$, where $R = I$ if $\mu = \mu_{\text{uni}}$.

After $k > 1$ steps, suppose we have the k -th DIRT given as the composition of mappings

$$\bar{T}_k = (\hat{T}_0 \circ R) \circ (\hat{T}_1 \circ R) \circ \dots \circ (\hat{T}_k \circ R),$$

where each \hat{T}_j is a SIRT. Denoting the pushforward of the reference probability measure μ under \bar{T}_k by $\hat{\nu}_k$, i.e., $\hat{\nu}_k \equiv (\bar{T}_k)_\# \mu$, and the density function of $\hat{\nu}_k$ by $\hat{f}_{\hat{\mathbf{X}}^k}(\mathbf{x})$, the pullback density of $\hat{\nu}_k$ under \bar{T}_k satisfies

$$\bar{T}_k^\# \hat{f}_{\hat{\mathbf{X}}^k}(\mathbf{u}) = (\hat{f}_{\hat{\mathbf{X}}^k} \circ \bar{T}_k)(\mathbf{u}) |\nabla_{\mathbf{u}} \bar{T}_k(\mathbf{u})| = f_{\mathbf{U}}(\mathbf{u}). \quad (47)$$

The density function of the pullback probability measure $\bar{T}_k^\# \nu_k$ is the reference product density $f_U(\mathbf{u})$. Suppose the corresponding approximate PDF $\hat{f}_{\hat{\mathbf{X}}^k}(\mathbf{x})$ can capture the range of variation and the correlation structure of the next PDF $f_{\mathbf{X}^{k+1}}(\mathbf{x})$, then the density function of the pullback probability measure $\bar{T}_k^\# \nu_{k+1}$,

$$\bar{T}_k^\# f_{\mathbf{X}^{k+1}}(\mathbf{u}) = (f_{\mathbf{X}^{k+1}} \circ \bar{T}_k)(\mathbf{u}) |\nabla_{\mathbf{u}} \bar{T}_k(\mathbf{u})|, \quad (48)$$

may become easier to factorise in the FTT format compared to the direct factorisation of the original target density function $f_{\mathbf{X}^{k+1}}(\mathbf{x})$. This way, for step $k+1$, the existing composition \bar{T}_k can be used to precondition the construction of the coupling between μ and ν_{k+1} : by building a coupling between the pullback measure $\bar{T}_k^\# \nu_{k+1}$ and the reference measure

$$\mathbf{U}^{k+1} = (T_{k+1} \circ R)(\mathbf{U}), \quad \text{where } \mathbf{U} \sim \mu \quad \text{and} \quad \mathbf{U}^{k+1} \sim \bar{T}_k^\# \nu_{k+1},$$

one can obtain a new composition of maps $(\bar{T}_k \circ T_{k+1} \circ R)$ such that

$$(\bar{T}_k \circ T_{k+1} \circ R)^\# \nu_{k+1} = \mu \quad \text{or} \quad (\bar{T}_k \circ T_{k+1} \circ R)_\# \mu = \nu_{k+1}.$$

We use SIRT to approximate T_{k+1} . Using (47), we have $|\nabla_{\mathbf{u}} \bar{T}_k(\mathbf{u})| = ((\hat{f}_{\hat{\mathbf{X}}^k} \circ \bar{T}_k)(\mathbf{u}))^{-1} f_U(\mathbf{u})$. Thus, the pullback density in (48) can be expressed as a *ratio function*

$$(\bar{T}_k)^\# f_{\mathbf{X}^{k+1}}(\mathbf{u}) = \frac{(f_{\mathbf{X}^{k+1}} \circ \bar{T}_k)(\mathbf{u})}{(\hat{f}_{\hat{\mathbf{X}}^k} \circ \bar{T}_k)(\mathbf{u})} f_U(\mathbf{u}). \quad (49)$$

This way, we can compute a FTT $\tilde{g}_{k+1}(\mathbf{u})$ to approximate the function

$$q_{k+1}(\mathbf{u}) \propto \left(\frac{(f_{\mathbf{X}^{k+1}} \circ \bar{T}_k)(\mathbf{u})}{(\hat{f}_{\hat{\mathbf{X}}^k} \circ \bar{T}_k)(\mathbf{u})} \frac{f_U(\mathbf{u})}{\omega(\mathbf{u})} \right)^{\frac{1}{2}}, \quad (50)$$

where $\omega(\mathbf{u})$ is the weighting function associated with the reference domain \mathcal{U} and $a \propto b$ denotes that a is proportional to b . Since z_k , the normalising constant of $f_{\mathbf{X}^{k+1}}$, is unknown, here we only need to decompose an unnormalised version of $q_{k+1}(\mathbf{u})$ into a FTT. The normalising constant is computed automatically during the marginalisation process of SIRT (cf. Proposition 2).

The SIRT $\mathbf{U}^{k+1} = \hat{T}_{k+1}(\mathbf{U}')$ built on the FTT $\tilde{g}_{k+1}(\mathbf{u})$ couples the uniform reference random variable $\mathbf{U}' \sim \mu_{\text{uni}}$ with $\mathbf{U}^{k+1} \sim (\hat{T}_{k+1})_\# \mu_{\text{uni}}$. Thus, the composition of transformations $\mathbf{U}^{k+1} = (\hat{T}_{k+1} \circ R)(\mathbf{U})$ couples the general reference random variable $\mathbf{U} \sim \mu$ with $\mathbf{U}^{k+1} \sim (\hat{T}_{k+1} \circ R)_\# \mu$, where $(\hat{T}_{k+1} \circ R)_\# \mu$ is an approximation to the pullback measure $\bar{T}_k^\# \nu_{k+1}$. Thus we have

$$(\hat{T}_{k+1} \circ R)^\# (\bar{T}_k^\# \nu_{k+1}) = (\bar{T}_k \circ \hat{T}_{k+1} \circ R)_\# \nu_{k+1} \approx \mu \quad \text{or} \quad (\bar{T}_k \circ \hat{T}_{k+1} \circ R)_\# \mu \approx \nu_{k+1}.$$

The next DIRT is therefore defined by the new composition of mappings

$$\bar{T}_{k+1} := \bar{T}_k \circ (\hat{T}_{k+1} \circ R).$$

The recursion is completed by obtaining \hat{T}_L and \bar{T}_L .

Proposition 6 *At the j -th DIRT step, the Jacobian of the incremental mapping \hat{T}_j is given by*

$$|\nabla_{\mathbf{u}} \hat{T}_j^{-1}(\mathbf{u})| = \hat{p}_{U^j}(\mathbf{u}) = \frac{1}{\hat{z}_j} \tilde{g}_j^2(\mathbf{u}) \omega(\mathbf{u}), \quad \text{where } \hat{z}_j = \int_{\mathcal{U}} \tilde{g}_j^2(\mathbf{u}) \omega(\mathbf{u}) d\mathbf{u} \quad (51)$$

is the normalising constant of the probability density function over the reference domain \mathcal{U} .

Proof The SIRT $\mathbf{U}^j = \hat{T}_j(\mathbf{U}')$, which is constructed by integrating $\tilde{g}_j^2(\mathbf{u})\omega(\mathbf{u})$, maps the uniform random variable $\mathbf{U}' \sim \mu_{\text{uni}}$ to $\mathbf{U}^j \sim (\hat{T}_j)_\# \mu_{\text{uni}}$. Thus, the pushforward measure $(\hat{T}_j)_\# \mu_{\text{uni}}$ has the density function $\hat{p}_{\mathbf{U}^j}(\mathbf{u})$ defined in (51), which yields

$$\hat{p}_{\mathbf{U}^j}(\mathbf{u}) \equiv (\hat{T}_j)_\# f_{\text{uni}}(\mathbf{u}) = |\nabla_{\mathbf{u}} \hat{T}_j^{-1}(\mathbf{u})|.$$

Lemma 1 *At step k of the DIRT construction, suppose we have an initial FTT factorisation $\tilde{g}_0(\mathbf{x}) \approx \sqrt{\pi_0}(\mathbf{x})$ and a sequence of FTT factorisations $\tilde{g}_j(\mathbf{u}) \approx q_j(\mathbf{u})$ for $j = 1, \dots, k$, where q_j is defined in (50), and the DIRTs*

$$\bar{T}_j = (\hat{T}_0 \circ R) \circ (\hat{T}_1 \circ R) \circ \dots \circ (\hat{T}_j \circ R), \quad \text{for } j \leq k.$$

For $j = 1, \dots, k$, suppose further we have normalised density functions over the reference domain \mathcal{U} defined in (51). Then, the pushforward measure $(\bar{T}_k)_\# \mu$ has the PDF

$$\hat{f}_{\hat{\mathbf{X}}^k}(\mathbf{x}) \equiv (\bar{T}_k)_\# f_{\mathcal{U}}(\mathbf{x}) = \hat{f}_{\hat{\mathbf{X}}^0}(\mathbf{x}) \prod_{j=1}^k \frac{(\hat{p}_{\mathbf{U}^j} \circ \bar{T}_{j-1}^{-1})(\mathbf{x})}{(f_{\mathcal{U}} \circ \bar{T}_{j-1}^{-1})(\mathbf{x})}. \quad (52)$$

Proof The result can be shown using induction. For the case $k = 0$, the result follows directly from (46). Suppose (52) holds for $k > 0$. We define the composition of mappings

$$\tilde{T}_k = \bar{T}_k \circ R^{-1} = \hat{T}_0 \circ (R \circ \hat{T}_1) \circ \dots \circ (R \circ \hat{T}_k).$$

Since $R_\# \mu = \mu_{\text{uni}}$, we have the identity $(\bar{T}_k)_\# \mu = (\tilde{T}_k)_\# \mu_{\text{uni}}$, which leads to

$$\hat{f}_{\hat{\mathbf{X}}^k}(\mathbf{x}) = (\bar{T}_k)_\# f_{\mathcal{U}}(\mathbf{x}) = (\tilde{T}_k)_\# f_{\text{uni}}(\mathbf{x}).$$

At step $k + 1$, we have the new composition of mappings $\tilde{T}_{k+1} = \tilde{T}_k \circ R \circ \hat{T}_{k+1}$, the pushforward measures, $(\tilde{T}_{k+1})_\# \mu$ and $(\tilde{T}_k)_\# \mu$, have the density functions

$$\begin{aligned} \hat{f}_{\hat{\mathbf{X}}^{k+1}}(\mathbf{x}) &= (\tilde{T}_{k+1})_\# f_{\text{uni}}(\mathbf{x}) = (f_{\text{uni}} \circ \tilde{T}_{k+1}^{-1})(\mathbf{x}) |\nabla_{\mathbf{x}} \tilde{T}_{k+1}^{-1}(\mathbf{x})| = |\nabla_{\mathbf{x}} \tilde{T}_{k+1}^{-1}(\mathbf{x})|, \\ \hat{f}_{\hat{\mathbf{X}}^k}(\mathbf{x}) &= (\tilde{T}_k)_\# f_{\text{uni}}(\mathbf{x}) = (f_{\text{uni}} \circ \tilde{T}_k^{-1})(\mathbf{x}) |\nabla_{\mathbf{x}} \tilde{T}_k^{-1}(\mathbf{x})| = |\nabla_{\mathbf{x}} \tilde{T}_k^{-1}(\mathbf{x})|, \end{aligned}$$

respectively. Applying the change of variables $\mathbf{u}' = \tilde{T}_k^{-1}(\mathbf{x})$ and $\mathbf{u} = R^{-1}(\mathbf{u}')$, the determinant of $\nabla_{\mathbf{x}} \tilde{T}_{k+1}^{-1}(\mathbf{x})$ can be expressed as

$$|\nabla_{\mathbf{x}} \tilde{T}_{k+1}^{-1}(\mathbf{x})| = |\nabla_{\mathbf{u}} \hat{T}_{k+1}^{-1}(\mathbf{u})| |\nabla_{\mathbf{u}'} R^{-1}(\mathbf{u}')| |\nabla_{\mathbf{x}} \tilde{T}_k^{-1}(\mathbf{x})|. \quad (53)$$

Note that the above change of variables implies also that $|\nabla_{\mathbf{u}'} R^{-1}(\mathbf{u}')| = f_{\mathcal{U}}(\mathbf{u})^{-1}$ and $\mathbf{u} = (\tilde{T}_k \circ R)^{-1}(\mathbf{x}) = \tilde{T}_k^{-1}(\mathbf{x})$. Together with Proposition 6, we have

$$|\nabla_{\mathbf{x}} \tilde{T}_{k+1}^{-1}(\mathbf{x})| = \frac{(\hat{p}_{\mathbf{U}^{k+1}} \circ \bar{T}_k^{-1})(\mathbf{x})}{(f_{\mathcal{U}} \circ \bar{T}_k^{-1})(\mathbf{x})} |\nabla_{\mathbf{x}} \tilde{T}_k^{-1}(\mathbf{x})|.$$

Thus, the result follows.

Corollary 3 *At step k of the DIRT construction, the composition of mappings, \bar{T}_k , satisfies*

$$|\nabla_{\mathbf{x}} \bar{T}_k^{-1}(\mathbf{x})| = \frac{\hat{f}_{\hat{\mathbf{X}}^k}(\mathbf{x})}{(f_{\mathcal{U}} \circ \bar{T}_k^{-1})(\mathbf{x})}.$$

Proof The result direct follows from $\bar{T}_k^{-1} = R^{-1} \circ \tilde{T}_k^{-1}$ and the proof of Lemma 1.

Remark 8 The normalised PDFs of the k -th DIRT step can be expressed as

$$\hat{f}_{\mathbf{X}^k}(\mathbf{x}) = \left(\prod_{j=0}^k \frac{1}{\hat{z}_j} \right) \tilde{g}_0^2(\mathbf{x}) \lambda(\mathbf{x}) \prod_{j=1}^k \left((\tilde{g}_j \circ \bar{T}_{j-1}^{-1})^2(\mathbf{x}) \frac{(\omega \circ \bar{T}_{j-1}^{-1})(\mathbf{x})}{(f_{\mathbf{U}} \circ \bar{T}_{j-1}^{-1})(\mathbf{x})} \right). \quad (54)$$

Thus, we define the constant $\bar{z}_k = \prod_{j=0}^k \hat{z}_j$ and the square root of the unnormalised PDF

$$\bar{g}_k(\mathbf{x}) = \tilde{g}_0(\mathbf{x}) \prod_{j=1}^k \left((\tilde{g}_j \circ \bar{T}_{j-1}^{-1})(\mathbf{x}) \frac{(\omega \circ \bar{T}_{j-1}^{-1})^{\frac{1}{2}}(\mathbf{x})}{(f_{\mathbf{U}} \circ \bar{T}_{j-1}^{-1})^{\frac{1}{2}}(\mathbf{x})} \right). \quad (55)$$

Here $\bar{g}_k^2(\mathbf{x})$ is an approximation to the unnormalised bridging density $\pi_k(\mathbf{x})$ and \bar{z}_k is an approximation to the normalising constant z_k .

4.2 Ratio functions and error analysis

We will first discuss the ratio function (50) and its approximation and then present the corresponding error analysis.

4.2.1 Ratio functions

Given the square root of the unnormalised PDF in (55), the pullback density in (49) can be expressed as

$$(\bar{T}_k)^\# f_{\mathbf{X}^{k+1}}(\mathbf{u}) = \frac{(f_{\mathbf{X}^{k+1}} \circ \bar{T}_k)(\mathbf{u})}{(\hat{f}_{\mathbf{X}^k} \circ \bar{T}_k)(\mathbf{u})} f_{\mathbf{U}}(\mathbf{u}) \propto \frac{(\pi_{k+1} \circ \bar{T}_k)(\mathbf{u})}{(\bar{g}_k \circ \bar{T}_k)(\mathbf{u})^2} f_{\mathbf{U}}(\mathbf{u}).$$

This way, we need to compute a FTT $\tilde{g}_{k+1}(\mathbf{u})$ to approximate the function

$$q_{k+1}(\mathbf{u}) = \frac{(\pi_{k+1} \circ \bar{T}_k)^{\frac{1}{2}}(\mathbf{u}) f_{\mathbf{U}}^{\frac{1}{2}}(\mathbf{u})}{(\bar{g}_k \circ \bar{T}_k)(\mathbf{u}) \omega^{\frac{1}{2}}(\mathbf{u})}, \quad (56)$$

to build the SIRT \hat{T}_{k+1} . We call this strategy the *exact ratio approach*.

Alternatively, the pullback density in (49) can be expressed as

$$(\bar{T}_k)^\# f_{\mathbf{X}^{k+1}}(\mathbf{u}) \propto \frac{(\pi_{k+1} \circ \bar{T}_k)(\mathbf{u})}{(\pi_k \circ \bar{T}_k)(\mathbf{u})} \frac{(\pi_k \circ \bar{T}_k)(\mathbf{u})}{(\bar{g}_k \circ \bar{T}_k)^2(\mathbf{u})} f_{\mathbf{U}}(\mathbf{u}) \quad (57)$$

Since the DIRT density function \bar{g}_k^2 approximates the k -th unnormalised bridging density function π_k , the pullback density in (57) can be approximated as

$$(\bar{T}_k)^\# f_{\mathbf{X}^{k+1}}(\mathbf{u}) \propto (r_{k+1,k} \circ \bar{T}_k)(\mathbf{u}) \frac{(\pi_k \circ \bar{T}_k)(\mathbf{u})}{(\bar{g}_k \circ \bar{T}_k)^2(\mathbf{u})} f_{\mathbf{U}}(\mathbf{u}) \approx (r_{k+1,k} \circ \bar{T}_k)(\mathbf{u}) f_{\mathbf{U}}(\mathbf{u}).$$

This way, we need to compute a FTT $\tilde{q}_{k+1}(\mathbf{u})$ that approximates the function

$$\tilde{q}_{k+1}(\mathbf{u}) = \left(\frac{(r_{k+1,k} \circ \bar{T}_k)(\mathbf{u}) f_{\mathbf{U}}(\mathbf{u})}{\omega(\mathbf{u})} \right)^{\frac{1}{2}}, \quad (58)$$

to build an alternative SIRT \hat{T}_{k+1} . We call this strategy the *approximate ratio approach*.

Remark 9 For all $k \geq 0$, we want the ratio π_k/\bar{g}_k^2 to be finite in \mathcal{U} . Otherwise, it may cause large errors in the FTT decomposition and may deteriorate the convergence of the resulting sampling schemes for characterising ν_π . Given Assumption 2, it can be shown (using induction) that the ratio π_k/\bar{g}_k^2 is bounded if the conditions

$$\sup_{\mathbf{x} \in \mathcal{X}} \frac{\pi_0(\mathbf{x})}{\bar{g}_0^2(\mathbf{x})} < \infty, \quad \text{and} \quad \sup_{\mathbf{u} \in \mathcal{U}} \frac{(r_{k,k-1} \circ \bar{T}_{k-1})(\mathbf{u}) f_{\mathcal{U}}(\mathbf{u})}{\bar{g}_k^2(\mathbf{u}) \omega(\mathbf{u})} < \infty, \quad (59)$$

are satisfied. As discussed in Remark 6, one can add a small positive constant $\gamma > 0$ to \bar{g}_0 to satisfy the first condition in (59). If the ratio $f_{\mathcal{U}}(\mathbf{u})/\omega(\mathbf{u})$ is bounded for $\forall \mathbf{u} \in \mathcal{U}$, then one can also add γ to \bar{g}_k to satisfy the second condition in (59) without affecting the integrability of $\bar{g}_k^2 \omega$.

Remark 10 In some situations, the ratio function $(r_{k+1,k} \circ \bar{T}_k)(\mathbf{u})$ may exhibit sharp boundary layers if the uniform reference measure μ_{uni} (with $R = I$) is used. This can increase the complexity of the resulting FTT factorisations. Apart from carefully choosing the bridging measures, a partial remedy to the boundary layer is to use a reference measure with the density $f_{\mathcal{U}}(\mathbf{u})$ decaying towards the boundary, such as the normal density truncated on a sufficiently large hypercube $[-\sigma, \sigma]^d$. The function $f_{\mathcal{U}}(\mathbf{u})$ in (56) and (58) smoothens the previous approximation errors, which can improve the accuracy of FTT approximations. With a reference measure defined on a hypercube, the collocation techniques based on Chebyshev and Fourier bases (cf. Section 3.2) can be applied to construct and evaluate FTT decompositions in DIRT.

4.2.2 DIRT error

Based on assumptions about the FTT error at each layer of the DIRT construction, here we establish error bounds of DIRT in terms of the TV distance, the Hellinger distance, and the χ^2 -divergence of the k -th bridging measure ν_k from the pushforward measure $(\bar{T}_k)_\# \mu$.

Theorem 3 (Exact ratio approach) *Suppose that at the k -th DIRT step the FTT decomposition $\bar{g}_k \approx q_k$ satisfies $\|\bar{g}_k - q_k\|_{L_\omega^2(\mathcal{U})} \leq \epsilon_k$, where q_k is defined in (56). Then the square root of the unnormalised PDF \bar{g}_k defined in (55) approximates the square root of the unnormalised density function of the k -th bridging measure π_k with the error*

$$\|\sqrt{\pi_k} - \bar{g}_k\|_{L_\lambda^2(\mathcal{X})} \leq \sqrt{\bar{z}_{k-1}} \epsilon_k,$$

where $\bar{z}_{k-1} = \prod_{j=0}^{k-1} \hat{z}_j$ is the normalising constant of the unnormalised PDF \bar{g}_{k-1}^2 .

Proof Let $I = \|\sqrt{\pi_k} - \bar{g}_k\|_{L_\lambda^2(\mathcal{X})}$, we have

$$\begin{aligned} I^2 &= \left\| \left(\frac{\sqrt{\pi_k}}{\bar{g}_{k-1}} - \frac{\bar{g}_k}{\bar{g}_{k-1}} \right) \bar{g}_{k-1} \right\|_{L_\lambda^2(\mathcal{X})}^2 \\ &= \int_{\mathcal{X}} \left(\frac{\pi_k^{\frac{1}{2}}(\mathbf{x})}{\bar{g}_{k-1}(\mathbf{x})} - (\bar{g}_k \circ \bar{T}_{k-1}^{-1})(\mathbf{x}) \frac{(\omega \circ \bar{T}_{k-1}^{-1})^{\frac{1}{2}}(\mathbf{x})}{(f_{\mathcal{U}} \circ \bar{T}_{k-1}^{-1})^{\frac{1}{2}}(\mathbf{x})} \right)^2 \bar{g}_{k-1}^2(\mathbf{x}) \lambda(\mathbf{x}) d\mathbf{x} \\ &= \int_{\mathcal{X}} \left(\frac{\pi_k^{\frac{1}{2}}(\mathbf{x}) (f_{\mathcal{U}} \circ \bar{T}_{k-1}^{-1})^{\frac{1}{2}}(\mathbf{x})}{\bar{g}_{k-1}(\mathbf{x})} - (\bar{g}_k \circ \bar{T}_{k-1}^{-1})(\mathbf{x}) (\omega \circ \bar{T}_{k-1}^{-1})^{\frac{1}{2}}(\mathbf{x}) \right)^2 \frac{\bar{z}_{k-1} \hat{f}_{\mathbf{X}^{k-1}}(\mathbf{x})}{(f_{\mathcal{U}} \circ \bar{T}_{k-1}^{-1})(\mathbf{x})} d\mathbf{x} \end{aligned}$$

Applying the change of variables $\mathbf{u} = \bar{T}_{k-1}^{-1}(\mathbf{x})$ and Corollary 3, I can be rewritten as

$$\begin{aligned} I &= \sqrt{\bar{z}_{k-1}} \left(\int_{\mathcal{U}} \left(\frac{(\pi_k \circ \bar{T}_{k-1})^{\frac{1}{2}}(\mathbf{u})}{(\bar{g}_{k-1} \circ \bar{T}_{k-1})(\mathbf{u})} \frac{f_{\mathcal{U}}^{\frac{1}{2}}(\mathbf{u})}{\omega^{\frac{1}{2}}(\mathbf{u})} - \tilde{g}_k(\mathbf{u}) \right)^2 \omega(\mathbf{u}) d\mathbf{u} \right)^{\frac{1}{2}} \\ &= \sqrt{\bar{z}_{k-1}} \|q_k - \tilde{g}_k\|_{L_{\omega}^2(\mathcal{U})} \\ &\leq \sqrt{\bar{z}_{k-1}} \epsilon_k. \end{aligned}$$

Theorem 4 (Approximate ratio approach) *Suppose that at the k -th DIRT step the FTT decompositions $\tilde{g}_0(\mathbf{u}) \approx \sqrt{\pi_0}$ and $\tilde{g}_j \approx \tilde{q}_j$ for $j = 1, \dots, k$ satisfy*

$$\|\tilde{g}_0 - \sqrt{\pi_0}\|_{L_{\lambda}^2(\mathcal{X})} \leq \epsilon_0, \quad \text{and} \quad \|\tilde{g}_j - \tilde{q}_j\|_{L_{\omega}^2(\mathcal{U})} \leq \epsilon_j, \quad \text{for } j = 1, \dots, k, \quad (60)$$

where \tilde{q}_j is defined in (58). Then the unnormalised PDF of DIRT defined by (55) approximates the k -th unnormalised bridging density function with the error

$$\|\sqrt{\pi_k} - \bar{g}_k\|_{L_{\lambda}^2(\mathcal{X})} \leq \bar{\epsilon}_k, \quad \text{where} \quad \bar{\epsilon}_k = \sqrt{c_{k,0}} \epsilon_0 + \sum_{j=1}^k \sqrt{c_{k,j} \bar{z}_{j-1}} \epsilon_j,$$

where $c_{k,j} = \sup_{\mathbf{x} \in \mathcal{X}} r_{k,j}(\mathbf{x})$ is given in Assumption 2, and $\bar{z}_k = \prod_{j=0}^k \hat{z}_j$.

Proof The difference between $\sqrt{\pi_k}$ and \bar{g}_k can be written as

$$\begin{aligned} \sqrt{\pi_k} - \bar{g}_k &= \left(\sqrt{\frac{\pi_k}{\pi_0}} \pi_0 - \sqrt{\frac{\pi_k}{\pi_0}} \bar{g}_0 \right) + \sum_{j=1}^k \left(\sqrt{\frac{\pi_k}{\pi_j} \frac{\pi_j}{\pi_{j-1}}} \bar{g}_{j-1} - \sqrt{\frac{\pi_k}{\pi_j} \frac{\bar{g}_j}{\bar{g}_{j-1}}} \bar{g}_{j-1} \right) \\ &= \sqrt{r_{k,0}} (\sqrt{\pi_0} - \bar{g}_0) + \sum_{j=1}^k \sqrt{r_{k,j}} \left(\sqrt{r_{j,j-1}} - (\tilde{g}_j \circ \bar{T}_{j-1}^{-1}) \sqrt{\frac{\omega \circ \bar{T}_{j-1}^{-1}}{f_{\mathcal{U}} \circ \bar{T}_{j-1}^{-1}}} \right) \bar{g}_{j-1}, \end{aligned}$$

Then, we have $\|\sqrt{\pi_k} - \bar{g}_k\|_{L_{\lambda}^2(\mathcal{X})} \leq I_0 + \sum_{j=1}^k I_j$, where

$$\begin{aligned} I_0 &= \|\sqrt{r_{k,0}} (\sqrt{\pi_0} - \bar{g}_0)\|_{L_{\lambda}^2(\mathcal{X})} \\ I_j &= \left(\int_{\mathcal{X}} r_{k,j}(\mathbf{x}) \left(r_{j,j-1}^{\frac{1}{2}}(\mathbf{x}) - (\tilde{g}_j \circ \bar{T}_{j-1}^{-1})(\mathbf{x}) \frac{(\omega \circ \bar{T}_{j-1}^{-1})^{\frac{1}{2}}(\mathbf{x})}{(f_{\mathcal{U}} \circ \bar{T}_{j-1}^{-1})^{\frac{1}{2}}(\mathbf{x})} \right)^2 \bar{g}_{j-1}^2(\mathbf{x}) \lambda(\mathbf{x}) d\mathbf{x} \right)^{\frac{1}{2}} \end{aligned}$$

Recalling that $c_{k,j} = \sup_{\mathbf{x} \in \mathcal{X}} r_{k,j}(\mathbf{x})$, we have

$$I_0 \leq \sqrt{c_{k,0}} \|\sqrt{\pi_0} - \bar{g}_0\|_{L_{\lambda}^2(\mathcal{X})} \leq \sqrt{c_{k,0}} \epsilon_0.$$

Applying the change of variables $\mathbf{u} = \bar{T}_{j-1}^{-1}(\mathbf{x})$ and Corollary 3 for each $j > 0$, we obtain

$$\begin{aligned} I_j &\leq \sqrt{c_{k,j}} \left(\int_{\mathcal{X}} \left(r_{j,j-1}^{\frac{1}{2}}(\mathbf{x}) (f_{\mathcal{U}} \circ \bar{T}_{j-1}^{-1})^{\frac{1}{2}}(\mathbf{x}) - (\tilde{g}_j \circ \bar{T}_{j-1}^{-1})(\mathbf{x}) (\omega \circ \bar{T}_{j-1}^{-1})^{\frac{1}{2}}(\mathbf{x}) \right)^2 \frac{\bar{z}_{j-1} \hat{f}_{\mathbf{X}^{j-1}}(\mathbf{x})}{(f_{\mathcal{U}} \circ \bar{T}_{j-1}^{-1})(\mathbf{x})} d\mathbf{x} \right)^{\frac{1}{2}} \\ &= \sqrt{c_{k,j} \bar{z}_{j-1}} \left(\int_{\mathcal{U}} \left(\left(\frac{(r_{j,j-1} \circ \bar{T}_{j-1})(\mathbf{u})}{\omega(\mathbf{u})} \right)^{\frac{1}{2}} - \tilde{g}_j(\mathbf{u}) \right)^2 \omega(\mathbf{u}) d\mathbf{u} \right)^{\frac{1}{2}} \\ &= \sqrt{c_{k,j} \bar{z}_{j-1}} \|\tilde{q}_j - \tilde{g}_j\|_{L_{\omega}^2(\mathcal{U})} \\ &\leq \sqrt{c_{k,j} \bar{z}_{j-1}} \epsilon_j, \end{aligned}$$

Thus, the result follows.

Remark 11 On the first glance it appears that Theorem 3 gives smaller errors than Theorem 4. However, this assumes that the two ratio functions in (56) and (58) are approximated with the same FTT error ϵ_k . Ideally this should also require the same number of degrees of freedom in TT cores. In practice this may not be the case: the exact ratio (57) carries the previous approximation errors in the term $((\bar{g}_k \circ \bar{T}_k)(\mathbf{u}))^{-1} (\pi_k \circ \bar{T}_k)^{\frac{1}{2}}(\mathbf{u})$, which can have a complicated structure that is difficult to approximate in FTT. In contrast, the approximate ratio involves only the target densities. For example, if the bridging densities π_k were introduced by tempering, the ratio $r_{k+1,k} = \pi^{\beta_{k+1}-\beta_k}$ is just another tempered density. For this reason, DIRT built using the approximate ratio approach may be more accurate in practice.

Corollary 4 *Given π_k and \bar{g}_k constructed using either the exact or the approximate ratio functions, we suppose the error of \bar{g}_k satisfies $\|\sqrt{\pi_k} - \bar{g}_k\|_{L^2_\lambda(\mathcal{X})} \leq e_k$. Then, the Hellinger distance between the k -th bridging measure ν_k and the pushforward measure $(\bar{T}_k)_\# \mu$ satisfies*

$$D_H(\nu_k \| (\bar{T}_k)_\# \mu) \leq \sqrt{\frac{2}{z_k}} e_k. \quad (61)$$

The total variation distance between ν_k and $(\bar{T}_k)_\# \mu$ satisfies

$$D_{\text{TV}}(\nu_k \| (\bar{T}_k)_\# \mu) \leq \frac{2 e_k}{\sqrt{z_k}}. \quad (62)$$

The χ^2 -divergence of ν_k from $(\bar{T}_k)_\# \mu$ satisfies

$$D_{\chi^2}(\nu_k \| (\bar{T}_k)_\# \mu) \leq \left(\nu_k(\pi_k^2 / \bar{g}_k^4)^{\frac{1}{2}} + ((\bar{T}_k)_\# \mu)(\pi_k^2 / \bar{g}_k^4)^{\frac{1}{2}} \right) \frac{2 \bar{z}_k}{z_k \sqrt{z_k}} e_k. \quad (63)$$

Proof The results follows directly from Theorem 1, Corollary 1, and Corollary 2. For the bound on the χ^2 -divergence, we also need the condition $\sup_{\mathbf{x} \in \mathcal{X}} \pi_k(\mathbf{x}) / \bar{g}_k^2(\mathbf{x}) < \infty$, which can be satisfied if one employs the treatment in Remark 9.

5 Debiasing

Applying either the SIRT or the DIRT, one can obtain an approximate map $T : \mathcal{U} \mapsto \mathcal{X}$ that enables the simulation of a random variable $\hat{\mathbf{X}} \sim T_\# \mu$ approximating the target random variable $\mathbf{X} \sim \nu_\pi$. In a situation where the SIRT or the DIRT have high accuracy in approximating the target measure, one can approximate the expectation $\nu_\pi(h)$ of a function of interest $h(\mathbf{x})$ directly, using the expectation of $h(\mathbf{x})$ over $T_\# \mu$, i.e., $(T_\# \mu)(h) \equiv \mu(h \circ T)$. The bias of the approximated expectation is proportional to the Hellinger distance $D_H(\nu_\pi \| T_\# \mu)$ (cf. Proposition 5). In addition, we can apply the approximate inverse Rosenblatt transport T within the Metropolis-Hastings method and importance sampling to reduce the bias in computing $\nu_\pi(h)$. For the sake of completeness, here we discuss some debiasing strategies based on existing work.

We first consider the IRT-MCMC (Algorithm 1), in which the approximate IRT is used as a proposal mechanism in the Metropolised independent sampler for constructing a Markov chain of random variables that converges to the target measure. In the acceptance probability (64), $f_{\mathbf{X}}(\cdot)$ is the PDF of the target measure ν_π and $\hat{f}_{\hat{\mathbf{X}}}(\cdot)$ is the PDF of $T_\# \mu$ that is defined by either the SIRT (19) or the DIRT (54). Following the result of Mengersen and Tweedie [39], the bounds in Remarks 6 and 9 can guarantee the uniform ergodicity of the Markov chain constructed by Algorithm 1. In addition, the average rejection probability is bounded by $2 D_{\text{TV}}(\nu_\pi \| T_\# \mu)$, see Lemma 1 of [14]. This provides an indicator on the performance of the Metropolised independent

Algorithm 1 IRT-MCMC

-
- 1: Choose an initial state $\mathbf{X}^{(0)} = \mathbf{x}^*$ for the Markov chain.
 - 2: **for** $j = 1, 2, \dots, N$ **do**
 - 3: Draw $\mathbf{U} \sim \mu$ and compute the proposal candidate $\hat{\mathbf{X}} = T(\mathbf{U})$.
 - 4: Given the previous state of the Markov chain $\mathbf{x} = \mathbf{X}^{(j-1)}$, with probability

$$\alpha(\mathbf{x}, \hat{\mathbf{X}}) = \min \left[1, \frac{f_{\mathbf{X}}(\hat{\mathbf{X}}) \hat{f}_{\hat{\mathbf{X}}}(\mathbf{x})}{f_{\mathbf{X}}(\mathbf{x}) \hat{f}_{\hat{\mathbf{X}}}(\hat{\mathbf{X}})} \right], \quad (64)$$

- accept $\hat{\mathbf{X}}$ by setting $\mathbf{X}^{(j)} = \hat{\mathbf{X}}$, otherwise set $\mathbf{X}^{(j)} = \mathbf{x}$.
 - 5: Evaluate the function $H_j = h(\mathbf{X}^{(j)})$.
 - 6: **end for**
 - 7: Estimate $\nu_\pi(h)$ by the sample average $\frac{1}{N} \sum_{j=1}^N H_j$.
-

sampler. However, our bound on $D_{\text{TV}}(\nu_\pi \| T_{\sharp} \mu)$ does not directly connect to the bound on the convergence rate of the Metropolised independent sampler, in which the use of acceptance/rejection may require a more precise control on the pointwise error, e.g., $\|\tilde{g} - \sqrt{\pi}\|_{L^\infty(\mathcal{X})}$, to assess the convergence rate of the sampler.

Algorithm 2 IRT-IS

-
- 1: **for** $j = 1, 2, \dots, N$ **do**
 - 2: Draw $\mathbf{U}^{(j)} \sim \mu$ and compute the approximate target random variable $\hat{\mathbf{X}}^{(j)} = T(\mathbf{U}^{(j)})$.
 - 3: Evaluate the unnormalised weight

$$W_j = w(\hat{\mathbf{X}}^{(j)}) := \frac{\pi(\hat{\mathbf{X}}^{(j)}) \lambda(\hat{\mathbf{X}}^{(j)})}{\hat{f}_{\hat{\mathbf{X}}}(\hat{\mathbf{X}}^{(j)})}$$

- and the function $\hat{H}_j = h(\hat{\mathbf{X}}^{(j)})$.
 - 4: **end for**
 - 5: Estimate the normalising constant using $\bar{z}_N = \frac{1}{N} \sum_{j=1}^N W_j$.
 - 6: Compute the sample average $\bar{h}_N = \frac{1}{N} \sum_{j=1}^N W_j \hat{H}_j$.
 - 7: Estimate $\nu_\pi(h)$ by the ratio estimator $I_N = \bar{h}_N / \bar{z}_N$.
-

One can also employ the approximate IRT built by either the SIRT or the DIRT as the biasing distribution in importance sampling, which leads to the IRT-IS algorithm (Algorithm 2). Compared to IRT-MCMC, IRT-IS generates random variables $\hat{\mathbf{X}}^{(j)}$ from the approximate IRT and correct the bias using the weights W_j . By avoiding the Markov chain, importance sampling offers several advantages over the Metropolised independent sampler: (i) it can be easily parallelised; and (ii) variance reduction techniques such as antithetic variable and control variates (see [51, Chapter 4] and references therein) and efficient high-dimensional quadrature methods such as quasi Monte Carlo [13] can be naturally applied within importance sampling.

The error bounds established in Sections 3 and 4 offer insights into the efficiency of IRT-IS. As discussed in [46, Chapter 9], for N approximate target random variables, one can use the effective sample size (ESS)

$$\text{ESS}(N) = N \frac{(T_{\sharp} \mu)(w)^2}{(T_{\sharp} \mu)(w^2)}$$

to measure the efficiency of importance sampling for representing the target measure ν_π .

Lemma 2 *Given the χ^2 -divergence of ν_π from $T_{\sharp} \mu$, the ESS of Algorithm 2 satisfies*

$$\text{ESS}(N) = \frac{N}{1 + D_{\chi^2}(\nu_\pi \| T_{\sharp} \mu)}.$$

Proof Since we have $(T_{\sharp}\mu)(w) = z$, where z is the normalising constant of the target density, the χ^2 -divergence of ν_{π} from $T_{\sharp}\mu$ satisfies

$$D_{\chi^2}(\nu_{\pi} \| T_{\sharp}\mu) = (T_{\sharp}\mu)(w^2) / (T_{\sharp}\mu)(w)^2 - 1,$$

where $w(\mathbf{x}) = \pi(\mathbf{x}) / \tilde{g}^2(\mathbf{x})$ for SIRT and $w(\mathbf{x}) = \pi(\mathbf{x}) / \tilde{g}_L^2(\mathbf{x})$ for DIRT. Thus, the result follows.

The bounds in Remarks 6 and 9 imply that \bar{z}_N and \bar{h}_N computed by Algorithm 2 are unbiased estimators for the normalising constant z and the expectation $(T_{\sharp}\mu)(wh)$, respectively. However the ratio estimator I_N is only asymptotically unbiased such that

$$\mathbb{P} \left[\lim_{N \rightarrow \infty} I_N = \nu_{\pi}(h) \right] = 1.$$

For a finite sample size, $N < \infty$, the ratio estimator I_N is a biased estimator of $\nu_{\pi}(h)$. However, for sufficiently large sample size N , one can apply the Delta method (cf. [46, Chapter 2] and references therein) to show that the mean square error (MSE) of I_N yields the approximation

$$\text{MSE}(I_N) \equiv \mathbb{E}[(I_N - \nu_{\pi}(h))^2] \approx \frac{1}{N} \frac{(T_{\sharp}\mu)(w^2(h - \nu_{\pi}(h))^2)}{(T_{\sharp}\mu)(w)^2}. \quad (65)$$

Thus, for a sufficiently regular function h , the MSE of the ratio estimator I_N can also be controlled by the χ^2 -divergence $D_{\chi^2}(\nu_{\pi} \| T_{\sharp}\mu)$.

6 Numerical examples

We demonstrate the efficacy and various aspects of DIRT, which employs SIRT within each layer, using four Bayesian inference problems arising in dynamical systems and PDEs. In all numerical examples, as efficiency measures of DIRT (or SIRT in the single layer case), we employ the integrated autocorrelation time (IACT) for IRT-MCMC (Algorithm 1) and the ratio between the total number of samples and the ESS, $N/\text{ESS}(N)$, for IRT-IS (Algorithm 2). For both IACT and $N/\text{ESS}(N)$, a lower value indicates a better sampling efficiency. The minimum value of both IACT and $N/\text{ESS}(N)$ is 1. Since $N/\text{ESS}(N) = 1 + D_{\chi^2}(\nu_k \| T_{\sharp}\mu)$, it also measures directly the accuracy of DIRT for approximating the posteriors.

6.1 Predator and prey

The predator-prey model is a system of coupled ODEs frequently used to describe the dynamics of biological systems. The populations of predator (denoted by Q) and prey (denoted by P) change over time according to a pair of ODEs

$$\begin{cases} \frac{dP}{dt} = rP \left(1 - \frac{P}{K}\right) - s \left(\frac{PQ}{a+P}\right), \\ \frac{dQ}{dt} = u \left(\frac{PQ}{a+P}\right) - vQ, \end{cases} \quad (66)$$

with initial conditions $P(t=0) = P_0$ and $Q(t=0) = Q_0$. The dynamical system is controlled by several parameters. In the absence of the predator, the population of the prey evolves according to the logistic equation characterised by r and K . In the absence of the prey, the population of the predator decreases exponentially with a rate v . In addition, the two populations have a nonlinear interaction characterised by a , s , and u . We often do not know the initial populations and the parameters r , K , a , s , u , and v . This way, we need to estimate unknowns

$$\mathbf{x} = [P_0, Q_0, r, K, a, s, u, v]^{\top},$$

from observed populations of the predator and prey at time instances t_i for $i = 1, \dots, n_T$.

6.1.1 Posterior density

Let $\mathbf{y} \in \mathbb{R}^{2n_T}$ denote the observed populations of the predator and prey. We define a forward model $G: \mathcal{X} \mapsto \mathbb{R}^{2n_T}$ in the form of $G(\mathbf{x}) = [P(t_i), Q(t_i)]_{i=1}^{n_T}$ to represent the populations of the predator and prey computed at $\{t_i\}_{i=1}^{n_T}$ for a given parameters \mathbf{x} . Assuming independent and identically distributed (i.i.d.) normal noise in the observed data and assigning a prior density $\pi_0(\mathbf{x})$ to the unknown parameter, one can define the unnormalized posterior density

$$\pi(\mathbf{x}) \propto \exp\left(-\frac{1}{2\sigma^2}\|G(\mathbf{x}) - \mathbf{y}\|_2^2\right) \pi_0(\mathbf{x}),$$

where σ is the standard deviation of the normally distributed noise. Synthetic observed data are used in this example. With $n_T = 13$ time instances $t_i = (i - 1) \times 25/6$ and a given parameter $\mathbf{x}_{true} = [50, 5, 0.6, 100, 1.2, 25, 0.5, 0.3]^\top$, we generate synthetic noisy data $\mathbf{y} = \mathbf{y}_{true} + \boldsymbol{\eta}$, where $\boldsymbol{\eta}$ is a realization of the i.i.d. zero mean normally distributed noise with the standard deviation $\sigma = \sqrt{2}$. A uniform prior density $\pi_0(\mathbf{x}) = \prod_{k=1}^8 \mathbb{1}_{[\mathbf{a}_k, \mathbf{b}_k]}(\mathbf{x}_k)$ is specified to restrict the support of \mathbf{x}_k to the interval $[\mathbf{a}_k, \mathbf{b}_k]$, where $\mathbf{a} = [30, 3, 0.36, 60, 0.72, 15, 0.3, 0.18]^\top$ and $\mathbf{b} = [80, 8, 0.96, 160, 1.92, 40, 0.8, 0.48]^\top$. To illustrate the behaviour of the posterior density, we plot the kernel density estimates of the marginal posterior densities in Figure 2. Note that some of the parameters are significantly correlated, which makes the posterior density function difficult to explore by both MCMC and a straightforward TT approximation.

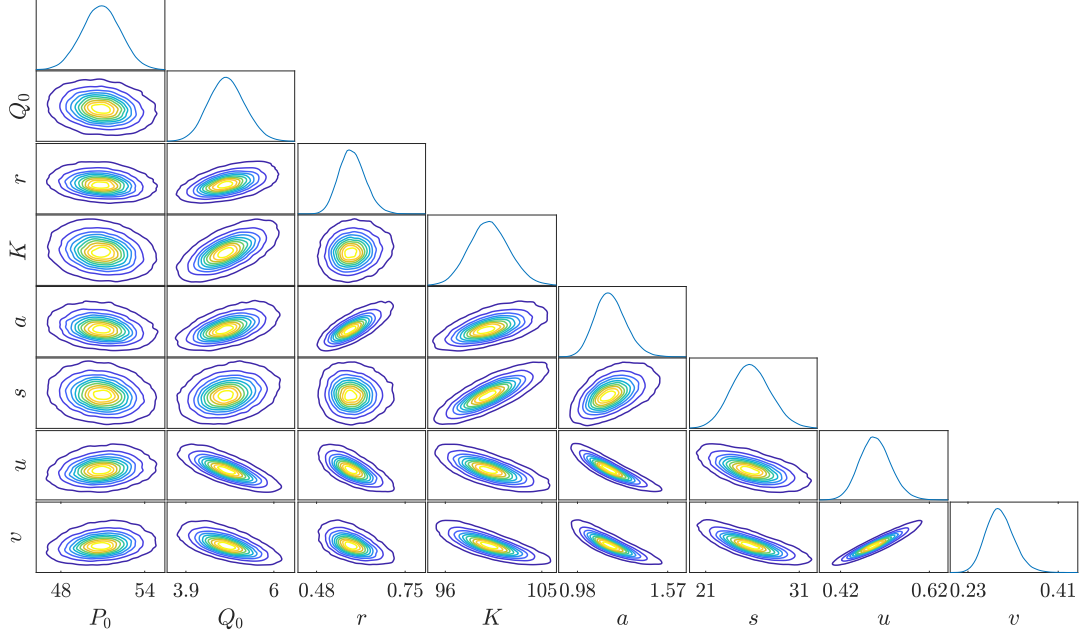


Fig. 2: Marginal posterior densities of the predator-prey model estimated from 10^6 posterior samples.

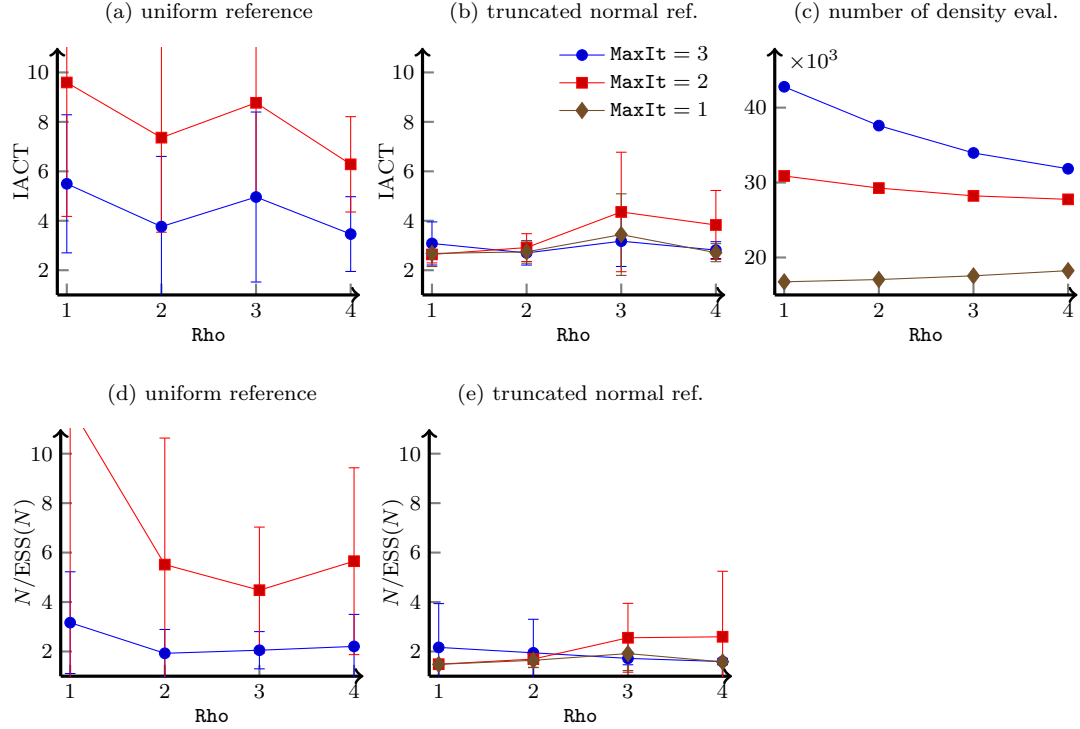


Fig. 3: (a): $\text{IACT} \pm \text{standard deviation}$ over 10 runs with the uniform reference measure. (b): $\text{IACT} \pm \text{standard deviation}$ with the truncated normal reference measure. (c): Number of density evaluations in TT-cross at each layer. (d): $N/\text{ESS}(N) \pm \text{standard deviation}$ over 10 runs with the uniform reference measure. (e): $N/\text{ESS}(N) \pm \text{standard deviation}$ with the truncated normal reference measure. Initial TT rank is adjusted such that the maximal TT rank is 13 in all tests, whereas enrichment ranks Rho and numbers of TT-cross iterations MaxIt are varied.

6.1.2 Numerical results

We use $L = 8$ bridging measures in the construction of DIRT by tempering the unnormalised posterior density with $\pi_k(\mathbf{x}) = \pi(\mathbf{x})^{\beta_k}$, starting from $\beta_0 = 10^{-4}$ and following by $\beta_{k+1} = \sqrt{10} \cdot \beta_k$. This way, $\beta_L = 1$ gives the target probability density. We consider two reference measures: the uniform reference measure μ_{uni} and the truncated normal reference measure μ_{TG} with the density $f_{\mathcal{U}}(\mathbf{u}) \propto \prod_{k=1}^8 \mathbb{1}_{[-4,4]}(\mathbf{u}_k) \exp(-\|\mathbf{u}_k\|_2^2/2)$. Note that at layer 0, the ratio function is just the tempered density $\pi_0(\mathbf{x})$ in the original domain $\mathbf{x}_k \in [\mathbf{a}_k, \mathbf{b}_k]$. We employ the piecewise-linear basis functions with n equally spaced interior collocation points for both reference measures. In addition, we tune TT-cross (Algorithm 4) using three parameters: the initial TT rank R0 , enrichment TT ranks $\rho_1 = \dots = \rho_{d-1} = \text{Rho}$, and the maximum number of TT-cross iterations MaxIt . Those define uniquely the maximum TT rank $\text{R}_{\text{max}} = \text{R0} + \text{Rho} \cdot \text{MaxIt}$.

Firstly, we vary one tuning variable at a time and investigate its impact on the efficiency and computational cost of the DIRT. We take the number of posterior density function evaluations in TT-cross in each DIRT layer to measure the computational cost for building DIRT.

In Figure 3, we vary the enrichment rank Rho and the number of TT-cross iterations MaxIt . The initial TT rank R0 is adjusted such that the maximum TT rank is 13 in all cases. We set the number of collocation points to be $n = 16$. All the DIRTs are constructed using the approximate ratio (58). With each Rho and MaxIt , we repeat the IRT-MCMC and IRT-IS for 10

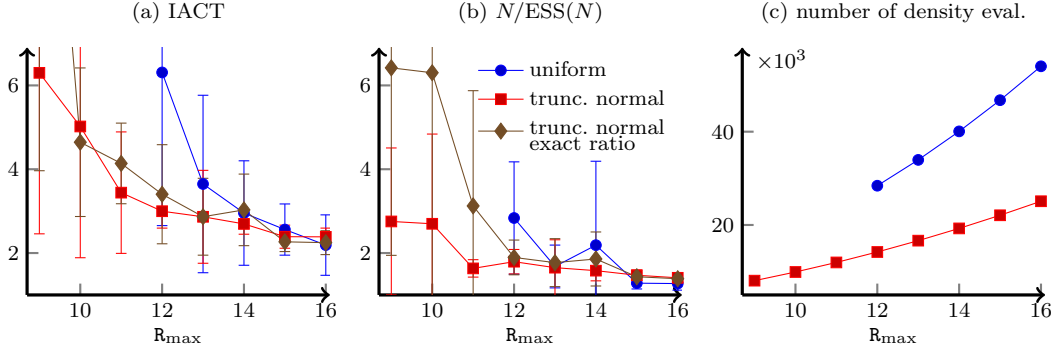


Fig. 4: $\text{IACT} \pm \text{standard deviation}$ over 10 runs (a), $N/\text{ESS}(N) \pm \text{standard deviation}$ over 10 runs (b), and number of density evaluations in TT-cross at each layer (c) with varying maximum TT ranks R_{\max} and different reference measures. For the uniform reference, $\text{MaxIt} = 3$ and $\text{Rho} = 3$ are used. For the truncated normal reference, $\text{MaxIt} = 1$ and $\text{Rho} = 0$ are used.

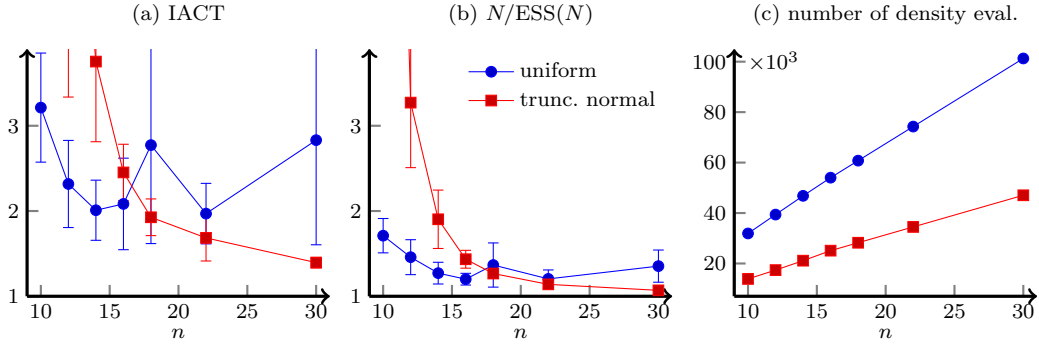


Fig. 5: $\text{IACT} \pm \text{standard deviation}$ over 10 runs (a), $N/\text{ESS}(N) \pm \text{standard deviation}$ over 10 runs (b), and number of density evaluations in TT-cross at each layer (c) for varying numbers of collocation points n and different reference measures. For the uniform reference, $\text{MaxIt} = 3$ and $\text{Rho} = 3$ are used. For the truncated normal reference, $\text{MaxIt} = 1$ and $\text{Rho} = 0$ are used.

experiments and report the estimated mean and standard deviation of the efficiency indicators. For the uniform reference (Figure 3 (a) and (d)), carrying out $\text{MaxIt} = 1$ iteration gives very inaccurate results with $\text{IACT} > 10$ and $N/\text{ESS}(N) > 10$. Increasing the number of TT-cross iterations for the uniform reference measure significantly improves the DIRT accuracy. Since the ratio function varies considerably from layer to layer, TT-cross needs at least 3 iterations and a nontrivial enrichment to adapt the approximation to the new function. This comes at the expense of tripling the number of density evaluations, in addition to those needed to compute the enrichment, as shown in Figure 3 (c). In contrast, using the truncated normal reference measure (Figure 3 (b) and (e)) can significantly improve the efficiency in this example. With only one TT-cross iteration, it can reduce the final IACT to below 4 and $N/\text{ESS}(N)$ to below 3.

Remark 12 At levels $k > 0$ of the DIRT construction, the ratio functions may have a similar shape (cf. Fig. 1). Thus, one can take the FTT of the ratio function at the previous level $k > 0$ as the initial guess for building FTT at level $k + 1$. This initialization provides good index sets in TT-cross, such that only one TT-cross iteration is sufficient with the truncated normal reference measure.

In Figure 4, we vary the maximum TT rank \mathbf{R}_{\max} . With the uniform reference, we set $\mathbf{Rho} = 3$ and $\mathbf{MaxIt} = 3$. With the truncated normal reference, we set $\mathbf{Rho} = 0$ and $\mathbf{MaxIt} = 1$, which makes the number of density evaluations equal to the number of degrees of freedom in the FTT decomposition, $n_1 r_1 + \sum_{k=2}^{d-1} n_k r_{k-1} r_k + r_{d-1} n_d = (d-2)n\mathbf{R}_{\max}^2 + 2n\mathbf{R}_{\max}$. We observe that the two reference measures give eventually comparable IACTs and ESSs with increasing \mathbf{R}_{\max} . However, the truncated normal reference achieves this with much fewer density evaluations.

In Figure 4, we compare also the approximate ratio (58) used in all experiments with the exact ratio (56). The diamond shaped markers in Figure 4 (a) and (b) show IACTs and ESSs obtained by the exact ratio approach. In this example, it gives worse results with a larger IACT and $N/\text{ESS}(N)$ for the truncated normal reference measure with lower \mathbf{R}_{\max} values, and does not lead to any meaningful results for the uniform reference measure.

In Figure 5, we vary the number of collocation points n used in each dimension. The truncated normal reference starts with a larger error since $n = 10$ points cannot resolve the rather large reference domain $[-4, 4]$. With increasing n , the IACT obtained using the truncated normal reference decays rapidly. In comparison, the IACT obtained using the uniform reference exhibits a spike and does not show rapid decay with increasing n . This may be caused by the boundary layers in the ratio function. Similar trends are observed in the reported $N/\text{ESS}(N)$. Again, the truncated normal reference requires significantly fewer density evaluations to achieve the same level of accuracy compared to the uniform reference in this experiment.

Next, we benchmark DIRT with the truncated normal reference, $\mathbf{MaxIt} = 1$, $\mathbf{Rho} = 0$, $n = 16$, and $\mathbf{R0} = \mathbf{R}_{\max} = 13$ against other sampling algorithms, including the Delayed Rejection Adaptive Metropolis (DRAM) [23] and the Stein variational Newton (SVN) [12]. DRAM is initialized with the covariance matrix $5I$, adaptation scale $2.4/\sqrt{d}$, adaptation interval 10 and delayed rejection scale 2. These parameters are commonly recommended in general case. For this example, SVN is sensitive to the choice of the step size and to the initial distribution of particles. We choose the step size to be $2 \cdot 10^{-2}$ and generate the initial particle set from the normal distribution $\mathcal{N}(\mathbf{x}_{\text{true}}, (2 \cdot 10^{-2} \mathbf{x}_{\text{true}})^2)$, which gives a reasonable balance between the stability and the rate of convergence. We carry out 23 Newton iterations in SVN to approach stationarity.

We simulate each method $M = 10$ times with N samples produced in each simulation, denoted by $\{\mathbf{x}^{(\ell,j)}\}_{j=1}^N$, where $\ell = 1, \dots, M$ indexes the simulations. For each simulation, we compute the empirical posterior covariance matrix $\mathbf{C}^\ell = \frac{1}{N} \sum_{j=1}^N (\mathbf{x}^{(\ell,j)} - \bar{\mathbf{x}}^\ell)(\mathbf{x}^{(\ell,j)} - \bar{\mathbf{x}}^\ell)^\top$, where $\bar{\mathbf{x}}^\ell = \frac{1}{N} \sum_{j=1}^N \mathbf{x}^{(\ell,j)}$ is the empirical posterior mean. Then, we use the average deviation of covariance matrices to benchmark the sampling performance of different sampling algorithms. Here we employ the Förstner-Moonen distance [16] over the cone of symmetric and positive definite (SPD) matrices,

$$d_{\text{FM}}(A, B) = \sum_{i=1}^d \ln^2(\lambda_i(\mathbf{A}, \mathbf{B})),$$

where $\lambda_i(\mathbf{A}, \mathbf{B})$ denotes the i -th generalised eigenvalue of the pair of SPD matrices (\mathbf{A}, \mathbf{B}) , to measure the deviation. This way, averaging the Förstner-Moonen distance between the ℓ -th empirical covariance matrix and the average covariance matrix over all M simulations,

$$\mathcal{E}_C = \frac{1}{M} \sum_{\ell=1}^M d_{\text{FM}}(\mathbf{C}^\ell, \bar{\mathbf{C}}), \quad \text{where} \quad \bar{\mathbf{C}} = \frac{1}{M} \sum_{\ell=1}^M \mathbf{C}^\ell, \quad (67)$$

provides an estimated deviation of empirical covariance matrices computed by a given algorithm.

In Figure 6, we plot the covariance deviations (67) obtained by IRT-MCMC, DRAM, and SVN versus the total number of target density function evaluations and the total CPU time needed by each algorithm. Here the reported total numbers of density evaluations and CPU

times include the construction of DIRT in each simulation experiment. The 10 independent simulations are run in parallel on a workstation with a Intel Xeon E5-2640v4 CPU at 2.4GHz. We can notice that DIRT produces estimated covariance matrices with smallest deviations in almost all tests. Moreover, DIRT is computationally more efficient in terms of the CPU time, because the evaluation of DIRT can take advantage of vector instructions.

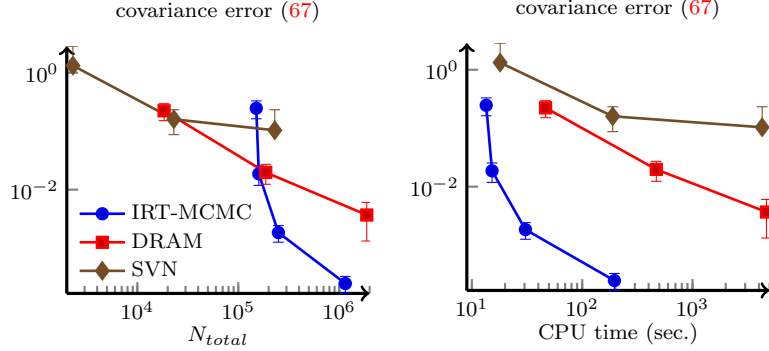


Fig. 6: Estimated deviation of empirical covariance matrices (67) computed by IRT-MCMC, DRAM and SVN for different total numbers of density evaluations (left) and CPU times (right).

6.2 Lorenz-96

This is a widely used benchmark model in atmospheric circulations. We consider a Lorenz-96 model that is specified by the system of ODEs

$$\frac{dP_i(t)}{dt} = (P_{i+1} - P_{i-2})P_{i-1} - P_i + 8, \quad \text{for } i = 1, \dots, d, \quad (68)$$

with periodic boundary conditions and an unknown initial condition $P_i(0) = \mathbf{x}_i$ for $i = 1, \dots, d$. The state dimension is set to $d = 40$. Observing noisy states with even indices at the final time $T = 0.1$, we aim to infer the initial state \mathbf{x} in this example. This way, we have observed data $\mathbf{y} \in \mathbb{R}^{\frac{d}{2}}$ and can define a forward model $G : \mathcal{X} \mapsto \mathbb{R}^{d/2}$ in the form of $G(\mathbf{x}) = [P_{2k}(T)]_{k=1}^{d/2}$ to represent simulated observables for a given initial condition \mathbf{x} .

Assuming i.i.d. normal noise in the observed data and assigning a truncated normal prior density to the initial condition, we have the unnormalized posterior density

$$\pi(\mathbf{x}) = \exp\left(-\frac{1}{2\sigma^2}\|G(\mathbf{x}) - \mathbf{y}\|_2^2\right) \prod_{k=1}^d \left(\mathbb{1}_{[-10,10]}(\mathbf{x}_k) \exp\left(-\frac{1}{2}(\mathbf{x}_k - 1)^2\right)\right).$$

We use a synthetic data set $\mathbf{y} = G(\mathbf{x}_{\text{true}}) + \boldsymbol{\eta}$, where \mathbf{x}_{true} is drawn from $\sim \mathcal{N}(1, 10^{-4}I_d)$, and $\boldsymbol{\eta}$ is a realisation of the i.i.d. zero mean normal noise with the standard deviation $\sigma = 10^{-1}$.

For the TT-cross approximations, we use the truncated normal reference measure on $[-3, 3]^d$, piecewise linear basis functions with $n = 15$ interior collocation points, $\text{MaxIt} = 1$ TT-cross iteration, and TT ranks $\mathbf{R}_{\text{max}} = 15$. DIRT is built with the tempered density

$$\pi_k(\mathbf{x}) = \exp\left(-\frac{\beta_k}{2\sigma^2}\|G(\mathbf{x}) - \mathbf{y}\|_2^2\right) \cdot \prod_{k=1}^d \left(\mathbb{1}_{[-10,10]}(\mathbf{x}_k) \exp\left(-\frac{\beta_k^{0.25}}{2}(\mathbf{x}_k - 1)^2\right)\right),$$

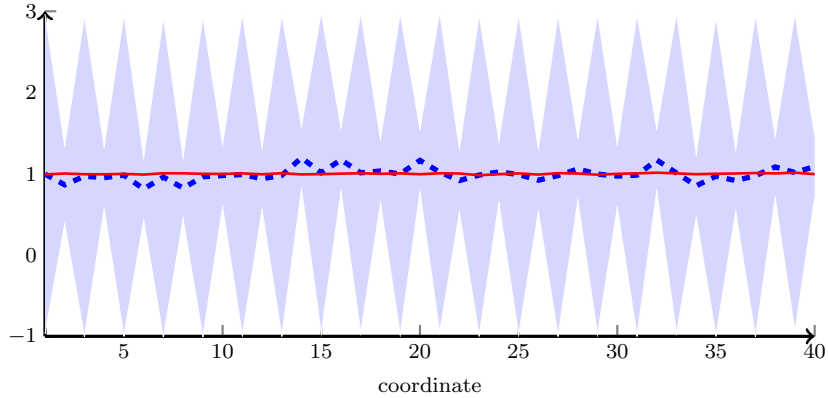


Fig. 7: Lorenz-96 model, true initial state (solid red) and posterior expectation, mean (blue dashed) ± 2 standard deviations (shaded area).

with $\beta_0 = 10^{-4}$ and $\beta_{k+1} = \sqrt{10} \cdot \beta_k$. This way, we need $L = 8$ layers to reach the posterior density. A weaker tempering of the prior is used to reduce its impact on the intermediate levels. This allows most of the intermediate DIRT levels to be used to bridge the more complicated likelihood. This setup requires a total of 1.2×10^6 density evaluations in TT-cross at all layers, and provides an average ESS of $N/1.55$ in IRT-IS and an average IACT of 2.6 in IRT-MCMC.

Using the posterior density, we can quantify the uncertainty of the inferred initial state and make predictions of the terminal state. The predicted initial state is shown in Figure 7. Note that the chaotic regime of Lorenz-96 makes it difficult to predict the unobserved odd coordinates. Nevertheless, DIRT demonstrates high numerical and sampling efficiency in approximating this complicated posterior.

6.3 Elliptic PDE

In the third example, we apply both SIRT and DIRT to the classical inverse problem governed by the stochastic diffusion equation

$$-\nabla \cdot (\kappa_d(s; \mathbf{x}) \nabla u(s)) = 0 \quad \text{on } s \in D := (0, 1)^2, \quad (69)$$

with Dirichlet boundary conditions $u|_{s_1=0} = 1$ and $u|_{s_1=1} = 0$ on the left and right boundaries, and homogeneous Neumann conditions on other boundaries. The goal is to infer the unknown diffusion coefficient $\kappa_d(s; \mathbf{x})$ from incomplete observations of the potential function $u(s)$. Here we adopt the same setup used in [14, 54].

6.3.1 Posterior density

The unknown diffusion coefficient $\kappa_d(s; \mathbf{x})$ is parametrized by a d -dimensional random variable \mathbf{x} . We take each of the parameters \mathbf{x}_k , $k = 1, \dots, d$, to be uniformly distributed on $[-\sqrt{3}, \sqrt{3}]$. Then, for any $\mathbf{x} \in [-\sqrt{3}, \sqrt{3}]^d$ and $s = (s_1, s_2) \in D$, the logarithm of the diffusion coefficient at s is defined by the following expansion

$$\ln \kappa_d(s; \mathbf{x}) = \sum_{k=1}^d \mathbf{x}_k \sqrt{\eta_k} \cos(2\pi \rho_1(k) s_1) \cos(2\pi \rho_2(k) s_2), \quad (70)$$

where

$$\eta_k = \frac{k^{-(\nu+1)}}{\sum_{k=1}^d k^{-(\nu+1)}}, \quad \rho_1(k) = k - \frac{\tau(k)^2 + \tau(k)}{2}, \quad \rho_2(k) = \tau(k) - \rho_1(k), \quad \text{and } \tau(k) = \left\lfloor \frac{\sqrt{1+k/2} - 1}{2} \right\rfloor.$$

To discretise the PDE in (69), we tessellate the spatial domain D with a uniform Cartesian grid with mesh size h . Then, we replace the infinite dimensional solution $u \in V \equiv H^1(D)$ by the continuous, piecewise bilinear finite element (FE) approximation $u_h \in V_h$ associated with the discretisation grid. To find u_h , we solve the resulting Galerkin system using a sparse direct solver. A fixed discretisation with $d = 11$, $h = 2^{-6}$, and $\nu = 2$ is used in this example.

The observed data $\mathbf{y} \in \mathbb{R}^m$ consist of m local averages of the potential function $u(s)$ over subdomains $D_i \subset D$, $i = 1, \dots, m$. To simulate the observable model outputs, we define the forward model $G^h : \mathcal{X} \mapsto \mathbb{R}^m$ with

$$G_i^h(\mathbf{x}) = \frac{1}{|D_i|} \int_{D_i} u_h(s; \mathbf{x}) ds, \quad i = 1, \dots, m.$$

The subdomains D_i are squares with side length $2/(\sqrt{m} + 1)$ centred at the interior vertices of a uniform Cartesian grid on $D = [0, 1]^2$ with grid size $1/(\sqrt{m} + 1)$, which form an overlapping partition of D . Synthetic data for these m local averages are produced from the “true” parameter $\mathbf{x}_{true} = (1.5, \dots, 1.5)$ by adding i.i.d. zero mean normally distributed noise with the standard deviation σ . This way, we have the unnormalized posterior density

$$\pi(\mathbf{x}) = \exp\left(-\frac{1}{2\sigma^2} \|G^h(\mathbf{x}) - \mathbf{y}\|_2^2\right) \prod_{k=1}^d \left(\mathbb{1}_{[-\sqrt{3}, \sqrt{3}]}(\mathbf{x}_k)\right).$$

6.3.2 Numerical results

In this example, we compare the impact of different tempering schemes, different numbers of measurements, and different measurement noise levels on DIRT. We also compare different basis functions used in the DIRT construction. In all experiments, we feed $N = 2^{16}$ independent samples generated by DIRT to both IRT-MCMC and IRT-IS.

In Figure 8, we compare DIRT with three different tempering sequences $\boldsymbol{\beta} = [\beta_0, \dots, \beta_L]$, varying the grid size n and the TT ranks \mathbf{R}_{\max} . Note that with $L = 0$ we have the single-layer SIRT. The reported number of density function evaluations is a sum of the numbers of evaluations in TT-cross at all layers. We use the truncated normal reference measure on $[-4, 4]^d$ with both piecewise linear and Fourier bases for the multilayer DIRT.

With the noise variance $\sigma^2 = 10^{-2}$ and a rather small data size $m = 3^2$, the posterior density is relatively simple to characterise, and hence can be tackled directly using the single-layer SIRT (see the case $L = 0$ in Figure 8 and [14]). However, the multilayer DIRT uses much smaller number of collocation points and TT ranks for producing an approximate posterior density with the same accuracy. Here the 3-layer DIRT needs only 10% of the density evaluations required for the single-layer counterpart.

Next, we test the multilayer DIRT on more difficult posterior densities, with larger numbers of measurements and smaller observation noise. We set the number of collocation points to be $n = 16$, maximum TT-cross iteration to be $\text{MaxIt} = 1$, and maximum TT rank to be $\mathbf{R}_{\max} = 12$. In Figure 9, we fix $\sigma^2 = 10^{-2}$ and vary the number of measurements. Since halving the measurement grid size $2/(\sqrt{m} + 1)$ corresponds to multiplying m by approximately a factor of 4, we use a different tempering strategy, starting with $\beta_0 = 4^{-\lceil \log_4 m \rceil}$, and setting $\beta_{k+1} = 4 \cdot \beta_k$ for next layers. This way, the number of layers grows proportionally to $\log m$, and the number of density

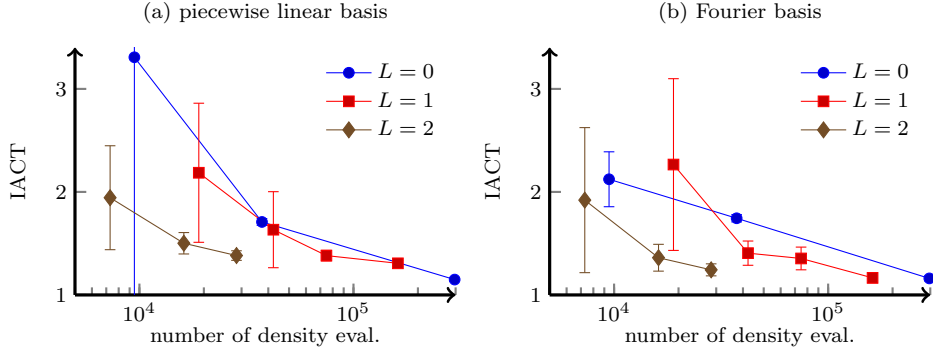


Fig. 8: Elliptic PDE with $\sigma^2 = 10^{-2}$ and $m = 3^2$. IACT vs. number of density evaluations in DIRT for different number of layers: $L = 0$ ($\beta = 1$), $L = 1$ ($\beta = \{0.1, 1\}$) and $L = 2$ ($\beta = \{0.1, \sqrt{0.1}, 1\}$). Note R_{\max} varying from 8 to 32 on $L = 0$, but only from 4 to 8 on $L = 2$.

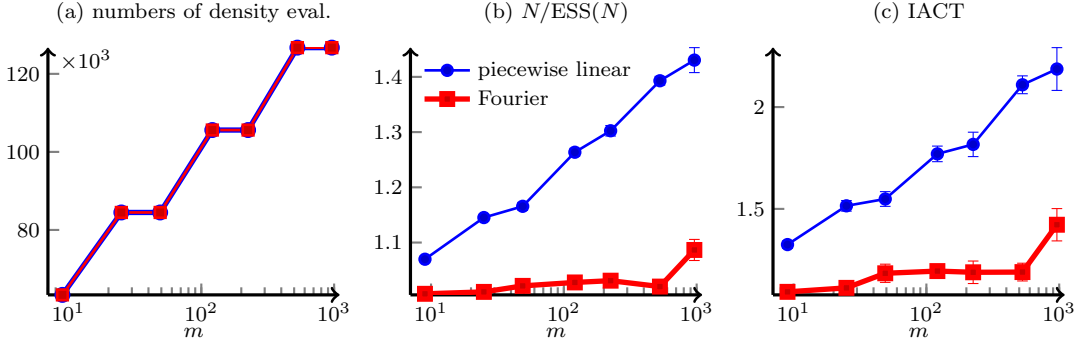


Fig. 9: Elliptic PDE with varying numbers of measurements m . (a): Total Number of density evaluations in all layers; (b): reciprocal sample size; and (c): IACT. Tempering is carried out with $\beta_0 = 4^{-\lceil \log_4 m \rceil}$, $\beta_{k+1} = 4 \cdot \beta_k$. TT-cross parameters: $n = 16$, $R_{\max} = R_0 = 12$, and $\text{MaxIt} = 1$.

evaluations in TT-cross for fixed TT ranks is also proportional to $\log m$, which can be confirmed by Figure 9 (a). Here we can see that the Fourier basis is significantly more accurate than the piecewise-linear basis for the same grid size. With the linear basis, both IACT and $N/\text{ESS}(N)$ grow logarithmically in the number of measurements. With the Fourier basis, the IACT stays almost constant below 1.5 and the $N/\text{ESS}(N)$ stays almost constant below 1.1, increasing slightly only for the most difficult case with $m = 31^2$ (Figure 9 (b) and (c)). With increasing number of measurements, the likelihood becomes more concentrated. This makes it more challenging to characterise the posterior using prior-based approaches such as QMC [54] or single-layer TT approximation. For example, even with a much larger number of collocation points $n = 65$ and 5 iterations of TT-cross (giving a maximal TT rank of 41), we still can not produce reasonable results for $m = 15^2$ with the single-layer SIRT.

We carry out an additional test with decreasing noise variance σ^2 . In Figure 10, we fix $m = 15^2$ and vary σ^2 from 10^{-1} to 10^{-5} . In this experiment, fixing TT ranks becomes insufficient for representing posterior densities with low observation noise. In particular, the piecewise linear basis does not have sufficient accuracy for the case of the smallest noise variance. In contrast, the Fourier basis can still retain low IACT and $N/\text{ESS}(N)$ for low noise variance cases, where IACT and $N/\text{ESS}(N)$ grow proportionally to $\log \sigma$. Together with the log-scaling of the number of evaluations, the effective complexity of the entire IRT-MCMC and IRT-IS schemes becomes

poly-logarithmic in the variance. Although the Fourier basis is computationally more expensive to evaluate than the piecewise-linear basis, with a factor of 2.5 in the worst case scenario in this experiment, this additional computational effort is well compensated by a much higher accuracy. This makes DIRT a viable approach for a range of concentrated distributions.

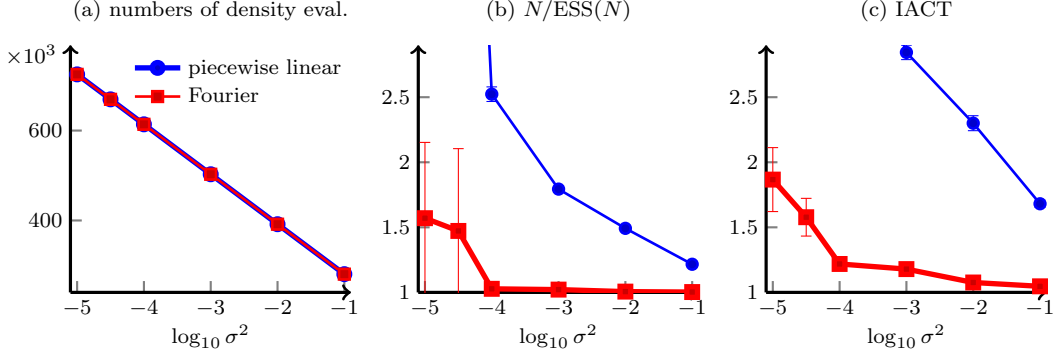


Fig. 10: Elliptic PDE with varying noise variances σ^2 . (a): Total numbers of density evaluations in all layers; (b): reciprocal sample size; (c) IACT. Tempering is carried out with $\beta_0 = 0.1\sigma^2$, $\beta_{k+1} = \sqrt{10} \cdot \beta_k$. TT parameters: $n = 16$, TT rank 20, one TT-cross iteration.

6.4 Parabolic PDE

In the fourth example, we consider an inverse problem of identifying the diffusion coefficient of a two-dimensional parabolic PDE from point observations of its solution. In the problem domain $D = [0, 3] \times [0, 1]$, with boundary ∂D , we model the time-varying potential function $p(s, t)$ for given diffusion coefficient field $\kappa_d(s)$ and forcing function $f(s, t)$ using the heat equation

$$\frac{\partial p(s, t)}{\partial t} = \nabla \cdot (\kappa_d(s; \mathbf{x}) \nabla p(s, t)) + f(s, t), \quad s \in D, t \in [0, T], \quad (71)$$

where $T = 10$. Parabolic PDEs of this type are widely used in modeling groundwater flow, optical diffusion tomography, the diffusion of thermal energy, and numerous other common scenarios for inverse problems. Let $\partial D_n = \{s \in \partial D \mid s_2 = 0\} \cup \{s \in \partial D \mid s_2 = 1\}$ denote the top and bottom boundaries, and $\partial D_d = \{s \in \partial \Omega \mid s_1 = 0\} \cup \{s \in \partial \Omega \mid s_1 = 3\}$ denote the left and right boundaries. For $t \geq 0$, we impose the mixed boundary condition:

$$p(s, t) = 0, \forall s \in \partial D_d, \quad \text{and} \quad (\kappa_d(s; \theta) \nabla p(s, t)) \cdot \mathbf{n}(s) = 0, \forall x \in \partial D_n,$$

where $\mathbf{n}(s)$ is the outward normal vector on the boundary. We also impose a zero initial condition, i.e., $p(s, 0) = 0, \forall s \in D$, and let the potential field be driven by a time-invariant forcing function

$$f(s, t) = c \left(\exp \left(-\frac{1}{2r^2} \|s - a\|^2 \right) - \exp \left(-\frac{1}{2r^2} \|s - b\|^2 \right) \right), \forall t \geq 0,$$

with $r = 0.05$, which is the superposition of two normal-shaped sink/source terms centered at $a = (0.5, 0.5)$ and $b = (2.5, 0.5)$, scaled by a constant $c = 5\pi \times 10^{-5}$.

6.4.1 Posterior density

The logarithm of the diffusion coefficient, $\ln \kappa_d(s; \mathbf{x})$, is endowed with the process convolution prior [25],

$$\ln \kappa_d(s; \mathbf{x}) = \ln \bar{\kappa} + \sum_{k=1}^d \mathbf{x}_k \exp\left(-\frac{1}{2}\|s - s^{(k)}\|^2\right), \quad (72)$$

where $d = 27$, $\ln \bar{\kappa} = -5$, each coefficient \mathbf{x}_k follows a standard normal prior $\mathcal{N}(0, 1)$ (which can be truncated to $[-5, 5]$ with sufficient accuracy), and $s^{(k)}, k = 1, \dots, d$ are centers of the kernel functions (shown as blue crosses in Figure 11 (a)). Similarly to the previous example, the potential function $p(s, t)$ in (71) is approximated by $p_h(s, t)$ using the finite element method with piecewise bilinear basis functions and implicit Euler time integration.

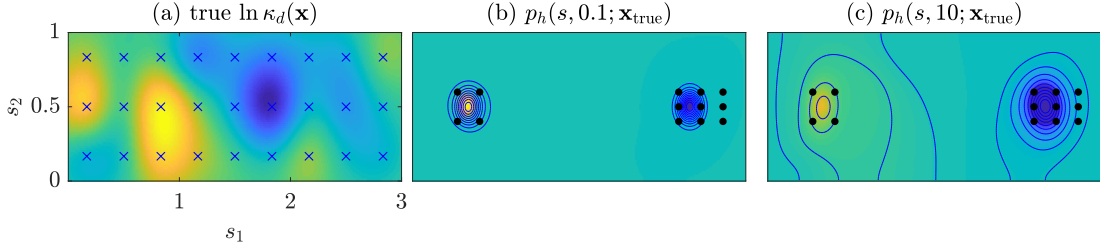


Fig. 11: Setup of the parabolic example. (a): Logarithm of the “true” diffusion coefficient and $d = 27$ centers of the process convolution prior (blue crosses); (b): the potential function $p_h(s, t; \mathbf{x}_{\text{true}})$ at $t = 0.1$, computed with $h = 1/80$; and (c): the potential function $p_h(s, t; \mathbf{x}_{\text{true}})$ at $t = 10$. Black dots in (b) and (c) are locations of measurements.

The observed data $\mathbf{y} \in \mathbb{R}^{m \times n_T}$ consist of the time-varying potential function $p(s, t)$ measured at $m = 13$ locations (shown as black dots in Figure 11 (b) and (c)) at $n_T = 10$ discrete time points equally spaced between $t = 1$ and $t = 10$. To simulate the observable model outputs, we define the forward model $G^h : \mathcal{X} \mapsto \mathbb{R}^{m \times n_T}$ with

$$G_{i,j}^h(\mathbf{x}) = p_h(s_i, t_j; \mathbf{x}), \quad i = 1, \dots, m, \quad j = 1, \dots, n_T.$$

Using a “true” parameter \mathbf{x}_{true} drawn from the prior distribution and a forward model with $h = 1/80$, synthetic data $\mathbf{y} \in \mathbb{R}^{m \times n_T}$ are produced by adding i.i.d. normal noise with zero mean and the standard deviation $\sigma = 1.65 \times 10^{-2}$ to $G^h(\mathbf{x}_{\text{true}})$. The corresponding $\ln \kappa_d(s; \mathbf{x}_{\text{true}})$ and the simulated potential function at several time snapshots are shown in Figure 11. The standard deviation $\sigma = 1.65 \times 10^{-2}$ corresponds to a signal-to-noise ratio of 10. This way, we have the unnormalized posterior density

$$\pi(\mathbf{x}) = \exp\left(-\frac{1}{2\sigma^2} \|G^h(\mathbf{x}) - \mathbf{y}\|_F^2\right) \prod_{k=1}^d \left(\mathbb{1}_{[-5,5]}(\mathbf{x}_k) \exp\left(-\frac{1}{2}\mathbf{x}_k^2\right)\right).$$

6.4.2 Numerical results

To construct DIRT, we employ a geometric grading in β , refining towards 1,

$$\log_{10} \beta_k \in \{-5, -4, -3, -2.5, -2, -1.5, -1, -0.75, -0.5, -0.25, 0\}.$$

The posterior is very concentrated in this example, so we employ separate tempering of prior and likelihood in the bridging densities,

$$\pi_k(\mathbf{x}) = \exp\left(-\frac{\beta_k}{2\sigma^2} \|G^h(\mathbf{x}) - \mathbf{y}\|_F^2\right) \prod_{k=1}^d \left(\mathbb{1}_{[-5,5]}(\mathbf{x}_k) \exp\left(-\frac{\beta_k^{0.01}}{2} \mathbf{x}_k^2\right)\right).$$

in which a weakly tempered prior is used. We use a truncated normal reference measure on the domain $(-4, 4]^d$ with the Fourier basis to build DIRT. In TT-cross, a maximum iteration $\text{MaxIt} = 1$ without enrichment ($\text{Rho} = 0$) is used. The number of collocation points in each dimension is set to be $n = 16$ and the TT ranks are chosen to be $\mathbf{R0} = \mathbf{R}_{\max} = \mathbf{R}_k$, where

$$\mathbf{R}_k \in \{15, 15, 15, 15, 15, 15, 13, 9, 9, 8, 7\}$$

at the k -th layer of DIRT.

The PDE in (71) is computationally expensive to solve. Here our goal is to explore the posterior density defined by a forward model, G^{h_f} , with refined grid size $h_f = 1/80$. A coarse forward model, G^{h_c} with $h_c = 1/20$, and an intermediate forward model, G^{h_m} with $h_m = 1/40$, are used in defining the bridge densities to speed-up the DIRT construction. In numerical experiments, we consider the CPU time of solving the coarse model evaluation as one work unit. The CPU times for evaluating the intermediate model and the fine model are about 12.5 work units and 160 work units, respectively.

In the first experiment, we employ the coarse forward model, G^{h_c} , to compare the sampling performance of DIRT with that of DRAM. The results are reported in Figure 12 (a), where the number of independent samples is calculated as the length of the Markov chain divided by the estimated IACT. The estimated IACTs for DRAM and DIRT are about 132 and 3.04, respectively, and the importance sampling with DIRT produces $\text{ESS} = N/1.5$. For DRAM, we exclude the burn-in samples in the number of work units, whereas the number of work units for the DIRT includes the construction cost of DIRT (993392 density evaluations). In this experiment, despite the high construction cost, DIRT can generate a Markov chain with almost independent samples, which is significantly more efficient than DRAM. Furthermore, the construction cost of DIRT will be less significant if one needs to generate more posterior samples, as shown in Figure 12 (a).

In the second experiment, we demonstrate the construction of DIRT using not only the bridge densities with different temperatures, but also the forward models with different grid resolutions. For initial temperatures such that $\beta_k < 10^{-0.5}$, we use the coarse forward model G^{h_c} . For $\beta_k = 10^{-0.5}$ and $\beta_k = 10^{-0.25}$, we use the intermediate forward model G^{h_m} . For $\beta_k = 1$ we use the fine forward model G^{h_f} , so that the fine model is used to define the target posterior density. We need 915024, 58544, and, 19824 evaluations of the coarse, intermediate, and fine models, respectively, to construct DIRT. Once the DIRT is constructed, Algorithm 1 generates a Markov chain with IACT 2.87 that samples the posterior defined by the fine model. Again, the importance sampling is more efficient with $\text{ESS} = N/1.78$. The number of independent samples versus the number of work units is reported in Figure 12 (b). In this experiment, it is computationally infeasible to apply DRAM directly (or any MCMC in general) to sample the posterior defined by the fine model. In contrast, the evaluation of DIRT and the corresponding posterior densities can be embarrassingly parallelised, which can further accelerate the posterior inference using high-performance computers. The IRT-IS algorithm can bypass the construction of Markov chains, which makes it suitable to be integrated into multilevel Monte Carlo or multilevel quasi Monte Carlo estimators to improve the convergence rate of the computation of posterior expectations. We leave this as a future research question.

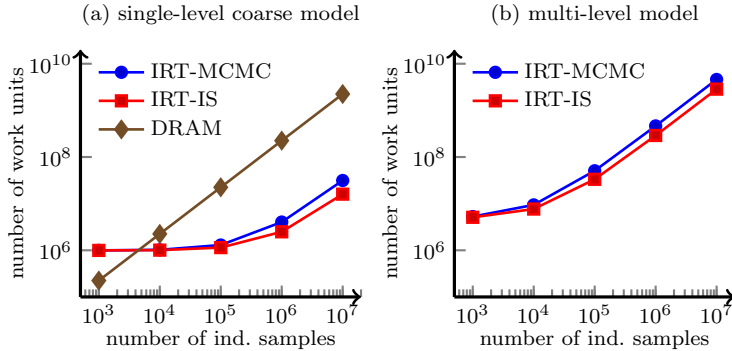


Fig. 12: Number of independent samples computed by IRT-MCMC, IRT-IS, and DRAM versus the total computational cost. (a): Comparison using a single level coarse model. (b) Comparison using the multilevel model in the DIRT construction. In both plots, the construction costs of IRT-MCMC and IRT-IS are included, whereas the burn-in cost of DRAM is not included. The work unit is the computational cost of one coarse model evaluation.

7 Conclusion

We have enabled functional tensor decompositions of complicated and concentrated continuous probability density functions that suffer from impractically large tensor ranks when approximated directly. Instead, we build an adaptive sequential change of coordinates that drives the target density towards a product function. This change of variables is realised by the composition of monotonicity-preserving SIRTs computed from FTT factorisations of ratios of bridging densities. Each of the ratio functions recovers one scale of correlations of the target density, and hence it can be approximated with fixed TT ranks. Together with the triangular structure of the Rosenblatt transport, this makes the total complexity linear in the number of variables.

This deep composition of the inverse Rosenblatt transports shares similarities with deep neural networks with nonlinear activation functions. However, DIRT has several advantages.

- Each DIRT layer, defined by the bridging densities, can be associated to the scale of noise or observation function. Any prior knowledge of model hierarchies can improve the selection of bridging densities. In contrast, the influence of a particular fully-connected layer in a neural network is difficult to predict or understand.
- DIRT layers can be computed independently. As soon as the layer is approximated up to the desired accuracy, it can be saved and never recomputed again. This enables a simple interactive construction, where the tuning parameters can be set layer per layer. Neural networks require optimisation of all layers simultaneously.
- The construction of each DIRT layer is powered by efficient TT-cross algorithms, which can converge much faster than the stochastic gradient descent used by neural networks in many cases. The dense linear algebra operations used by FTT decompositions can take full advantage of modern CPU and GPU vectorisations, whereas an embarrassing parallelism with respect to target density evaluations is well scalable to modern high performance computers.

This work opens many potential applications and further enhancements of DIRT. For example, the transport maps defined by DIRT can be naturally extended to approximate the optimal biasing density in importance sampling, which can be valuable for solving rare event simulations. In Section 6.4, we offered some preliminary investigation on constructing DIRT using multilevel models. The multilevel idea can be further integrated with DIRT to improve the convergence rate of the importance sampling estimator. For problems involving extremely high-dimensional

or infinite-dimensional random variables, DIRT can be combined with the likelihood informed subspace (LIS) [9, 57, 62] to characterise the highly non-Gaussian effective random variable dimensions identified by LIS. In addition, for sequential Bayesian inference, we can apply DIRT to iteratively characterise the filtered posterior measures changing over time, where the evolution of the random states and time-dependent observations naturally define a sequence of bridging measures.

8 Appendices

8.1 Appendix A: construction of FTT by cross interpolation

Here we recall an alternating iteration algorithm for constructing the FTT decomposition of a multivariate function $h : \mathcal{X} \mapsto \mathbb{R}$. We seek an FTT of the form

$$h(\mathbf{x}) \approx \tilde{h}(\mathbf{x}) = \sum_{\alpha_0=1}^{r_0} \sum_{\alpha_1=1}^{r_1} \dots \sum_{\alpha_d=1}^{r_d} \mathcal{H}_1^{(\alpha_0, \alpha_1)}(\mathbf{x}_1) \dots \mathcal{H}_k^{(\alpha_{k-1}, \alpha_k)}(\mathbf{x}_k) \dots \mathcal{H}_d^{(\alpha_{d-1}, \alpha_d)}(\mathbf{x}_d), \quad (73)$$

with $r_0 = r_d = 1$. Each univariate function $\mathcal{H}_k^{(\alpha_{k-1}, \alpha_k)}(\mathbf{x}_k) : \mathcal{X}_k \mapsto \mathbb{R}$ is represented as a linear combination of a set of n_k basis functions $\{\phi_k^{(i)}(\mathbf{x}_k)\}_{i=1}^{n_k}$, that is,

$$\mathcal{H}_k^{(\alpha_{k-1}, \alpha_k)}(\mathbf{x}_k) = \sum_{i=1}^{n_k} \phi_k^{(i)}(\mathbf{x}_k) \mathcal{A}_k[\alpha_{k-1}, i, \alpha_k], \quad (74)$$

where $\mathcal{A}_k \in \mathbb{R}^{r_{k-1} \times n_k \times r_k}$ is (the coefficient tensor of) the k -th TT core. The number of degrees of freedom in the FTT decomposition, that is, in the tensors $\{\mathcal{A}_k\}_{k=1}^d$, is linear in d provided the TT ranks r_0, \dots, r_d are bounded. For the numerical efficiency it is essential that the TT cores can be constructed using a similar number of evaluations of $h(\mathbf{x})$. This can be achieved using cross interpolation methods. The following definition is used to construct cross interpolations.

Definition 1 For each variable \mathbf{x}_k , we consider a set of *interpolation basis functions* that can be represented by a vector-valued function $\phi_k(\mathbf{x}_k) = [\phi_k^{(1)}(\mathbf{x}_k), \dots, \phi_k^{(n_k)}(\mathbf{x}_k)] \in \mathbb{R}^{1 \times n_k}$, and a set of collocation points $\mathbf{X}_k = \{\mathbf{x}_k^{(i)}\}_{i=1}^{n_k}$ such that the Vandermonde matrix

$$\phi_k(\mathbf{X}_k) \equiv [\phi_k(\mathbf{x}_k^{(i)})] \in \mathbb{R}^{n_k \times n_k}, \quad (75)$$

is an identity matrix. A typical construction is the (piecewise) Lagrange basis functions defined by a point set \mathbf{X}_k . We can also construct the interpolation basis from other basis functions of a separable Hilbert space, denoted by $\psi_k(\mathbf{x}_k) = [\psi_k^{(1)}(\mathbf{x}_k), \dots, \psi_k^{(n_k)}(\mathbf{x}_k)] \in \mathbb{R}^{1 \times n_k}$, and a point set \mathbf{X}_k with a nonsingular Vandermonde matrix by setting

$$\phi_k(\mathbf{x}_k) = \psi_k(\mathbf{x}_k) \psi_k(\mathbf{X}_k)^{-1}.$$

Specifically, if $\psi_k(\mathbf{x}_k)$ is a set of λ_k -orthogonal functions and \mathbf{X}_k are the roots of the function $\psi_k^{(n_k+1)}(\mathbf{x}_k)$, we recover the pseudo-spectral methods and have

$$\psi_k(\mathbf{X}_k)^{-1} = \psi_k(\mathbf{X}_k)^\top \text{diag}(\boldsymbol{\omega}_k),$$

where the vector $\boldsymbol{\omega}_k \in \mathbb{R}^{n_k}$ contains quadrature weights associated with \mathbf{X}_k and $\text{diag}(\cdot)$ brings a vector into a diagonal matrix.

Furthermore, we define the mass matrix $\mathbf{M}_k = \int \phi_k(\mathbf{x}_k)^\top \phi_k(\mathbf{x}_k) \lambda_k(\mathbf{x}_k) d\mathbf{x}_k$. We let $\mathbf{L}_k \in \mathbb{R}^{n_k \times n_k}$ be the Cholesky factor of the mass matrix, i.e., $\mathbf{L}_k \mathbf{L}_k^\top = \mathbf{M}_k$. For an interpolation basis constructed from λ_k -orthogonal functions and the roots of $\psi_k^{(n_k+1)}(\mathbf{x}_k)$, we have $\mathbf{M}_k = \text{diag}(\boldsymbol{\omega}_k)$.

8.1.1 Two dimensional case

Consider first the FTT decomposition of a bivariate function

$$h(\mathbf{x}_1, \mathbf{x}_2) \approx \tilde{h}(\mathbf{x}_1, \mathbf{x}_2) = \sum_{\alpha=1}^r \mathcal{H}_1^{(\alpha)}(\mathbf{x}_1) \mathcal{H}_2^{(\alpha)}(\mathbf{x}_2), \quad (76)$$

where the rank- r cores

$$\mathcal{H}_1(\mathbf{x}_1) \equiv \phi_1(\mathbf{x}_1) \mathcal{A}_1 \in \mathbb{R}^{1 \times r} \quad \text{and} \quad \mathcal{H}_2(\mathbf{x}_2) \equiv \mathcal{A}_2 \phi_2(\mathbf{x}_2)^\top \in \mathbb{R}^{r \times 1}$$

are specified by basis functions $\phi_1(\mathbf{x}_1) \in \mathbb{R}^{1 \times n_1}$ and $\phi_2(\mathbf{x}_2) \in \mathbb{R}^{1 \times n_2}$, and the corresponding coefficient matrices $\mathcal{A}_1 \in \mathbb{R}^{n_1 \times r}$ and $\mathcal{A}_2 \in \mathbb{R}^{r \times n_2}$, respectively. We aim to recover \mathcal{A}_1 and \mathcal{A}_2 such that the L^2 norm of the error

$$\|h(\mathbf{x}_1, \mathbf{x}_2) - \mathcal{H}_1(\mathbf{x}_1) \mathcal{H}_2(\mathbf{x}_2)\|_{L_\lambda^2(\mathcal{X})},$$

is minimised. Note that with interpolation bases, the matrices \mathcal{A}_1 and \mathcal{A}_2 are also pointwise evaluations of the functions $\mathcal{H}_1(\mathbf{x}_1)$ and $\mathcal{H}_2(\mathbf{x}_2)$ at collocation points \mathbf{X}_1 and \mathbf{X}_2 , respectively. This way, $h(\mathbf{x}_1, \mathbf{x}_2)$ yields a discrete approximation

$$h(\mathbf{x}_1, \mathbf{x}_2) \approx \phi_1(\mathbf{x}_1) h(\mathbf{X}_1, \mathbf{X}_2) \phi_2(\mathbf{x}_2)^\top, \quad (77)$$

where $h(\mathbf{X}_1, \mathbf{X}_2) \equiv [h(\mathbf{x}_1^{(i)}, \mathbf{x}_2^{(j)})] \in \mathbb{R}^{n_1 \times n_2}$ for $\mathbf{x}_1^{(i)} \in \mathbf{X}_1$ and $\mathbf{x}_2^{(j)} \in \mathbf{X}_2$ is the matrix of nodal values of $h(\mathbf{x}_1, \mathbf{x}_2)$ similarly to (75). This way, the L^2 error of the continuous factorisation yields a discrete approximation

$$\begin{aligned} \|h(\mathbf{x}_1, \mathbf{x}_2) - \mathcal{H}_1(\mathbf{x}_1) \mathcal{H}_2(\mathbf{x}_2)\|_{L_\lambda^2(\mathcal{X})} &\approx \|\phi_1(\mathbf{x}_1) (h(\mathbf{X}_1, \mathbf{X}_2)^\top - \mathcal{A}_1 \mathcal{A}_2) \phi_2(\mathbf{x}_2)^\top\|_{L_\lambda^2(\mathcal{X})} \\ &= \|\mathbf{L}_1^\top (h(\mathbf{X}_1, \mathbf{X}_2) - \mathcal{A}_1 \mathcal{A}_2) \mathbf{L}_2\|_F. \end{aligned} \quad (78)$$

Thus, we can recover the matrices \mathcal{A}_1 and \mathcal{A}_2 by solving some low-rank matrix factorisation of $h(\mathbf{X}_1, \mathbf{X}_2)$. However, assembling the matrix $h(\mathbf{X}_1, \mathbf{X}_2)$ requires evaluating the function $h(\mathbf{x}_1, \mathbf{x}_2)$ at the Cartesian union of the collocation points $\mathbf{X}_1 \times \mathbf{X}_2$, which can be computationally prohibitive in the generalisation to $d > 2$.

Instead, we can use some *interpolation point sets* $\bar{\mathbf{X}}_1 \subset \mathbf{X}_1$ and $\bar{\mathbf{X}}_2 \subset \mathbf{X}_2$ of cardinality $\#\bar{\mathbf{X}}_1 = \#\bar{\mathbf{X}}_2 = r$ such that the matrix $h(\bar{\mathbf{X}}_1, \bar{\mathbf{X}}_2) \in \mathbb{R}^{r \times r}$ is nonsingular, and rank- r *interpolation cores*

$$\mathcal{G}_1(\mathbf{x}_1) \equiv \phi_1(\mathbf{x}_1) \mathcal{B}_1 \quad \text{and} \quad \mathcal{G}_2(\mathbf{x}_2) \equiv \mathcal{B}_2 \phi_2(\mathbf{x}_2)^\top,$$

with $\mathcal{B}_1 \in \mathbb{R}^{n_1 \times r}$ and $\mathcal{B}_2 \in \mathbb{R}^{r \times n_2}$, to approximate $h(\mathbf{x}_1, \mathbf{x}_2)$ by interpolation. The interpolation cores satisfy the property that $\mathcal{G}_1(\bar{\mathbf{X}}_1)$ and $\mathcal{G}_2(\bar{\mathbf{X}}_2)$ are identity matrices. This yields interpolated approximations to $h(\mathbf{x}_1, \mathbf{x}_2)$, for example,

$$h(\mathbf{x}_1, \mathbf{x}_2) \approx \mathcal{G}_1(\mathbf{x}_1) h(\bar{\mathbf{X}}_1, \bar{\mathbf{X}}_2) \quad \text{and} \quad h(\mathbf{x}_1, \mathbf{x}_2) \approx \mathcal{G}_1(\mathbf{x}_1) h(\bar{\mathbf{X}}_1, \bar{\mathbf{X}}_2) \mathcal{G}_2(\mathbf{x}_2).$$

This way, the goal becomes identifying the optimal point sets $(\bar{\mathbf{X}}_1, \bar{\mathbf{X}}_2)$ and the cores $(\mathcal{G}_1, \mathcal{G}_2)$ that minimise the interpolated rank- r factorisation error

$$\|h(\mathbf{x}_1, \mathbf{x}_2) - \mathcal{G}_1(\mathbf{x}_1) h(\bar{\mathbf{X}}_1, \bar{\mathbf{X}}_2) \mathcal{G}_2(\mathbf{x}_2)\|_{L_\lambda^2(\mathcal{X})}. \quad (79)$$

In practice, an *alternating direction* strategy can be employed to solve the above nonlinear minimisation problem via a sequence of subproblems at a lower computational cost compared

to that of the full matrix factorisation induced by (78). For example, we start from some initial guess of \mathcal{B}_2 and $\bar{\mathbf{X}}_2$ to solve for \mathcal{B}_1 and $\bar{\mathbf{X}}_1$ via the minimisation problem

$$\mathcal{B}_1, \bar{\mathbf{X}}_1 = \arg \min_{\mathcal{B}'_1, \bar{\mathbf{X}}'_1} \left\| h(\mathbf{x}_1, \bar{\mathbf{X}}_2) \mathcal{B}_2 \phi_2(\mathbf{x}_2)^\top - \phi_1(\mathbf{x}_1) \mathcal{B}'_1 h(\bar{\mathbf{X}}'_1, \bar{\mathbf{X}}_2) \mathcal{B}_2 \phi_2(\mathbf{x}_2)^\top \right\|_{L^2_\lambda(\mathcal{X})}, \quad (80)$$

then we use the updated \mathcal{B}_1 and $\bar{\mathbf{X}}_1$ to renew \mathcal{B}_2 and $\bar{\mathbf{X}}_2$ via

$$\mathcal{B}_2, \bar{\mathbf{X}}_2 = \arg \min_{\mathcal{B}'_2, \bar{\mathbf{X}}'_2} \left\| \phi_1(\mathbf{x}_1) \mathcal{B}_1 h(\bar{\mathbf{X}}_1, \mathbf{x}_2) - \phi_1(\mathbf{x}_1) \mathcal{B}_1 h(\bar{\mathbf{X}}_1, \bar{\mathbf{X}}'_2) \mathcal{B}'_2 \phi_2(\mathbf{x}_2)^\top \right\|_{L^2_\lambda(\mathcal{X})},$$

and repeat until convergence. Given the collocation points $\bar{\mathbf{X}}_1$ and $\bar{\mathbf{X}}_2$, the coefficient matrices \mathcal{B}_1 and \mathcal{B}_2 satisfy a simple quadratic optimisation, and can be computed from

$$\mathcal{B}_1 h(\bar{\mathbf{X}}_1, \bar{\mathbf{X}}_2) = h(\mathbf{X}_1, \bar{\mathbf{X}}_2) \quad \text{and} \quad h(\bar{\mathbf{X}}_1, \bar{\mathbf{X}}_2) \mathcal{B}_2 = h(\bar{\mathbf{X}}_1, \mathbf{X}_2), \quad (81)$$

respectively. Solving (81) only requires $(n_1 + n_2 - r)r$ evaluations of $h(\mathbf{x}_1, \mathbf{x}_2)$.

In (81), one needs to find the interpolation point sets $\bar{\mathbf{X}}_1$ and $\bar{\mathbf{X}}_2$ so that the resulting interpolation operator is an optimal approximation to the projection operator that spans the same linear subspace. However, finding the optimal interpolation point sets is an NP-hard problem. In practice, accurate quasi-optimal solutions can be obtained by greedy algorithms such as the (discrete) empirical interpolation [1, 8] or the maximum volume (*MaxVol*) [19, 20, 21] methods. Here we outline the procedure of the *MaxVol* algorithm [19] for solving (80), which can be equivalently expressed as the problem of searching for an index set $\mathbf{I} \subset \{1, \dots, n\}$ of cardinality r such that the norm of $\mathbf{B} = \mathbf{H}\mathbf{H}^{-1} \in \mathbb{R}^{n \times r}$ is minimized. Here $\bar{\mathbf{H}} = \mathbf{H}[\mathbf{I}, :] \in \mathbb{R}^{r \times r}$ is the submatrix of a given matrix \mathbf{H} in the MATLAB notation. For example, one can have $\mathbf{H} = h(\mathbf{X}_1, \bar{\mathbf{X}}_2)$, and then the interpolation point set $\bar{\mathbf{X}}_1$ is given by \mathbf{I} and the coefficient matrix is set by $\mathcal{B}_1 = \mathbf{B}$.

Algorithm 3 MaxVol

- 1: Choose an initial set \mathbf{I} and a stopping threshold $\delta > 0$.
 - 2: **while** $\max_{i,j} |\mathbf{B}[i, j]| > 1 + \delta$ **do**
 - 3: Let $i_*, j_* = \arg \max_{i,j} |\mathbf{B}[i, j]|$.
 - 4: Replace the index $\mathbf{I}[j_*]$ in the set by i_* .
 - 5: Recompute $\bar{\mathbf{H}} = \mathbf{H}[\mathbf{I}, :]$ and $\mathbf{B} = \mathbf{H}\mathbf{H}^{-1}$.
 - 6: **end while**
-

Given an initial index set, which can be chosen as the r dominant pivots from Gaussian elimination, *MaxVol* proceeds as Algorithm 3. Note that $\mathbf{B}[\mathbf{I}, :] \in \mathbb{R}^{r \times r}$ is an identity matrix by construction. *MaxVol* ensures that no other row is more ‘‘important’’ by searching for a *dominant* submatrix $\bar{\mathbf{H}}$ such that $|\mathbf{B}[i, j]| \leq 1 + \delta$, which is a proxy to the *maximum volume* submatrix $\bar{\mathbf{H}}_*$ such that $|\det(\bar{\mathbf{H}}_*)| = \max_{\mathbf{I}} |\det(\mathbf{H}[\mathbf{I}, :])|$. The update of \mathbf{B} can be computed efficiently via the Sherman-Morrison-Woodbury formula [19] with a total cost of $\mathcal{O}(nr^2)$ per iteration.

For the numerical stability it is beneficial to compute the thin generalised QR factorization $\mathbf{H}\mathbf{R} = h(\mathbf{X}_1, \bar{\mathbf{X}}_2)$, where the matrix \mathbf{H} has \mathbf{M}_1 -orthonormal columns. This way, the set of functions $\phi_1(\mathbf{x}_1)\mathbf{H}$ forms a λ_1 -orthogonal basis. The factorisation $\mathbf{H}\mathbf{R} = h(\mathbf{X}_1, \bar{\mathbf{X}}_2)$ can be obtained by the thin QR factorization $\mathbf{Q}\mathbf{R} = \mathbf{L}_1^\top h(\mathbf{X}_1, \bar{\mathbf{X}}_2)$ and $\mathbf{H} = \mathbf{L}_1^{-\top} \mathbf{Q}$. Then, one can apply *MaxVol* to \mathbf{H} , which is the evaluation of $\phi_1(\mathbf{x}_1)\mathbf{H}$ at \mathbf{X}_1 , to select the index set \mathbf{I} , and thus the interpolation points $\bar{\mathbf{X}}_1 \subset \mathbf{X}_1$. We have $\mathbf{H}[\mathbf{I}, :] = h(\bar{\mathbf{X}}_1, \bar{\mathbf{X}}_2)\mathbf{R}^{-1}$, which yields $\mathbf{B} = \mathbf{H}\mathbf{H}[\mathbf{I}, :]^{-1} = h(\mathbf{X}_1, \bar{\mathbf{X}}_2)h(\bar{\mathbf{X}}_1, \bar{\mathbf{X}}_2)^{-1}$. Thus, we can set the coefficient matrix as $\mathcal{B}_1 = \mathbf{B}$ and define the interpolation core $\mathcal{G}_1(\mathbf{x}_1) \equiv \phi_1(\mathbf{x}_1)\mathcal{B}_1$ such that $\mathcal{G}_1(\mathbf{X}_1)$ is an identity matrix.

We can obtain $(\mathcal{B}_1, \bar{\mathbf{X}}_1)$ and $(\mathcal{B}_2, \bar{\mathbf{X}}_2)$ by applying *MaxVol* within alternating iterations. Then, we can set $\mathcal{A}_1 = \mathcal{B}_1$ and $\mathcal{A}_2 = h(\bar{\mathbf{X}}_1, \bar{\mathbf{X}}_2)\mathcal{B}_2$ to recover the factorisation in the form of (76).

8.1.2 Multi-dimensional case

The TT-cross algorithm [43] recursively extends (81) to $d > 2$. In the first step, we assume that a reduced point set $\bar{\mathbf{X}}_{>1} = \{(\mathbf{x}_2^{(\alpha_1)}, \dots, \mathbf{x}_d^{(\alpha_1)})\}$ of r_1 points is given. We can for example draw it from some tractable reference measure. We compute an analogue of the first equation in (81)

$$\mathcal{A}_1 h(\bar{\mathbf{X}}_1, \bar{\mathbf{X}}_{>1}) = h(\mathbf{X}_1, \bar{\mathbf{X}}_{>1}) \in \mathbb{R}^{n_1 \times r_1},$$

where $h(\mathbf{X}_1, \bar{\mathbf{X}}_{>1}) = [h(\mathbf{x}_1^{(i_1)}, \mathbf{x}_2^{(\alpha_1)}, \dots, \mathbf{x}_d^{(\alpha_1)})]$ is a matrix filled with the function $h(\mathbf{x})$ evaluated at the “reduced” set of points $\mathbf{X}_1 \times \bar{\mathbf{X}}_{>1}$. Now we apply *MaxVol* to compute reduced subsets $\mathbf{I}_1 \subset \{1, \dots, n_1\}$ and $\bar{\mathbf{X}}_{<2} = \mathbf{X}_1(\mathbf{I}_1) \subset \mathbf{X}_1$. Similarly to the matrix \mathbf{B}_1 in the two dimensional case, we let the actual TT core be the “stabilized” matrix $\mathcal{A}_1 = \mathbf{H}_1 \mathbf{H}_1[\mathbf{I}_1, :]^{-1}$, where $\mathbf{H}_1 \mathbf{R}_1 = h(\mathbf{X}_1, \bar{\mathbf{X}}_{>1})$ is the generalised QR decomposition.

In the k -th step, we assume reduced point sets $\bar{\mathbf{X}}_{<k} = \{\mathbf{x}_1^{(\alpha_{k-1})}, \dots, \mathbf{x}_{k-1}^{(\alpha_{k-1})}\}$ and $\bar{\mathbf{X}}_{>k} = \{\mathbf{x}_{k+1}^{(\alpha_k)}, \dots, \mathbf{x}_d^{(\alpha_k)}\}$ are given. We can compute a third order tensor

$$\mathcal{H}_k := \left[h(\mathbf{x}_1^{(\alpha_{k-1})}, \dots, \mathbf{x}_{k-1}^{(\alpha_{k-1})}, \mathbf{x}_k^{(i_k)}, \mathbf{x}_{k+1}^{(\alpha_k)}, \dots, \mathbf{x}_d^{(\alpha_k)}) \right] \in \mathbb{R}^{r_{k-1} \times n_k \times r_k}, \quad (82)$$

which consists of evaluations of $h(\mathbf{x})$ at the Cartesian union of the sets $\bar{\mathbf{X}}_{<k} \times \mathbf{X}_k \times \bar{\mathbf{X}}_{>k}$. We let $\bar{\mathbf{X}}_{<1} = \bar{\mathbf{X}}_{>d} = \emptyset$ to enable the notation for all k . We can *unfold* \mathcal{H}_k into matrices of the form

$$\mathbf{H}_k^{(L)} \in \mathbb{R}^{(r_{k-1} n_k) \times r_k}, \quad \mathbf{H}_k^{(R)} \in \mathbb{R}^{r_{k-1} \times (n_k r_k)}, \quad (83)$$

such that

$$\mathcal{H}_k[\alpha_{k-1}, i_k, \alpha_k] = \mathbf{H}_k^{(L)}[\alpha_{k-1} + (i_k - 1)r_{k-1}, \alpha_k] = \mathbf{H}_k^{(R)}[\alpha_{k-1}, i_k + (\alpha_k - 1)n_k].$$

The union of the indices α_{k-1} and i_k corresponds to the union of the point sets $\mathbf{X}_{\leq k} := \bar{\mathbf{X}}_{<k} \times \mathbf{X}_k$. Therefore, we can apply *MaxVol* to $\mathbf{H}_k^{(L)}$ (or a generalised QR factor thereof) to obtain a discrete set $\mathbf{I}_k \subset \{1, \dots, r_{k-1} n_k\}$, and take a subsample of $\mathbf{X}_{\leq k}$ for the next recursion step, $\bar{\mathbf{X}}_{<k+1} = \mathbf{X}_{\leq k}(\mathbf{I}_k)$. Similarly for the k th TT core we define

$$\mathbf{B}_k^{(L)} = \mathbf{H}_k^{(L)} \mathbf{H}_k^{(L)}(\mathbf{I}_k, \cdot)^{-1}, \quad (84)$$

$$\mathcal{A}_k[\alpha_{k-1}, i_k, \alpha_k] = \mathbf{B}_k^{(L)}[\alpha_{k-1} + (i_k - 1)r_{k-1}, \alpha_k]. \quad (85)$$

If the function $h(\mathbf{x})$ admits an exact TT decomposition, and the initial point sets were chosen such that all $\mathbf{H}_k^{(L)}$ are full-rank, the recursion defined above reconstructs the decomposition exactly. However, in practice the initial point sets can be a poor interpolation sets. In this case we can *refine* them by carrying out several iterations. Having computed \mathcal{A}_d , we reverse the recursion and iterate backwards, computing discrete sets $\mathbf{J}_k \subset \{1, \dots, n_k r_k\}$ via *MaxVol* applied to $(\mathbf{H}_k^{(R)})^\top$, and setting $\bar{\mathbf{X}}_{>k-1} = \mathbf{X}_{>k}(\mathbf{J}_k)$, where $\mathbf{X}_{>k} = \mathbf{X}_k \times \bar{\mathbf{X}}_{>k}$.

The second key ingredient is the adaptation of TT ranks. The TT ranks can be easily reduced. For example, it is sufficient to replace the generalised QR factorization of $\mathbf{H}_k^{(L)}$ or $(\mathbf{H}_k^{(R)})^\top$ by a generalised SVD, where the singular values below the desired threshold are truncated. To increase the TT ranks, we can apply *oversampling*. Using the forward iteration (with k increasing) as an example, we can compute the tensor $\mathcal{H}_k \in \mathbb{R}^{r_{k-1} \times n_k \times (r_k + \rho_k)}$ on the enriched point set $\bar{\mathbf{X}}_{<k} \times \mathbf{X}_k \times (\bar{\mathbf{X}}_{>k} \cup \tilde{\mathbf{X}}_{>k})$, where $\tilde{\mathbf{X}}_{>k} = \{(\mathbf{x}_{k+1}^{(\alpha_k)}, \dots, \mathbf{x}_d^{(\alpha_k)})\}_{\alpha_k=1}^{\rho_k}$ are auxiliary points. These auxiliary points can be sampled at random [44], or more accurately, from a surrogate of the error [15]. In the latter case, we carry out a second TT-cross to approximate the error

$h(\mathbf{x}) - \tilde{h}(\mathbf{x})$ by a TT decomposition with TT ranks $\rho_1, \dots, \rho_{d-1}$, and take the *MaxVol* points of the error as $\tilde{\mathbf{X}}_{>k}$. This *enrichment* of the solution with error or residual information has proven to accelerate the convergence drastically even for small expansion ranks ρ_k when applied to solving linear systems [15]. The pseudocode of the TT-cross is provided in Algorithm 4.

Algorithm 4 TT-cross

```

1: Choose initial sets  $\bar{\mathbf{X}}_{<k}$ ,  $k = 2, \dots, d$ , stopping threshold  $\delta > 0$ , enrichment TT ranks  $\rho_k$ .
2: while first iteration or  $\|\tilde{h}(\mathbf{x}) - \tilde{h}_{\text{prev}}(\mathbf{x})\| > \delta \|\tilde{h}(\mathbf{x})\|$  do
3:   for  $k = d, d-1, \dots, 2$  do ▷ backward iteration
4:     Sample  $\mathcal{H}_k$  as shown in (82), optionally expanding  $\bar{\mathbf{X}}_{<k}$  to  $\bar{\mathbf{X}}_{<k} \cup \tilde{\mathbf{X}}_{<k}$ .
5:     Compute  $\mathbf{J}_k$  from MaxVol on  $(\mathbf{H}_k^{(R)})^\top$  or its SVD factor, let  $\bar{\mathbf{X}}_{>k-1} = \mathbf{X}_{\geq k}(\mathbf{J}_k)$ .
6:   end for
7:   for  $k = 1, 2, \dots, d-1$  do ▷ forward iteration
8:     Sample  $\mathcal{H}_k$  as shown in (82), optionally expanding  $\bar{\mathbf{X}}_{>k}$  to  $\bar{\mathbf{X}}_{>k} \cup \tilde{\mathbf{X}}_{>k}$ .
9:     Compute  $\mathbf{I}_k$  from MaxVol on  $\mathbf{H}_k^{(L)}$  or its SVD factor, let  $\bar{\mathbf{X}}_{<k+1} = \mathbf{X}_{\leq k}(\mathbf{I}_k)$ .
10:    Reconstruct TT cores as shown in (84)–(85).
11:  end for
12:  Sample the last TT core  $\mathcal{A}_d = \mathcal{H}_d$  as shown in (82).
13: end while

```

The construction of the tensor in (82) suggests that the TT-cross requires $\sum_{k=1}^d r_{k-1} n_k r_k$ evaluations of $h(\mathbf{x})$ per iteration, which is proportional to the number of unknowns in the TT cores. To enhance the robustness (at the expense of a larger number of function evaluations), one may oversample \mathbf{X}_k beyond n_k basis functions, and use the *rectangular MaxVol* algorithm [40] to oversample $\mathbf{I}_k, \mathbf{J}_{k+1}$ beyond r_k indices. In this case, the matrix inverse in (84) is replaced by a pseudoinverse. For our DIRT framework, the standard *MaxVol* equipped with the error enrichment is sufficiently robust to factorise the ratio functions, so we proceed with Algorithm 4.

8.2 Appendix B: proof of Proposition 2

Recall the marginal function

$$\hat{\pi}_{\leq k}(\mathbf{x}_{\leq k}) = \sum_{\ell_k=1}^{r_k} \left(\mathcal{G}_1(\mathbf{x}_1) \cdots \mathcal{G}_{k-1}(\mathbf{x}_{k-1}) \mathcal{L}_k^{(:, \ell_k)}(\mathbf{x}_k) \right)^2, \quad (86)$$

where $\mathcal{L}_k(\mathbf{x}_k) : \mathcal{X}_k \mapsto \mathbb{R}^{r_{k-1} \times r_k}$ is given by (25) with a coefficient tensor $\mathcal{B}_k \in \mathbb{R}^{r_{k-1} \times n_k \times r_k}$. The next marginal function $\hat{\pi}_{<k}(\mathbf{x}_{<k})$ is defined by

$$\begin{aligned} \hat{\pi}_{<k}(\mathbf{x}_{<k}) &= \sum_{\ell_k=1}^{r_k} \int \left(\mathcal{G}_1(\mathbf{x}_1) \cdots \mathcal{G}_{k-1}(\mathbf{x}_{k-1}) \mathcal{L}_k^{(:, \ell_k)}(\mathbf{x}_k) \right)^2 \lambda_k(\mathbf{x}_k) d\mathbf{x}_k \\ &= \sum_{\ell_k=1}^{r_k} \int \left(\sum_{\alpha_{k-1}=1}^{r_{k-1}} \mathcal{G}_{<k}^{(\alpha_{k-1})}(\mathbf{x}_{<k}) \mathcal{L}_k^{(\alpha_{k-1}, \ell_k)}(\mathbf{x}_k) \right) \left(\sum_{\beta_{k-1}=1}^{r_{k-1}} \mathcal{G}_{<k}^{(\beta_{k-1})}(\mathbf{x}_{<k}) \mathcal{L}_k^{(\beta_{k-1}, \ell_k)}(\mathbf{x}_k) \right) \lambda_k(\mathbf{x}_k) d\mathbf{x}_k \\ &= \sum_{\alpha_{k-1}=1}^{r_{k-1}} \sum_{\beta_{k-1}=1}^{r_{k-1}} \mathcal{G}_{<k}^{(\alpha_{k-1})}(\mathbf{x}_{<k}) \mathcal{G}_{<k}^{(\beta_{k-1})}(\mathbf{x}_{<k}) \overline{\mathcal{M}}_k[\alpha_{k-1}, \beta_{k-1}], \end{aligned} \quad (87)$$

where the symmetric matrix $\overline{\mathcal{M}}_k \in \mathbb{R}^{r_{k-1} \times r_{k-1}}$ is given by

$$\overline{\mathcal{M}}_k[\alpha_{k-1}, \beta_{k-1}] = \sum_{\ell_k=1}^{r_k} \int \mathcal{L}_k^{(\alpha_{k-1}, \ell_k)}(\mathbf{x}_k) \mathcal{L}_k^{(\beta_{k-1}, \ell_k)}(\mathbf{x}_k) \lambda_k(\mathbf{x}_k) d\mathbf{x}_k, \quad (88)$$

and $\mathcal{G}_{<k}$ is defined in (24). Plugging the expression (25) of $\mathcal{L}_k(\mathbf{x}_k)$ into (88), we obtain

$$\begin{aligned} \overline{\mathcal{M}}_k[\alpha_{k-1}, \beta_{k-1}] &= \sum_{\ell_k=1}^{r_k} \int \left(\sum_{i=1}^{n_k} \phi_k^{(i)}(\mathbf{x}_k) \mathbf{B}_k[\alpha_{k-1}, i, \ell_k] \right) \left(\sum_{j=1}^{n_k} \phi_k^{(j)}(\mathbf{x}_k) \mathbf{B}_k[\beta_{k-1}, j, \ell_k] \right) \lambda_k(\mathbf{x}_k) d\mathbf{x}_k \\ &= \sum_{\ell_k=1}^{r_k} \sum_{i=1}^{n_k} \sum_{j=1}^{n_k} \mathbf{B}_k[\alpha_{k-1}, i, \ell_k] \mathbf{B}_k[\beta_{k-1}, j, \ell_k] \int \phi_k^{(i)}(\mathbf{x}_k) \phi_k^{(j)}(\mathbf{x}_k) \lambda_k(\mathbf{x}_k) d\mathbf{x}_k \\ &= \sum_{\ell_k=1}^{r_k} \sum_{i=1}^{n_k} \sum_{j=1}^{n_k} \mathbf{B}_k[\alpha_{k-1}, i, \ell_k] \mathbf{B}_k[\beta_{k-1}, j, \ell_k] \mathbf{M}_k[i, j] \end{aligned} \quad (89)$$

where $\mathbf{M}_k \in \mathbb{R}^{n_k \times n_k}$ is the symmetric positive definite mass matrix defined in 21. Given the Cholesky factorisation $\mathbf{L}_k \mathbf{L}_k^\top = \mathbf{M}_k$, we have $\mathbf{M}_k[i, j] = \sum_{\tau=1}^{n_k} \mathbf{L}_k[i, \tau] \mathbf{L}_k[j, \tau]$. Substituting the above identity into (89), we have

$$\begin{aligned} \overline{\mathcal{M}}_k[\alpha_{k-1}, \beta_{k-1}] &= \sum_{\ell_k=1}^{r_k} \sum_{i=1}^{n_k} \sum_{j=1}^{n_k} \sum_{\tau=1}^{n_k} \mathbf{B}_k[\alpha_{k-1}, i, \ell_k] \mathbf{B}_k[\beta_{k-1}, j, \ell_k] \mathbf{L}_k[i, \tau] \mathbf{L}_k[j, \tau] \\ &= \sum_{\ell_k=1}^{r_k} \sum_{\tau=1}^{n_k} \left(\sum_{i=1}^{n_k} \mathbf{B}_k[\alpha_{k-1}, i, \ell_k] \mathbf{L}_k[i, \tau] \right) \left(\sum_{j=1}^{n_k} \mathbf{B}_k[\beta_{k-1}, j, \ell_k] \mathbf{L}_k[j, \tau] \right). \end{aligned} \quad (90)$$

Denoting $\mathbf{C}_k[\alpha_{k-1}, \tau, \ell_k] = \sum_{i=1}^{n_k} \mathbf{B}_k[\alpha_{k-1}, i, \ell_k] \mathbf{L}_k[i, \tau]$ and unfolding \mathbf{C}_k along the first coordinate similarly to (83) to obtain a matrix $\mathbf{C}_k^{(R)} \in \mathbb{R}^{r_{k-1} \times (n_k r_k)}$, we have

$$\overline{\mathcal{M}}_k[\alpha_{k-1}, \beta_{k-1}] = \sum_{\ell_k=1}^{r_k} \sum_{\tau=1}^{n_k} \mathbf{C}_k[\alpha_{k-1}, \tau, \ell_k] \mathbf{C}_k[\beta_{k-1}, \tau, \ell_k] = \sum_{\iota=1}^{n_k r_k} \mathbf{C}_k^{(R)}[\alpha_{k-1}, \iota] \mathbf{C}_k^{(R)}[\beta_{k-1}, \iota].$$

Equivalently, we have $\overline{\mathcal{M}}_k = \mathbf{C}_k^{(R)} (\mathbf{C}_k^{(R)})^\top$. This way, computing the thin QR factorisation

$$\mathbf{Q}_k \mathbf{R}_k = (\mathbf{C}_k^{(R)})^\top,$$

we obtain the Cholesky factorisation $\mathbf{R}_k^\top \mathbf{R}_k = \overline{\mathcal{M}}_k$ where $\mathbf{R}_k \in \mathbb{R}^{r_{k-1} \times r_{k-1}}$ is upper-triangular. Substituting the identity

$$\overline{\mathcal{M}}_k[\alpha_{k-1}, \beta_{k-1}] = \sum_{\ell_{k-1}=1}^{r_{k-1}} \mathbf{R}_k[\ell_{k-1}, \alpha_{k-1}] \mathbf{R}_k[\ell_{k-1}, \beta_{k-1}],$$

into (87), the next marginal function $\hat{\pi}_{<k}(\mathbf{x}_{<k})$ is defined by

$$\begin{aligned} \hat{\pi}_{<k}(\mathbf{x}_{<k}) &= \sum_{\ell_{k-1}=1}^{r_{k-1}} \sum_{\alpha_{k-1}=1}^{r_{k-1}} \sum_{\beta_{k-1}=1}^{r_{k-1}} \mathcal{G}_{<k}^{(\alpha_{k-1})}(\mathbf{x}_{<k}) \mathcal{G}_{<k}^{(\beta_{k-1})}(\mathbf{x}_{<k}) \mathbf{R}_k[\ell_{k-1}, \alpha_{k-1}] \mathbf{R}_k[\ell_{k-1}, \beta_{k-1}] \\ &= \sum_{\ell_{k-1}=1}^{r_{k-1}} \left(\sum_{\alpha_{k-1}=1}^{r_{k-1}} \mathcal{G}_{<k}^{(\alpha_{k-1})}(\mathbf{x}_{<k}) \mathbf{R}_k[\ell_{k-1}, \alpha_{k-1}] \right)^2 \\ &= \sum_{\ell_{k-1}=1}^{r_{k-1}} \left(\mathcal{G}_1(\mathbf{x}_1) \cdots \mathcal{G}_{k-2}(\mathbf{x}_{k-2}) \sum_{\alpha_{k-1}=1}^{r_{k-1}} \mathcal{G}_{k-1}^{(\cdot, \alpha_{k-1})}(\mathbf{x}_{k-1}) \mathbf{R}_k[\ell_{k-1}, \alpha_{k-1}] \right)^2, \end{aligned} \quad (91)$$

where the last line follows from the identity in (24). Following the recursive definition of $\mathcal{L}_k(\mathbf{x}_k)$ in Proposition 2, we have

$$\mathcal{L}_{k-1}^{(:, \ell_{k-1})}(\mathbf{x}_{k-1}) = \sum_{\alpha_{k-1}=1}^{r_{k-1}} \mathcal{G}_{k-1}^{(:, \alpha_{k-1})}(\mathbf{x}_{k-1}) \mathbf{R}_k[\ell_{k-1}, \alpha_{k-1}]. \quad (92)$$

Substituting the definition of the FTT core

$$\mathcal{G}_{k-1}^{(\alpha_{k-1}-1, \alpha_{k-1})}(\mathbf{x}_{k-1}) = \sum_{i=1}^{n_{k-1}} \phi_{k-1}^{(i)}(\mathbf{x}_{k-1}) \mathcal{A}_{k-1}[\alpha_{k-2}, i, \alpha_{k-1}]$$

into (92), we have

$$\mathcal{L}_{k-1}^{(\alpha_{k-2}, \ell_{k-1})}(\mathbf{x}_{k-1}) = \sum_{i=1}^{n_{k-1}} \phi_{k-1}^{(i)}(\mathbf{x}_{k-1}) \left(\sum_{\alpha_{k-1}=1}^{r_{k-1}} \mathcal{A}_{k-1}[\alpha_{k-2}, i, \alpha_{k-1}] \mathbf{R}_k[\ell_{k-1}, \alpha_{k-1}] \right).$$

Thus, defining the coefficient tensor

$$\mathcal{B}_{k-1}[\alpha_{k-2}, i, \ell_{k-1}] = \sum_{\alpha_{k-1}=1}^{r_{k-1}} \mathcal{A}_{k-1}[\alpha_{k-2}, i, \alpha_{k-1}] \mathbf{R}_k[\ell_{k-1}, \alpha_{k-1}],$$

we obtain the result of Proposition 2:

$$\mathcal{L}_{k-1}^{(\alpha_{k-2}, \ell_{k-1})}(\mathbf{x}_{k-1}) = \sum_{i=1}^{n_{k-1}} \phi_{k-1}^{(i)}(\mathbf{x}_{k-1}) \mathcal{B}_{k-1}[\alpha_{k-2}, i, \ell_{k-1}].$$

By setting index $k = 1$ and repeating the above procedure, we can obtain the normalising constant $\hat{z} = \int_{\mathcal{X}_1} \hat{\pi}_{\leq 1}(\mathbf{x}_1) \lambda_1(\mathbf{x}_1) d\mathbf{x}_1 = \mathbf{R}_1^2$, where $\mathbf{R}_1 \in \mathbb{R}$ as the unfolded \mathcal{C}_1 along the first coordinate is a row vector $\mathbf{C}_1^{(R)} \in \mathbb{R}^{1 \times (n_1 r_1)}$.

Acknowledgements The author would like to thank Y. Marzouk and R. Scheichl for for many insightful discussions. T. Cui acknowledges support from the Australian Research Council, under grant number CE140100049. S. Dolgov acknowledges support from the International Visitor Program of Sydney Mathematical Research Institute.

References

1. Barrault, M., Maday, Y., Nguyen, N.C., Patera, A.T.: An empirical interpolation method: application to efficient reduced-basis discretization of partial differential equations. *Comptes Rendus Mathematique* **339**(9), 667–672 (2004)
2. Bigoni, D., Engsig-Karup, A.P., Marzouk, Y.M.: Spectral tensor-train decomposition. *SIAM Journal on Scientific Computing* **38**(4), A2405–A2439 (2016)
3. Bigoni, D., Zahm, O., Spantini, A., Marzouk, Y.: Greedy inference with layers of lazy maps. arXiv preprint arXiv:1906.00031 (2019)
4. Blei, D.M., Kucukelbir, A., McAuliffe, J.D.: Variational inference: A review for statisticians. *Journal of the American statistical Association* **112**(518), 859–877 (2017)
5. Boyd, J.P.: Chebyshev and Fourier spectral methods. Courier Corporation (2001)
6. Bungartz, H.J., Griebel, M.: Sparse grids. *Acta Numerica* **13**(1), 147–269 (2004). DOI 10.1017/S0962492904000182
7. Carlier, G., Galichon, A., Santambrogio, F.: From knothe’s transport to brenier’s map and a continuation method for optimal transport. *SIAM Journal on Mathematical Analysis* **41**(6), 2554–2576 (2010)
8. Chaturantabut, S., Sorensen, D.C.: Nonlinear model reduction via discrete empirical interpolation. *SIAM Journal on Scientific Computing* **32**(5), 2737–2764 (2010)

9. Cui, T., Martin, J., Marzouk, Y.M., Solonen, A., Spantini, A.: Likelihood-informed dimension reduction for nonlinear inverse problems. *Inverse Problems* **30**(11), 114015 (2014)
10. Cui, T., Marzouk, Y.M., Willcox, K.E.: Data-driven model reduction for the bayesian solution of inverse problems. *International Journal for Numerical Methods in Engineering* **102**, 966–990 (2015). DOI 10.1002/nme.4748
11. Cui, T., Marzouk, Y.M., Willcox, K.E.: Scalable posterior approximations for large-scale bayesian inverse problems via likelihood-informed parameter and state reduction. *Journal of Computational Physic* **315**, 363–387 (2016)
12. Detommaso, G., Cui, T., Marzouk, Y., Spantini, A., Scheichl, R.: A stein variational newton method. In: *Advances in Neural Information Processing Systems*, pp. 9169–9179 (2018)
13. Dick, J., Kuo, F.Y., Sloan, I.H.: High-dimensional integration: The quasi-Monte Carlo way. *Acta Numerica* **22**, 133–288 (2013). DOI 10.1017/S0962492913000044
14. Dolgov, S., Anaya-Izquierdo, K., Fox, C., Scheichl, R.: Approximation and sampling of multivariate probability distributions in the tensor train decomposition. *Statistics and Computing* **30**, 603–625 (2020). DOI 10.1007/s11222-019-09910-z
15. Dolgov, S.V., Savostyanov, D.V.: Alternating minimal energy methods for linear systems in higher dimensions. *SIAM Journal on Scientific Computing* **36**(5), A2248–A2271 (2014)
16. Förstner, W., Moonen, B.: A metric for covariance matrices. In: *Geodesy-the Challenge of the 3rd Millennium*, pp. 299–309. Springer (2003)
17. Gelman, A., Meng, X.L.: Simulating normalizing constants: From importance sampling to bridge sampling to path sampling. *Statistical science* pp. 163–185 (1998)
18. Girolami, M., Calderhead, B.: Riemann manifold Langevin and Hamiltonian Monte Carlo methods. *Journal of the Royal Statistical Society: Series B (Statistical Methodology)* **73**(2), 123–214 (2011)
19. Goreinov, S.A., Oseledets, I.V., Savostyanov, D.V., Tyrtysnikov, E.E., Zamarashkin, N.L.: How to find a good submatrix. In: *Matrix Methods: Theory, Algorithms And Applications: Dedicated to the Memory of Gene Golub*, pp. 247–256. World Scientific (2010)
20. Goreinov, S.A., Tyrtysnikov, E.E., Zamarashkin, N.L.: A theory of pseudoskeleton approximations. *Linear algebra and its applications* **261**(1-3), 1–21 (1997)
21. Goreinov, S.A., Zamarashkin, N.L., Tyrtysnikov, E.E.: Pseudo-skeleton approximations by matrices of maximal volume. *Mathematical Notes* **62**(4), 515–519 (1997)
22. Gorodetsky, A., Karaman, S., Marzouk, Y.M.: A continuous analogue of the tensor-train decomposition. *Computer Methods in Applied Mechanics and Engineering* **347**, 59–84 (2019)
23. Haario, H., Laine, M., Mira, A., Saksman, E.: DRAM: efficient adaptive MCMC. *Statistics and Computing* **16**(4), 339–354 (2006). DOI 10.1007/s11222-006-9438-0
24. Hackbusch, W.: *Tensor spaces and numerical tensor calculus*, vol. 42. Springer Science & Business Media (2012)
25. Higdon, D.: Space and space-time modeling using process convolutions. In: *Quantitative methods for current environmental issues*, pp. 37–56. Springer (2002)
26. Holtz, S., Rohwedder, T., Schneider, R.: The alternating linear scheme for tensor optimization in the tensor train format. *SIAM Journal on Scientific Computing* **34**(2), A683–A713 (2012)
27. Hukushima, K., Nemoto, K.: Exchange monte carlo method and application to spin glass simulations. *Journal of the Physical Society of Japan* **65**(6), 1604–1608 (1996)
28. Jordan, M.I., Ghahramani, Z., Jaakkola, T.S., Saul, L.K.: An introduction to variational methods for graphical models. *Machine learning* **37**(2), 183–233 (1999)
29. Kantas, N., Beskos, A., Jasra, A.: Sequential Monte Carlo methods for high-dimensional inverse problems: A case study for the Navier-Stokes equations. *SIAM/ASA Journal on Uncertainty Quantification* **2**(1), 464–489 (2014)
30. Knothe, H.: Contributions to the theory of convex bodies. *The Michigan Mathematical Journal* **4**(1), 39–52 (1957)
31. Kobayev, I., Prince, S., Brubaker, M.A.: Normalizing flows: Introduction and ideas. arXiv preprint arXiv:1908.09257 (2019)
32. Kolda, T.G., Bader, B.W.: Tensor decompositions and applications. *SIAM review* **51**(3), 455–500 (2009)
33. Kruse, J., Detommaso, G., Scheichl, R., Koethe, U.: HINT: Hierarchical invertible neural transport for density estimation and Bayesian inference. arXiv preprint 1905.10687 (2019). URL <http://arxiv.org/abs/1905.10687>
34. Liu, J.S.: *Monte Carlo strategies in Scientific Computing*. Springer, New York (2001)
35. Liu, Q., Wang, D.: Stein variational gradient descent: A general purpose bayesian inference algorithm. In: *Advances In Neural Information Processing Systems*, pp. 2378–2386 (2016)
36. Mahoney, M.W., Drineas, P.: Cur matrix decompositions for improved data analysis. *Proceedings of the National Academy of Sciences* **106**(3), 697–702 (2009)
37. Marzouk, Y., Moselhy, T., Parno, M., Spantini, A.: Sampling via measure transport: An introduction. *Handbook of Uncertainty Quantification* pp. 1–41 (2016)

38. Meng, X.L., Wong, W.H.: Simulating ratios of normalizing constants via a simple identity: a theoretical exploration. *Statistica Sinica* pp. 831–860 (1996)
39. Mengersen, K.L., Tweedie, R.L., et al.: Rates of convergence of the hastings and metropolis algorithms. *The Annals of Statistics* **24**(1), 101–121 (1996)
40. Mikhalev, A.Y., Oseledets, I.V.: Rectangular maximum–volume submatrices and their applications. *Linear Algebra Appl.* **538**, 187–211 (2018). DOI 10.1016/j.laa.2017.10.014
41. Moselhy, T., Marzouk, Y.: Bayesian inference with optimal maps. *Journal of Computational Physics* **231**(23), 7815–7850 (2012)
42. Neal, R.M.: Sampling from multimodal distributions using tempered transitions. *Statistics and computing* **6**(4), 353–366 (1996)
43. Oseledets, I., Tyrtshnikov, E.: Tt-cross approximation for multidimensional arrays. *Linear Algebra and its Applications* **432**(1), 70–88 (2010)
44. Oseledets, I.V.: DMRG approach to fast linear algebra in the TT-format. *Comput. Meth. Appl. Math.* **11**(3), 382–393 (2011). DOI 10.2478/cmam-2011-0021
45. Oseledets, I.V.: Tensor-train decomposition. *SIAM Journal on Scientific Computing* **33**(5), 2295–2317 (2011)
46. Owen, A.B.: Monte Carlo theory, methods and examples (2013)
47. Papamakarios, G., Nalisnick, E., Rezende, D.J., Mohamed, S., Lakshminarayanan, B.: Normalizing flows for probabilistic modeling and inference. arXiv preprint arXiv:1912.02762 (2019)
48. Parno, M.D., Marzouk, Y.M.: Transport map accelerated markov chain monte carlo. *SIAM/ASA Journal on Uncertainty Quantification* **6**(2), 645–682 (2018)
49. Peherstorfer, B., Marzouk, Y.: A transport-based multifidelity preconditioner for markov chain monte carlo. *Advances in Computational Mathematics* **45**(5-6), 2321–2348 (2019)
50. Rezende, D.J., Mohamed, S.: Variational inference with normalizing flows. arXiv preprint arXiv:1505.05770 (2015)
51. Robert, C., Casella, G.: Monte Carlo statistical methods. Springer Science & Business Media (2013)
52. Rohrbach, P.B., Dolgov, S., Grasedyck, L., Scheichl, R.: Rank bounds for approximating Gaussian densities in the Tensor-Train format. arXiv preprint 2001.08187 (2020). URL <http://arxiv.org/abs/2001.08187>
53. Rosenblatt, M.: Remarks on a multivariate transformation. *The annals of mathematical statistics* **23**(3), 470–472 (1952)
54. Scheichl, R., Stuart, A.M., Teckentrup, A.L.: Quasi-Monte Carlo and Multilevel Monte Carlo methods for computing posterior expectations in elliptic inverse problems. *SIAM/ASA Journal on Uncertainty Quantification* **5**(1), 493–518 (2017). DOI 10.1137/16M1061692
55. Shen, J., Tang, T., Wang, L.L.: Spectral methods: algorithms, analysis and applications, vol. 41. Springer Science & Business Media (2011)
56. Spantini, A., Bigoni, D., Marzouk, Y.: Inference via low-dimensional couplings. *The Journal of Machine Learning Research* **19**(1), 2639–2709 (2018)
57. Spantini, A., Solonen, A., Cui, T., Martin, J., Tenorio, L., Marzouk, Y.: Optimal low-rank approximations of bayesian linear inverse problems. *SIAM Journal on Scientific Computing* **37**(6), A2451–A2487 (2015)
58. Swendsen, R.H., Wang, J.S.: Replica monte carlo simulation of spin-glasses. *Physical review letters* **57**(21), 2607 (1986)
59. Trefethen, L.N.: Approximation theory and approximation practice, vol. 164. Siam
60. Villani, C.: Optimal transport: old and new, vol. 338. Springer Science & Business Media (2008)
61. White, S.R.: Density-matrix algorithms for quantum renormalization groups. *Physical Review B* **48**(14), 10345 (1993)
62. Zahm, O., Cui, T., Law, K., Spantini, A., Marzouk, Y.: Certified dimension reduction in nonlinear bayesian inverse problems. arXiv preprint arXiv:1807.03712 (2018)